Spiro Compounds for Organic Optoelectronics

Tobat P. I. Saragi, Till Spehr, Achim Siebert, Thomas Fuhrmann-Lieker, and Josef Salbeck*

Macromolecular Chemistry and Molecular Materials (mmCmm), Institute of Chemistry, Department of Science and Center for Interdisciplinary Nanostructure Science and Technology (CINSaT), University of Kassel, Heinrich-Plett-Strasse 40, D-34109 Kassel, Germany

Received October 31, 2006

Contents

* To whom correspondence should be addressed. Tel: +49-561-8044425. Fax: +49-561-8044555. E-mail: salbeck@uni-kassel.de.

1. Introduction

Advances in organic semiconductors and the knowledge of their corresponding physical and chemical properties drive the development of low-cost optoelectronic applications such as light-emitting devices,[1−7] solar cells,[8−15] nonvolatile-memory devices,[16−23] photosensing devices,[24−28] vapor sensors,[29−31] biological and chemical sensors,[32−42] and field-effect transistors.[43−45]

Organic semiconductors as active materials in thin film electronic devices offer several major advantages over their inorganic counterparts. They can be processed by a multitude of different methods, the most important of which are vapor deposition and solution-based processes, such as spin-coating and different printing techniques. The deposition of thin films can be carried out at room temperature, and the production costs are considerably lower than those of the corresponding inorganic optoelectronic devices. The optoelectronic devices can be fabricated on low-cost flexible substrates, paving the way for all-plastic electronics and transparent devices.

Nevertheless, controlling the reproducibility of device performance and the lifetime (stability) of the device become major issues in organic optoelectronics devices, challenging materials scientists and device engineers. This issue is

10.1021/cr0501341 CCC: $65.00
Published on Web 03/24/2007

Tobat P. I. Saragi was born in 1974 in Serui, Irian Jaya, Indonesia. He received his B.Sc. and M.Sc. degrees in physics from the Bandung Institute of Technology, Indonesia, in 1996 and 2000. He worked on the electrical and optical properties of conjugated polymers under the direction of Prof. Tjia May On. His doctoral degree was obtained from the University of Kassel, Germany, in 2004 under the direction of Prof. Josef Salbeck. His doctoral thesis included studies of charge transport properties in thin films of spiro compounds and organic thin film phototransistors. He currently is pursuing his habilitation at the University of Kassel and his research interests are transistors, phototransistors, solar cells, and ultraviolet detectors.

Till Spehr was born on September 28, 1971, in Kassel, Germany. He received his Diploma of Chemistry from Kassel University in 2001. He is currently working on his Ph.D. in physical chemistry under the direction of Prof. Josef Salbeck. His research is focused on the solid-state photoluminescent properties of spiro compounds.

Achim Siebert was born on October 29, 1975, in Kassel, Germany. He studied chemistry at the University of Kassel and is currently working on his Ph.D. thesis under the supervison of Prof. Josef Salbeck. His research is focused on synthesis of spiro compounds.

addressed in industrial research as well as on an academic level in universities and institutional laboratories around the world. For instance, understanding the morphology and microscopic organization of the materials used in the active films, that is, single crystals, polycrystals, liquid crystals, and amorphous glasses, is of paramount importance to control and to optimize the corresponding optoelectronic device performance.

Thomas Fuhrmann-Lieker, born in 1968, studied chemistry in Bologna (Italy) and Marburg (Germany) where he received his Ph.D. in 1997 for work on optical data storage with azo polymers. After a 2-year postdoctoral stay at Kyushu University (Japan) in the group of Prof. Tetsuo Tsutsui, he joined the group Prof. Josef Salbeck at Duisburg University (Germany) and finished his habilitation at the University of Kassel (Germany) where he was appointed as Privatdozent in 2005. His research interests comprise the physical chemistry of photonic materials, self-organization phenomena in thin layers and composites, and the application of biomaterials.

Josef Salbeck is professor of Macromolecular Chemistry and Molecular Materials (mmCmm) in the Science Department at the University of Kassel, Germany. He was born 1956 in Verau, Germany. After training and working as a chemical laboratory assistant, he studied Chemistry at the University of Regensburg, where he obtained his Ph.D. degree in 1988 under the supervision of Prof. Dr. J. Daub. He finished his habilitation in Organic Chemistry in 1992 in the field of electrochemical–optical combination methods and obtained the lectureship in Organic Chemistry at the University of Regensburg. In 1993, Salbeck went to Hoechst AG in Frankfurt as a laboratory leader working in a research group about light-emitting polymers within the Corporate Research. As a Heisenberg fellow of the German Research Foundation (Deutsche Forschungsgemeinschaft), he joined in 1995 the group of Prof. Dr. K. Müllen at the Max-Planck-Institute for Polymer Research in Mainz and was appointed as professor of Electrochemistry and Optoelectronic Materials at University Duisburg in 1998. Since 2000, he has been full professor at the University of Kassel and is one of the founders of the recently established Center for Interdisciplinary Nanostructure Science and Technology (CINSaT) there. His research interests mainly involve functional molecular and hybrid materials and organic glasses for electronic, optical, and optoelectronic applications.

The amorphous glassy state is particularly desirable in active materials for various optoelectronics applications for several reasons. First, the amorphous state is relatively easy to achieve compared with single-crystal growth, and second, the amorphous character of the resulting thin films prevents any grain boundaries, leading to spatial homogeneity of the transport properties. In contrast to polycrystalline thin films, where grain boundaries between adjacent microcrystallites act as traps for charge carriers, deteriorating the device performance,[46,47] reproducibility of the device characteristics is thus facilitated with amorphous active materials. Third, the optical properties are favorable in an isotropic stable glassy state. Polycrystalline materials lead to a large amount of scattering, and single crystals introduce birefringence, which is not always wanted. Therefore, when the simple manufacturing process of amorphous films is applied, a high stability of the glassy state is needed in order to prevent the degradation of devices in applications.

An important physical parameter indicating the stability of the amorphous state of a given material is the glass transition temperature (T_g). If an amorphous film is heated above this temperature, molecular motion increases rapidly, allowing the transition into the crystalline state. Therefore it is of utmost importance to design the molecular structure of low molecular weight compounds in such a way that a high T_g is achieved. A relationship between molecular structure and stability of the amorphous state was shown by Naito and Miura.[48,49] They found that molecules with a symmetric globular structure, large molecular weight, and small intermolecular cohesion result in a high stability of the amorphous state. Several concepts addressing this issue have been proposed, including the development of dendritic architectures[50] and tetrahedral structures.[51] A broad range of amorphous organic semiconductors was developed by Shirota and co-workers.[52−58]

In this article, the important class of spiro compounds as organic molecular materials with high T_g that evolved as a very promising approach for optoelectronic materials are reviewed. An overview summarizing the literature about spiro compounds up to the year 2004 was published by us recently.[59] Since then, new light was shed on the interpretation of optical and electronic properties due to the finding of strong coupling in donor−acceptor-type materials. In order to account for these new developments, we focus in this review on the physicochemical properties of spiro compounds in solution as well as in the solid state. In the last section, however, we will also give a comprehensive overview on synthetic pathways, which exhibit some new approaches as well.

We will concentrate on compounds based on the spirobifluorene core. Materials based on other spiro structures, for instance, spirobisindane,[60] spirooxazine,[61−66] spiropyran,[67−70] or polymers like polyspirobifluorene[71−76] will not be included in this review. Spirosilabifluorenes will be touched briefly.

2. Basic Physicochemical Properties of Spiro Compounds

2.1. Molecular and Electronic Structure

2.1.1. The Spiro Linkage

Improving the morphological stability of low molar mass materials while retaining their electronic properties is based on the concept of connecting two more or less extended π-systems with identical or different functions (emission, charge transport) via a common sp^3-hybridized atom. This is the basic idea of the spiro concept.[77] The general structure of the resulting molecules is displayed in Figure 1a. This approach has several benefits. First, the perpendicular arrangement of the two molecular halves leads to a high steric demand of the resulting rigid structure, efficiently suppressing molecular interactions between the π-systems. Furthermore, this results in a higher solubility of the spiro compounds compared with the corresponding non-spiro-linked parent compounds. The sterically demanding structure of fluorescent emitters, based on the spiro concept, also suppresses very effectively excimer formation, frequently encountered in solid-state fluorescent dyes. In addition, doubling of the molecular weight in combination with the cross-shaped molecular structure along with the rigidity of spiro compounds causes entanglement in the amorphous state and hinders recrystallization.[59]

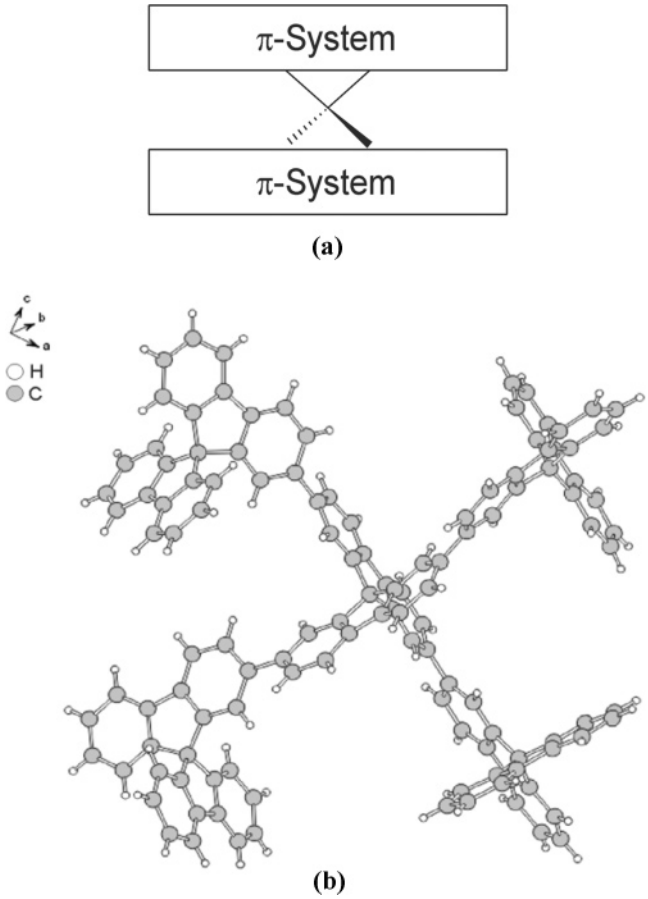

Figure 1. (a) General structure of spiro-linked low molecular mass molecules (Reprinted from ref 59. Copyright 2006. With kind permission of Springer Science and Business Media.) and (b) crystal structure of 4-Spiro[2] showing the perpendicular arrangement of the aryl chains.

Spiro compounds based on the spirobifluorene core are conceptually derived mostly from the corresponding biphenyl compounds (like spiro-6Φ **2** from *p*-sexiphenyl **1** or spiro-TAD **4** from TAD **3**). The spiro atom, however, forces the adjacent aryl rings in a coplanar arrangement. Thus, with respect to the parent compounds derived from biphenyl as

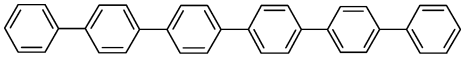

p-sexiphenyl **1**

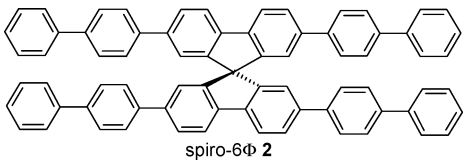
spiro-6Φ **2**

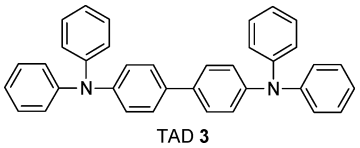
TAD **3**

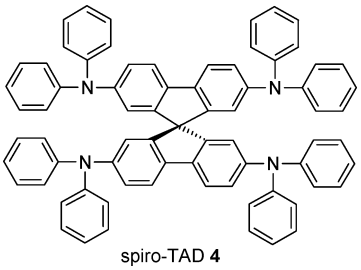
spiro-TAD **4**

central structure unit, one rotational degree of freedom is lost in the corresponding fluorene derivative. As an example of the arrangement of aryl chains in spiro compounds, the crystal structure of 4-spiro[2] (**5**) is given in Figure 1b.

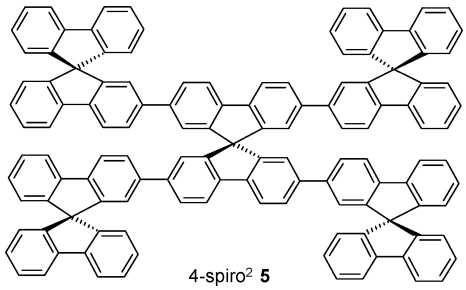
4-spiro[2] **5**

As far as the electronic properties are concerned, the molecules resemble fluorene compounds, and deviations of the spectroscopic and electrochemical properties from the parent biphenyl analogous compounds can be expected. Generally, however, the functional characteristic of the chromophores in each half of the spiro molecule is retained. As already mentioned, the perpendicular arrangement of the π-systems reduces the electronic interaction between the halves to a large extent, with some restrictions given in the next section.

2.1.2. Electronic Coupling via the Spiro Linkage?

The electronic independence of the two halves is based on the perpendicular arrangement of the π-systems and the spectroscopic transition moments. There is, however, experimental evidence for interactions in the excited states that are discussed within the model of so-called "spiro-conjugation".[78] If we consider the molecular orbital picture of two perpendicularly arranged spiro-linked π-systems, both of which are in the ground state, the only nodal plane of the highest occupied π-molecular orbital is the plane of each chromophore. In this configuration, interaction is prevented by symmetry mismatch of the wave functions. On the other hand, higher π-orbitals that can be occupied in excited states may exhibit a second nodal plane perpendicular to the first one but parallel to the plane of the second chromophore. The 4-fold symmetry of these molecular orbitals allows an interaction of both halves (Figure 2).

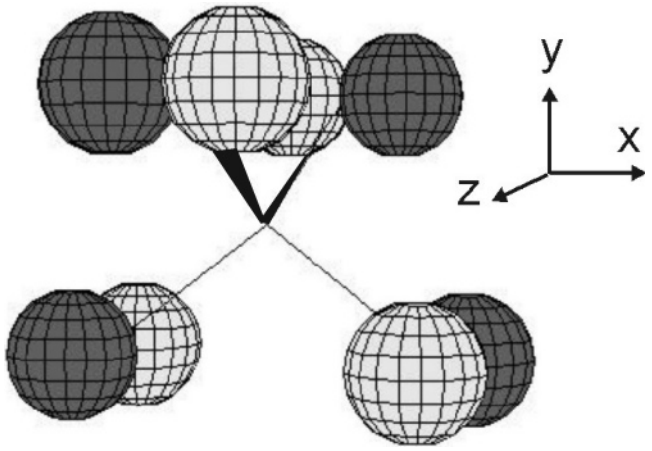

Figure 2. Model of spiro conjugation of higher molecular orbitals. The upper chromophore lies in the $y-z$ plane, the lower chromophore in the $x-y$ plane. Reprinted from ref 59. Copyright 2006. With kind permission of Springer Science and Business Media.

Along with the spiro-conjugation, other mechanisms capable of causing an interaction between both halves are vibronic coupling[79,80] or, for some compounds, coupling occurring because the transition moments are not perpendicular.[81] Schartel et al. demonstrated energy transfer between two identical halves from vibrationally excited states by means of fluorescence polarization spectroscopy.[82] Yip et al. estimated the rate of symmetry-forbidden but vibronically allowed energy transfer between spiro-linked donor−acceptor pairs to be on the order of 1×10^{12} s^{-1}.[83]

In the following, the basic spectroscopic and electrochemical properties derived from measurements in dilute solution and quantum chemical calculations will be discussed and compared with the parent compounds. Solid-state properties will be described in the next section.

2.2. Spectroscopic Properties

2.2.1. Oligophenyls

Oligophenyls are very interesting chromophores since they are excellent blue emitters exhibiting high fluorescence quantum yields and high stability. The color can be tuned by extending the oligophenyl chain, but only to a certain extent (Davydov rule).[84] With increasing number of phenyl rings, the extinction coefficient increases, and the fluorescence lifetime decreases.[85] Oligophenyls exhibit a large Stokes shift; typical data measured in solution are as follows: for *p*-terphenyl **6**, $\lambda_{Abs} = 280$ nm and $\lambda_{Em} = 340$ nm; for *p*-quaterphenyl **7**, $\lambda_{Abs} = 300$ nm and $\lambda_{Em} = 370$ nm; for *p*-quinquephenyl **8**, $\lambda_{Abs} = 310$ nm and $\lambda_{Em} = 390$

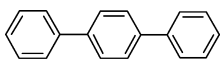
p-terphenyl **6**

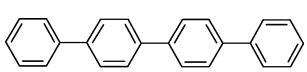
p-quaterphenyl **7**

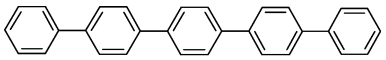

p-quinquephenyl **8**

nm, and for *p*-sexiphenyl **1**, $\lambda_{Abs} = 320$ nm and $\lambda_{Em} = 393$ nm.[86]

In the ground state of these molecules, the torsional angle between adjacent phenyl rings is 23°. In fluorenes and spiro compounds, however, the electronic system is altered due to forced planar alignment of phenyl rings that are linked by the spiro atom. Since the equilibrium geometries of the ground state and the excited state differ, the modifications of the oligophenyl chain have a considerable influence on the photophysical properties, namely, on the Stokes shift. In the series of spiro-oligophenyls with four (spiro-4Φ **9**), six (spiro-6Φ **2**), eight (spiro-8Φ **10**), and ten (spiro-10Φ **11**) phenyl rings in the chromophore, the

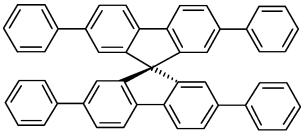

spiro-4Φ **9**

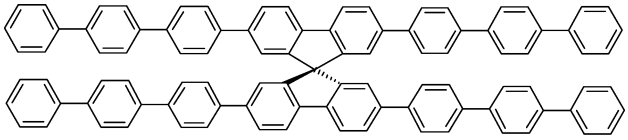

spiro-8Φ **10**

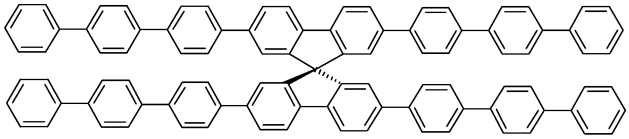

spiro-10Φ **11**

absorption maxima are 332, 342, 344, and 344 nm in dichloromethane, respectively.[77,87−89] As in the case of the unsubstituted oligophenyls, a limiting value for long chains exists. The wavelengths of the fluorescence maxima of the first of the homologous series of spiro oligophenyls increase steadily in the order 359, 385, 395, and 402 nm. The vibrational fine structure of the emission spectra is more pronounced than that of the corresponding absorption spectra due to the increased planarity and rigidity in the excited state. For spiro-6Φ **2**, a detailed analysis shows that the vibrational splitting of 0.20 eV corresponds to a phenyl breathing mode in the Raman spectrum.[90] In 4-spiro^2 **5** and other oligofluorenes, the torsional constraint is even more pronounced: only rigid fluorene units are coupled together. For 4-spiro^2 **5** in comparison with spiro-6Φ **2**, absorption and emission maxima are shifted bathochromically by approximately 10 nm while maintaining the Stokes shift. The unsubstituted perpendicular fluorene units in 4-spiro^2 **5** show an additional characteristic absorption band at 310 nm. Energy transfer from the shorter chains of one half to the longer chains of the other half is possible. Cascade energy transfer is demonstrated for compounds of higher dendrimer generations like 4-spiro^3 **12**.[91]

The fluorescence quantum yields of spiro-oligophenyls with six, eight, and ten phenyl rings measured in dilute

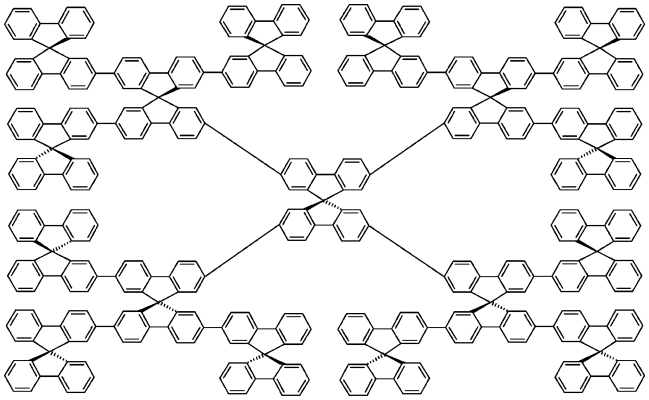

4-spiro^3 **12**

solution are 95%; that of spiro-4Φ **9** is 92%.[92] The fluorescence lifetime was determined to be 1124 ps for spiro-4Φ **9**, 785 ps for spiro-6Φ **2**, and 831 ps for 4-spiro^2 **5** in dichloromethane, which is similar to that of the parent oligophenyls but different from that of unsubstituted fluorene (10 ns).[93] Theoretical studies on these compounds have been published, including the calculation of polarizabilities and second hyperpolarizabilities.[94,95] Lukeš et al. modeled the electrical and optical properties of spiro-4Φ **9**, spiro-6Φ **2**, and 4-spiro^2 **5** by means of the collective electronic oscillator method and have supported their findings by optical measurements.[94,95] Spiro-4Φ **9** shows the smallest Stokes shift in solution (2214 cm^{-1}), which is due to small geometry differences between the ground and excited states.[95] The increasing number of nonhindered inter-ring torsional angles (spiro-6Φ **2**) leads to a larger Stokes shift (2979 cm^{-1}). In contrast, 4-spiro^2 **5** has a ∼200 cm^{-1} smaller Stokes shift with respect to spiro-6Φ **2**, which is probably due to the reduction of nonhindered inter-ring torsional angles.

Katsis et al. extended the oligofluorene chain up to seven fluorene units and showed that spiro compounds with five and with seven fluorene units exhibit no difference in their emission maxima.[96] Below this limiting value, the emission wavelength of short oligophenyls and oligofluorenes, however, can be slightly shifted by appropriate electron donor or acceptor substituents such as in spiro-6Φ(MeO)$_4$ **13**[89] or in spiro-4Φ-F$_4$ **14**,[97] respectively.

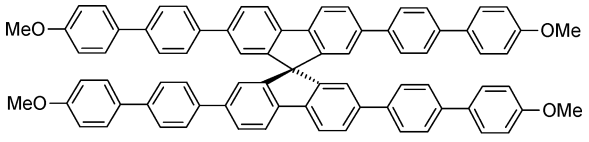

spiro-6Φ(MeO)$_4$ **13**

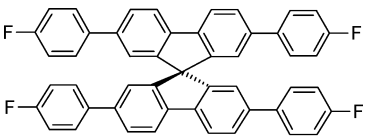

spiro-4Φ-F$_4$ **14**

When oligophenyls are applied as luminescent films, however, it has to be taken into consideration that photooxidation may occur in the presence of molecular oxygen.[98] The proposed pathway for the decomposition is based on the attack of singlet oxygen, which is formed by spin transfer from the excited oligophenyl molecules. *exo*-Peroxides as suggested in ref 98 or, more probably, *endo*-peroxides are formed, which may open to form quinones. This mech-

anism is supported by the infrared spectroscopic detection of carbonyl groups after irradiation in the presence of oxygen.[98]

2.2.2. Arylamines and Carbazoles

Arylamines usually show relatively low fluorescence quantum yields and are not used frequently as emitters. Most of the spiro compounds based on arylamines show a strong absorption in the ultraviolet (UV) range (between 375 and 383 nm) with extinction coefficients between 42 000 and 82 000 M^{-1} cm^{-1}.[91] Notable is the strong bathochromic shift in emission when a diphenylamino group such as that in spiro-TAD **4** (403 nm in CH_2Cl_2) is replaced with an α-naphthyl-phenyl-amino substituent (485 nm for spiro-α-NPB **15** in CH_2Cl_2).

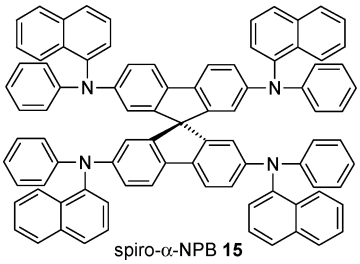

spiro-α-NPB **15**

Phenoxazine (spiro-PhOx-TAD **16**) and phenothiazine derivatives (spiro-PhTh-TAD **17**) with similar emission

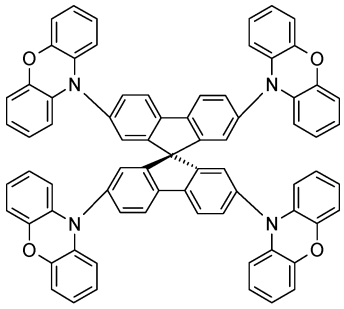

spiro-PhOx-TAD **16**

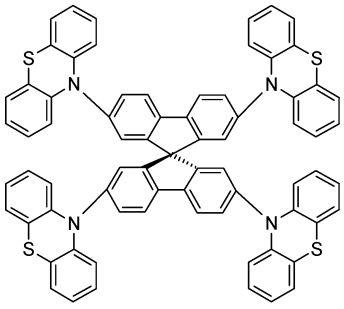

spiro-PhTh-TAD **17**

characteristics are reported.[91] On the other hand, replacement of the diphenylamino substituents of spiro-arylamines with a carbazole moiety results in a distinct hypsochromic shift of absorption and emission. The fluorescence quantum yield of spiro-Carb **18** is relatively high (83%),[89] which can be attributed to the increased rigidity of the carbazole moiety with respect to arylamines. Carbazoles are also interesting as hosts for triplet emitters since their own triplet energy is quite high (3.26 eV).[99] Avilov et al. studied various combinations of spirobifluorene and carbazole moieties theoretically indicating the correlation of the triplet energy

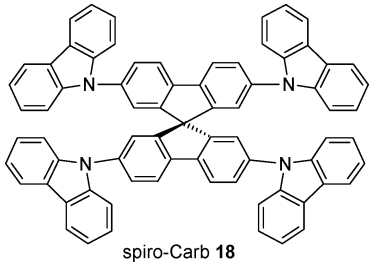

spiro-Carb **18**

and the substitution pattern. Maps for the distribution of spin density in the triplet state were calculated.[99]

2.2.3. Stilbene and Azobenzene Chromophores

A quite interesting blue emitter is spiro-DPVBi **19**, the spiro version of 4,4′-bis(2,2′-diphenylethenyl)-biphenyl **20** (DPVBi), which was introduced by Hosokawa et al. as an

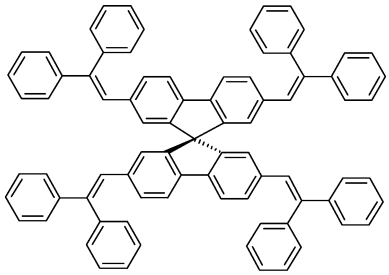

spiro-DPVBi **19**

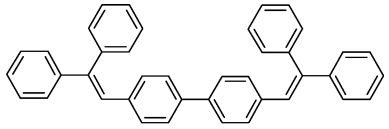

DPVBi **20**

excellent blue emitter.[100] Spiro-DPVBi **19** absorbs at λ_{max} = 377 nm and emits at 453 nm in dichloromethane, exhibiting a large Stokes shift. The fluorescence quantum yield measured in cyclohexane is 82%.[89]

Photochromic spiro compounds based on azo chromophores have also been reported; for a discussion, see the section about solid film properties.

2.2.4. Spirobifluorenes with Asymmetric Substitution Patterns on the Fluorene Units

The compounds discussed up to now have a symmetric substitution pattern at the 2,2′,7,7′ positions of spirobifluorene. They belong to the point group D_{2d} and do not exhibit chirality. If different substituents are applied at the 2,2′- and 7,7′-positions (2,2′-A,7,7′-B substitution, "left-right asymmetric"), the molecular point group changes to C_2 and optically active materials are obtained. Usually racemic mixtures have been prepared and characterized, but in a few cases, the enantiomers were separated and the chiroptical properties of the individual enantiomers were reported.[81,101−103] In circular dichroism (CD) spectra, the main UV absorption bands are split into a couplet with positive and negative sign.[81,101] These results indicate substantial coupling between the two crossed chromophores in the investigated naphthalene and anthracene compounds, (*R*)-(+)-**21** and (R)-(+)-**22**, which is rendered possible by the existence of parallel components of the transition moment. From the sign of the CD bands of the coupled chromophores, the absolute stereochemistry of the spiro center can be determined. In

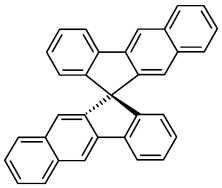

(R)-(+)-**21**

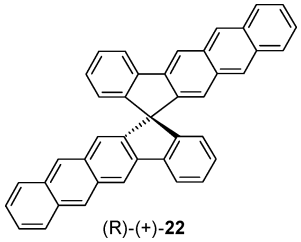

(R)-(+)-**22**

the following discussion, however, only racemic mixtures are considered.

If the 4- and 4′-positions of 2,2′,7,7′-substituted spiro-oligophenyles are additionally substituted, like in the "octo" compounds, the influence of the additional substitution on the electron system is minor. For example, the additional two biphenyl units in the 4,4′-positon in **24** do not disturb the conjugation along the two *p*-sexiphenyl chains because the central two phenyl rings in each chain are fixed planar by the spiro atom. Thus the compounds spiro-octo-1 **23**, spiro-octo-2 **24**, and spiro-octo-3 **25** exhibit spectra similar to their linear oligophenyl counterparts.[88,89]

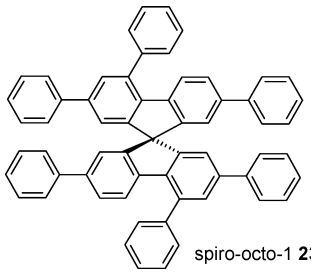

spiro-octo-1 **23**

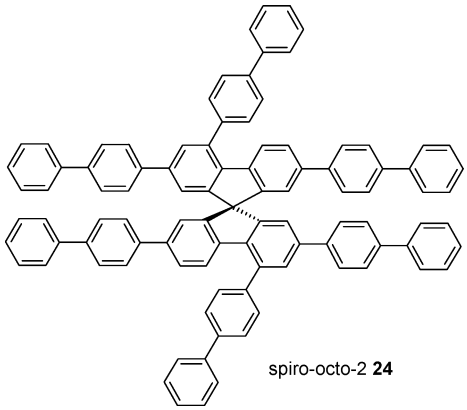

spiro-octo-2 **24**

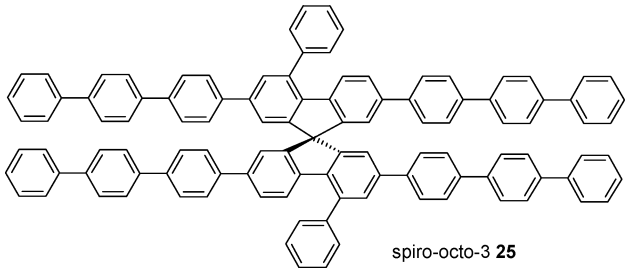

spiro-octo-3 **25**

If only the 2- and 2′-positions of spirobifluorene are substituted, molecules with short conjugation lengths are feasible. Compounds with excellent fluorescence properties for UV emission include spiro-terphenyl **26**,[104] compound SSS **27** containing two bis(fluorene) chromophores,[105,106] spiro-PBD **28**, and spiro-CN-PBD **29**.[107] Interestingly, the

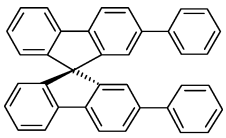

spiro-terphenyl **26**

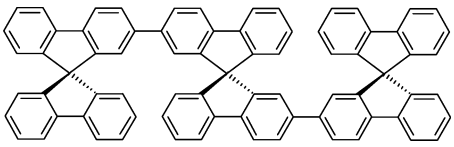

SSS **27**

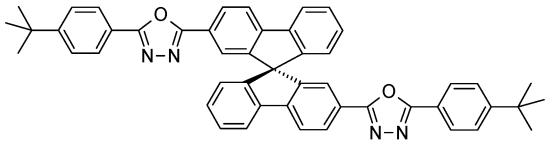

spiro-PBD **28**

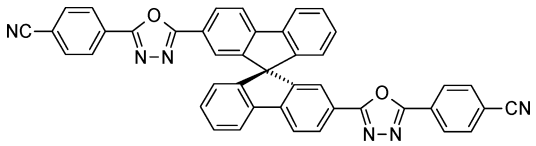

spiro-CN-PBD **29**

more restricted geometry in SSS **27** has a minor influence on absorption and emision as shown in comparison with spiro-4Φ **9** in which the bonds between the first and second and between the third and fourth phenyl rings are subject to rotation. The phosphorescence spectra of SSS **27** and related compounds have been measured in thin films at 77 K; a λ_{max} value of 545 nm (2.28 eV) was obtained.[105]

For the spiro-oxadiazole, spiro-PBD **28**, a detailed study of the electronic structure and optical properties was published.[90] The vibronic structure of the lowest energy absorption band is well resolved in solution as well as in the amorphous film, with a 0−0 transition at 351 nm (3.53 eV), and as strongest absorption peaks the 0−1 and 0−2 phonon bands at 336 nm (3.69 eV) and 318 nm (3.90 eV), respectively. The fluorescence spectrum of this compound is mirror symmetrical to the absorption spectrum with a Stokes shift of 43 nm in solution. In neat films, the second vibronic emission band is more pronounced ($\lambda_{Abs} = 334$ nm; $\lambda_{Em} = 406$ nm).

Wu et al. examined the photophysical properties of compounds containing phenanthroline **30** and indole **31** substituents in the 2- and 2′-positions. They obtained fluorescence lifetimes of 1.2 and 1.8 ns with quantum yields of 48% and 75%, respectively.[108] Investigations of phenanthroline (**32**)-, biphenyl (**33**)-, pyridyl (**34**)-, and phenyl

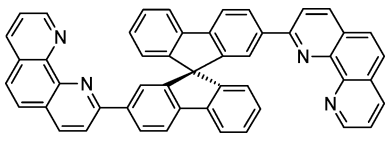

30

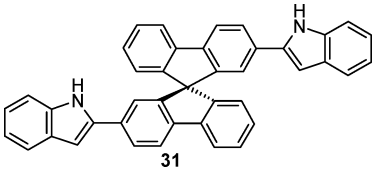

31

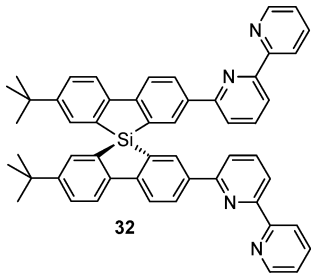

32

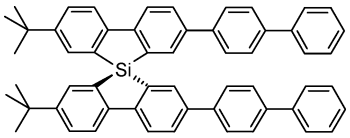

33

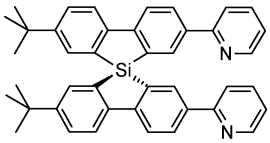

34

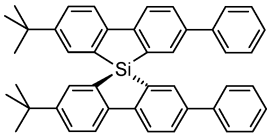

35

(**35**)-substituted spirosilabifluorenes have shown that the substitution of the spiro C atom by Si yields compounds with similarly favorable optical properties.[109] The absorbance spectra showed significant bathochromic shifts relative to those of their carbon analogues as a result of the effective $\sigma^*-\pi^*$ conjugation between the σ^* orbital of the exocyclic Si−C bond and the π^* orbital of the oligoarylene fragment. All compounds exhibit intense violet-blue emission (398−415 nm) with relative high solid-state photoluminescence quantum yield (30−55%). Recently, Yang et al. calculated the static second-order polarizability of those compounds.[110] They found a second-order polarizability of 12.7×10^{-30} esu, which agrees very well with the experimental value (14.4×10^{-30} esu).[110]

Described as an efficient blue emitter is the spirobifluorene-linked bis(phenylanthracene) spiro-FPA **36** with an

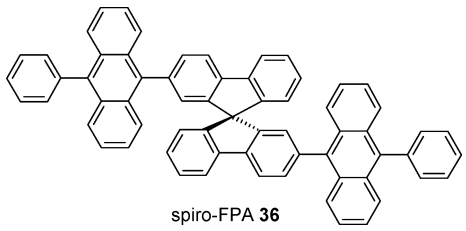

spiro-FPA **36**

emission maximum at 425 nm in toluene.[111] Spiro-DPA **37** has absorption maxima measured in dichloromethane at 360, 378, and 399 nm. The emission maximum is at 429 nm with a shoulder at 443 nm.[112]

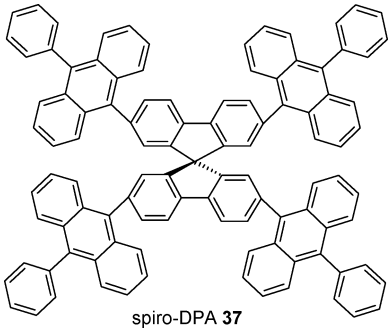

spiro-DPA **37**

The introduction of different substitutions at the 2- and 7-positions of the fluorene moieties in spirobifluorenes, for example, with electron-donating and -accepting groups, respectively, allows highly conjugated systems with red-shifted low-energy emission. The fluorescence quantum yields however, are generally not as high as in the case of oligophenyls. Additionally, solvatochromic effects can be quite large for these compounds.[107] Compounds include the series spiro-AMO-*t*-Bu **38**, spiro-AMPO-*t*-Bu **39**, spiro-AMO-CN **40**, and spiro-AMPO-CN **41**[107,113] and the series

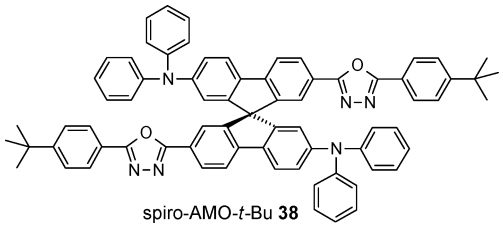

spiro-AMO-*t*-Bu **38**

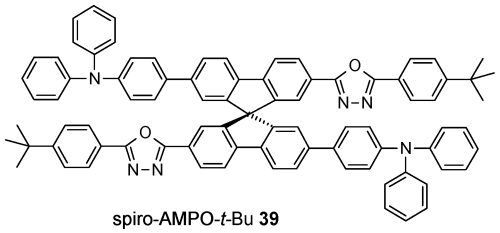

spiro-AMPO-*t*-Bu **39**

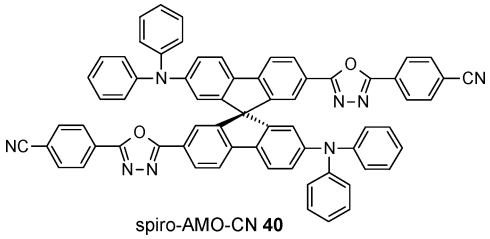

spiro-AMO-CN **40**

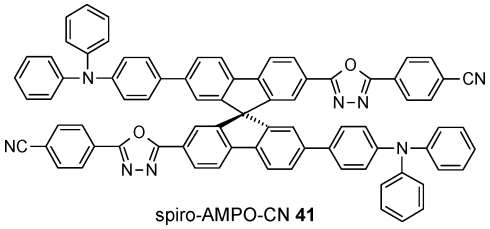

spiro-AMPO-CN **41**

DPASF **42**, DPVSF **43**, CHOSF **44**, BTSF **45**, BTCNSF **46**, and CNSF **47**.[114] Derivatives featuring oxadiazole groups as acceptor give the highest quantum yields,[107,113] and with a dicyanoethenyl substituent as acceptor, the emission can be shifted well into the red spectral range. Interestingly, no fluorescence was found for BTSF **45** in chlorobenzene.[114]

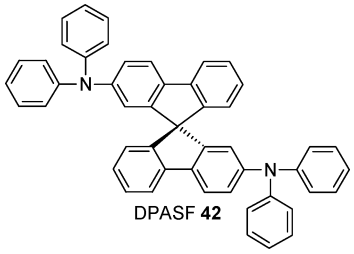
DPASF **42**

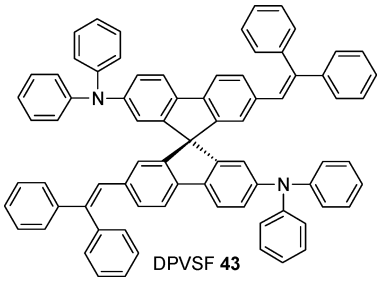
DPVSF **43**

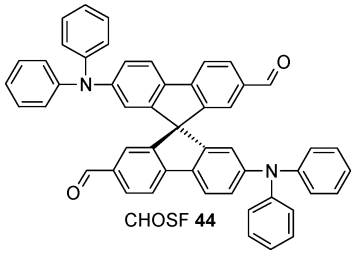
CHOSF **44**

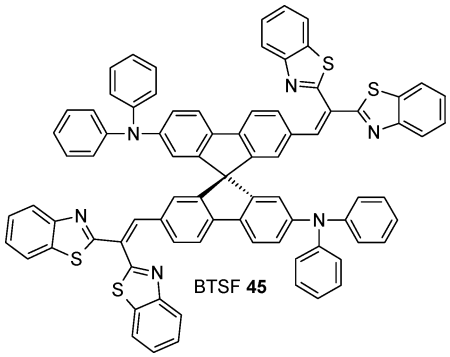
BTSF **45**

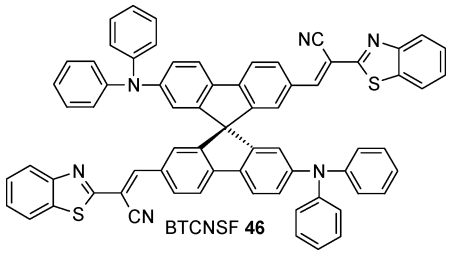
BTCNSF **46**

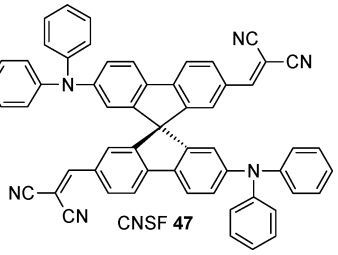
CNSF **47**

The introduction of strong donor−acceptor substitution patterns raises the question about the nonlinear optical properties. Kim et al. presented an interesting study about the influence of the perpendicular arrangement of identical chromophores on the second hyperpolarizability (γ) in 2,2′-diamino-7,7′-dinitrospirobifluorene **48**.[115] They obtained a value

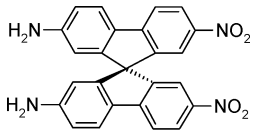
48

of 4.7 × 10^{-31} esu, ten times higher than that for a single chromophore, not four times as expected from geometric considerations, and concluded that electronic coupling effects have to be involved. Unfortunately, data on the first hyperpolarizability (β) of these spiro molecules are not reported.

Long-wavelength red fluorescence is achieved by incorporating a diarylamino electron donor and a dicyanovinyl electron acceptor.[116] Two example compounds are PhSPDCV **49** with a diphenylamino substituent as donor and pTSPDCV **50** with a di(4-tolyl)amino donor. Both compounds, pTSPDCV **50** and PhSPDCV **49**, exhibit strong solvatochromism in their fluorescence. They emit green in hexane, yellow-orange in 1,4-dioxane, and red in dichloromethane or acetonitrile. This effect can be understood by partial charge transfer between donor and acceptor moieties. The fluorescence quantum yields of these compounds measured in 1,4-dioxane range between 70% and 75%.

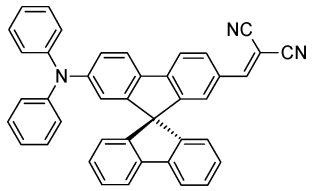
PhSPDCV **49**

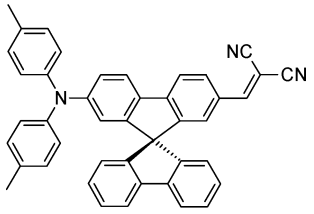
pTSPDCV **50**

2.2.5. Spirobifluorenes with Different Fluorene Units

Connecting two different chromophores by the spiro linkage (2,7-A,2′,7′-B substitution pattern, "top-down asymmetric compounds") can result in quite unexpected optical properties if there is an electronic interaction via the spiro carbon atom. A wide range of spiro compounds have been reported in which one half is unsubstituted fluorene, for example, the bipyrene dye SDPF **51**,[117] TDAF-1 **52**,[118] or the pyrimidine dye TBPSF **53**.[119] Since in most cases the orthogonally linked fluorene unit has no influence on the

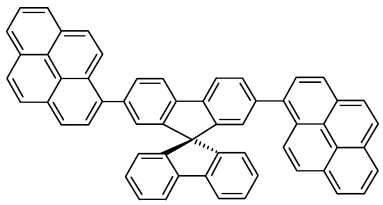
SDPF **51**

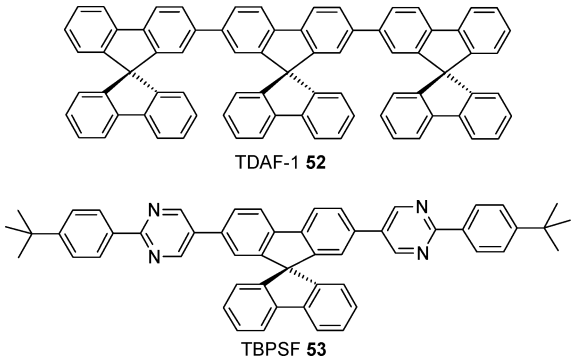

other chromophore, they behave in principle like the parent chromophores from which they are derived. Especially interesting, on the other hand, are spiro compounds consisting of electron-donating and electron-accepting halves since even in highly dilute solution photoinduced electron transfer from the donor half to the acceptor half is frequently observed. Examples are spiro compounds in which one half consists of one or two arylamines and the other of one or two oxadiazoles, that is, D1A1 **54**, D1A2 **55**, D2A1 **56** (synonym spiro-DPO **56**[107]), and D2A2 **57**.[120,121] These compounds

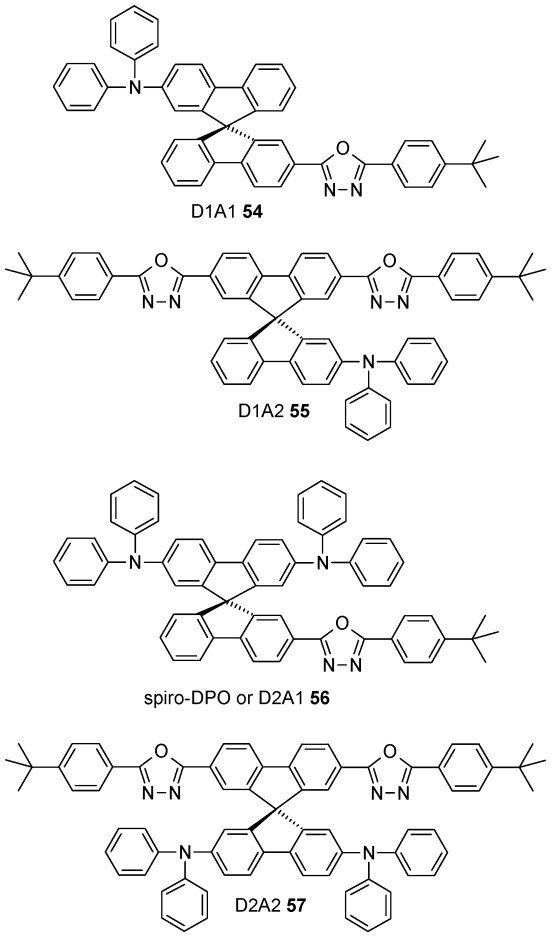

exhibit strong solvatochromic effects in emission, but not in the absorption spectra. Spiro-DPO **56**, for example, exhibits fluorescence in hexane with a maximum at 434 nm. By addition of dichloromethane, the fluorescence intensity decreases, and the maximum is shifted toward longer wavelengths. In pure dichloromethane, only a broad and weak fluorescence band, centered around 570 nm can be detected (Figure 3).[107] The strong solvent dependence of the

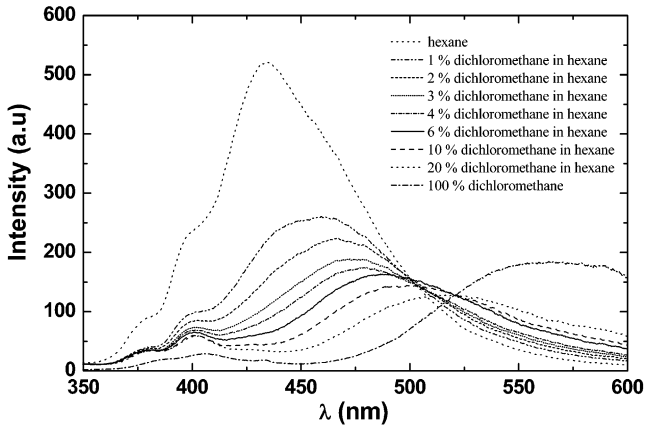

Figure 3. Fluorescence of spiro-DPO **56** with increasing solvent polarity.

emission spectra, accompanied by no significant change in absorption spectra, indicates that the two halves of the molecule have negligible interaction in the ground state but strong interaction in the vibrationally relaxed excited state.[107,121]

Wong and co-workers have investigated the photoinduced electron transfer by means of femtosecond fluorescence up-conversion spectroscopy.[121] A time constant of 430 fs was measured for the photoinduced electron transfer in D2A1 **56** (monitoring at 460 nm). Whereas for D1A1 **54** a similar time constant of 410 fs was obtained, the electron transfer in the compounds with two oxadiazole moieties as acceptors, D1A2 **55** and D2A2 **57**, is substantially faster (below 150 fs). In addition, the free energy change favoring electron transfer was also larger for the latter compounds, as calculated from electrochemical, spectroscopic, and structure parameters ($\Delta G \approx -0.6$ eV in apolar solvents).[120,121] Polar solvents stabilize the charge-separated state significantly. The change in dipole moment between ground and charge-separated excited state was calculated from the slope of the linear relationship between the frequency of the emission maximum and the solvent polarity function $\Delta f = (\epsilon - 1)/(2\epsilon + 1)$, depending on the dielectric constant of the solvent ϵ. Values as large as 30 D were obtained.[121]

A similar solvatochromic behavior with transition to an electron transfer state upon excitation can be observed if the electron-accepting moiety is replaced by an oligophenyl/oligofluorene chain (spiro-DPSP **58**, spiro-DPSP[2] **59**)[122,123]

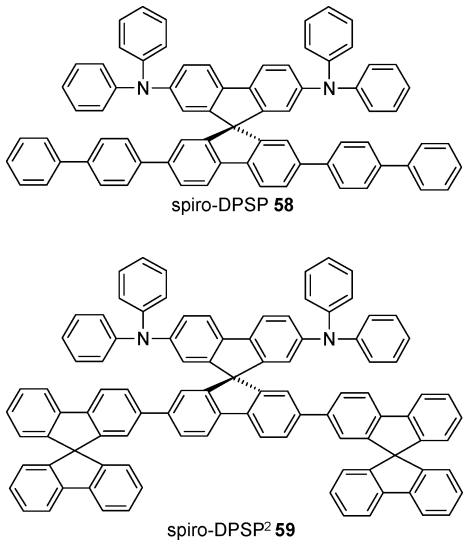

but not if the electron donor is replaced by an oligophenyl chain (spiro-SPO **60**). The emission maximum of spiro-DPSP

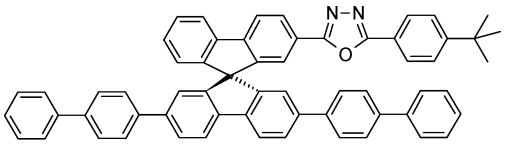

spiro-SPO **60**

58 shifts from 419 nm in hexane to 520 nm in dichloromethane solution. Thus, similarly to oxadiazoles, oligophenyls may also act as acceptors in photoinduced charge transfer. Applications of these materials in photoresponsive devices are described in a later section.

Oligophenyls with spiro-linked 3,6-substituded alkoxyfluorenes, such as **61**, **62**, and **63**, show a similar absorption

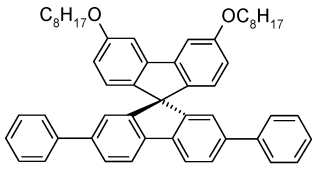

61

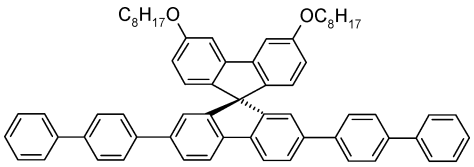

62

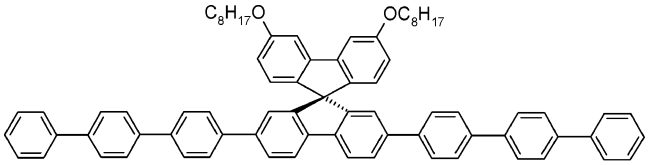

63

and emission behavior to the corresponding spiro oligophenyls (spiro-4Φ **9**, spiro-6Φ **2**, and spiro-8Φ **10)**. The photoluminescence maxima are at 365 and 382 nm for compound **61**, at 387 and 407 nm for compound **62**, and at 396 and 416 nm for compound **63**.[124] The alkoxy side chains in these compounds help to increase the solubility but lower the glass transition temperatures.

A compound has been synthesized by connecting two truxene moieties via a spirobifluorene unit (compound **64**).[125]

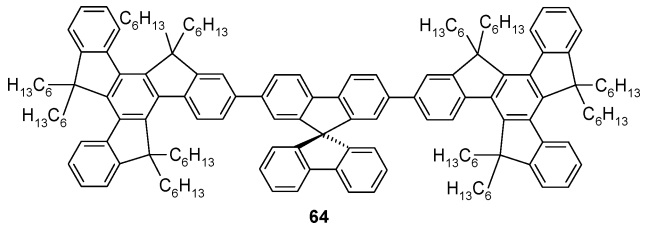

64

The absorption maximum of this compound is at 362 nm, which corresponds to a slight red shift as compared with truxene, owing to the increased conjugation length. The second absorption peak is at 309 nm, which originated from the truxene moiety. The fluorescence maximum is at 411 nm with another peak at 388 nm.

2.2.6. Other Compounds

The absorption spectrum of methyl-substituted spirobifluorene-based pyrazoloquinolines (spiro-PAQ-Me **65**) measured in ethyl acetate comprises a broad, low-energy absorption at 420 nm with two weak absorptions in the region 340−360 nm and a strong peak at 288 nm.[126] The maximum of the absorption spectrum of phenyl-substituted spirobifluorene-based pyrazoloquinolines (spiro-PAQ-Ph **66**) is

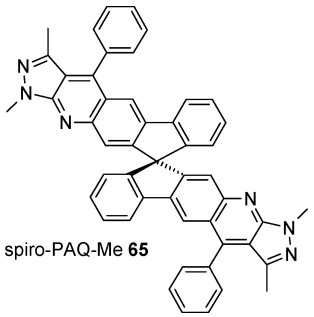

spiro-PAQ-Me **65**

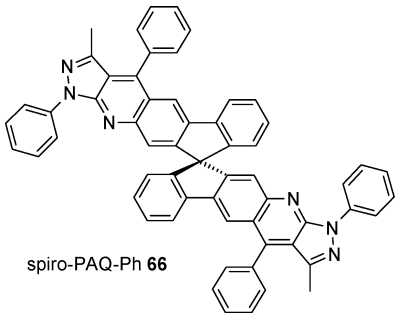

spiro-PAQ-Ph **66**

slightly red-shifted (2−6 nm). The emission spectra are at 438 and 455 nm with corresponding fluorescence quantum yields of 67% and 95% for spiro-PAQ-Me **65** and spiro-PAQ-Ph **66**, respectively.[126]

Dispirofluorene-indenofluorene compounds, a new family of double spiro compounds, have been also synthesized.[127] Three compounds of this class are **67**, **68**, and **69**. The UV−vis spectra of **67**, **68**, and **69** show absorption bands around 230, 254, 300, and 310 nm, as for spirobifluorene. The

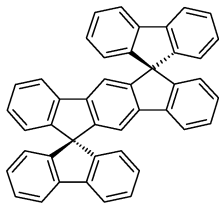

67

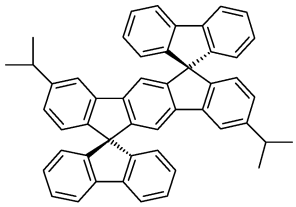

68

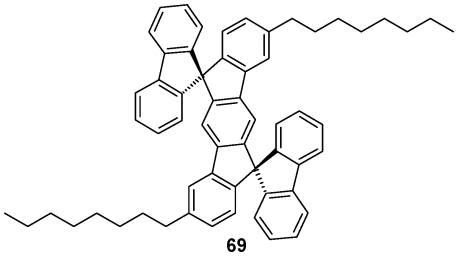

69

emission peaks of compounds **67**, **68**, and **69** measured in dichloromethane are at 367, 372, and 373 nm, respectively. Compound **67** shows a fluorescence quantum yield of 1.5% measured in dichloromethane, which is 7.5 times larger than that of spirobifluorene (0.2%).[127]

2.3. Electrochemical Properties

The electrochemical properties of spirobifluorene derivatives are of course dominated by the functional substituents in each half, but the electrostatic interaction between the two molecular halves may have a significant influence on the redox potentials. Before we start discussing several functional groups, a few words on the comparability of electrochemical data found in the literature are appropriate. Because classical (and mostly aqueous) reference electrodes are usually not defined in nonaqueous solvents, electrochemically determined redox potentials in nonaqueous solvents should be referred to a stable and nearly solvent-independent reference redox system, for example, ferrocene/ferricinium (Fc/Fc^+) or cobaltocene/cobaltoinium ($CoCp_2/CoCp_2^+$) as recommended by IUPAC for more than 20 years.[128] At least the redox potential of ferrocene/ferricinium in the used electrolyte system against the reference electrode used should be given. In this review, redox potentials are generally given against Fc/Fc^+ unless noted otherwise. Positive values are typically measured in CH_2Cl_2 and negative values in THF.

In order to derive "HOMO (highest occupied molecular orbital)" and "LUMO (lowest unoccupied molecular orbital)" values and to be able to compare the data with photoelectron spectroscopy data measured in solid films, an offset value of 4.8 eV is usually suggested. The molecular orbital energy is then given as, for example, $\epsilon(\mathrm{MO}) = -(4.8\ \mathrm{eV} + eE_{1/2})$, $E_{1/2}$ being the reversible half wave potential with respect to ferrocene.[129]

Recently, Forrest and co-workers refined the relationship between the HOMO obtained from solid-state measurements and the oxidation potential obtained from electrochemical measurements.[130] The HOMO levels of a number of organic semiconductors were determined by ultraviolet photoemission spectroscopy and compared with the relative oxidation potential (V_{cv}) measured using pulsed cyclic voltammetry, leading to the relationship $E_{HOMO} = -(1.4 \pm 0.1)(eV_{cv}) - (4.6 \pm 0.08)$ eV, consistent with theoretical predictions. Here, e is the electron charge.

Relative redox potentials in solution are assumed to reflect the relative potentials in the solid state, but of course, not all interactions with the molecular environment can be accounted for by this approximation. Often, the "band gap" energy is defined from the onset of the absorption spectra. The electrochemical pendant, that is, the energy difference between first oxidation and reduction potential, may be substantially different. This can be seen immediately in the case of the spiro compounds with two different chromophores, discussed in the previous section. If one half is easily oxidized and the second easily reduced, the resulting energy difference cannot be seen in the absorption spectra but is reflected in the position of the red-shifted charge-transfer emission band. This was, for example, nicely demonstrated by Fungo et al.[131] for the donor−acceptor compounds D1A1 **54**, D1A2 **55**, D2A1 (spiro-DPO) **56**, and D2A2 **57** by means of electrogenerated chemiluminescence. They found electrochemiluminescence spectra similar to that of the photogenerated charge-separated state, with energies correlated to the difference between oxidation and reduction potentials.

2.3.1. Arylamines

We will reverse the order of the discussion with respect to the previous sections and start with the spiro compounds featuring two different halves, since in this case the oxidation steps of the arylamine half are not significantly influenced by the spiro-linked second molecular half with significantly higher oxidation potentials.[132] For spiro-DPSP **58**, spiro-DPO (D2A1) **56**, and D2A2 **57**, the first oxidation potential is lower, whereas the second is higher, as in TAD **3** (0.29 and 0.52 V vs Fc/Fc^+ in CH_2Cl_2). These differences can be attributed to the planarization by the spiro linkage. In the case of spiro-DPO (D2A1) **51**, we measured values of 0.21 and 0.54 V[133] (Figure 4), whereas Wong et al. reported lower

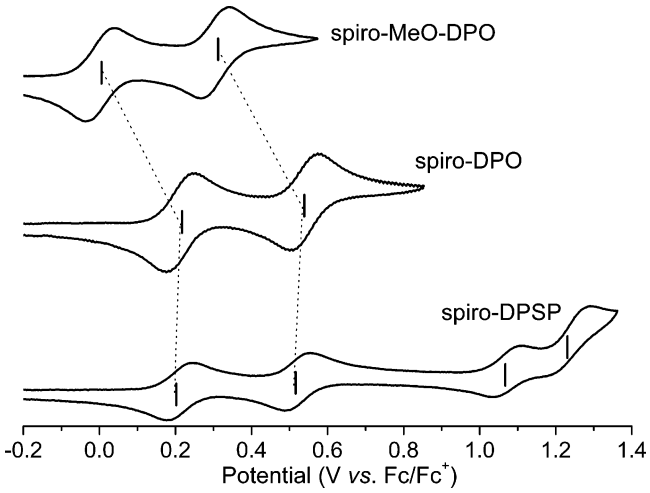

Figure 4. Oxidation of spiro-DPSP **58**, spiro-DPO **56**, and spiro-MeO-DPO **72** containing arylamine moieties. The measurement was carried out in dichloromethane containing 0.1 M TBAHFP as supporting electrolyte: working electrode, platinum disc electrode; counter electrode, glassy carbon electrode; reference electrode, Ag/AgCl pseudo-reference electrode. The scan rate for all measurements was 50 mV/s performed at room temperature under nitrogen. The vertical bars indicate the half-wave potentials.

values under similar conditions.[121] The origin of this mismatch is not clear; however, the positions of the potentials given above are reasonable in comparison with spiro-DPSP **58** (0.20 V, 0.52 V),[133] D2A2 **57** (0.23 V, 0.55 V),[121] and measurements of D2A1 **56** in benzene/acetonitrile (0.28 V, 0.46 V).[131]

If the second half of the spiro molecule is identically electroactive (e.g., in spiro-TAD **4**), the first oxidation steps of the two halves split: The first charge is transferred at a low potential (0.20 V) and the second one, which has to overcome Coulombic repulsion, at 0.44 V. The first two electron-transfer steps are followed by a formal two-electron-transfer step to the tetracation at 0.65 V (all values vs Fc/Fc^+ in CH_2Cl_2).

The first oxidation potential is barely reduced by replacing the phenyl substituents by naphthyl (spiro-α-NPB **15**, 0.20 V), but it is substantially lowered if the terminal phenyl groups have methoxy or methyl substituents at the *para* position (spiro-MeO-TAD **73** 0.11 V, spiro-TTB **74** 0.08 V).[91] The cyclic voltammogramms for some compounds are

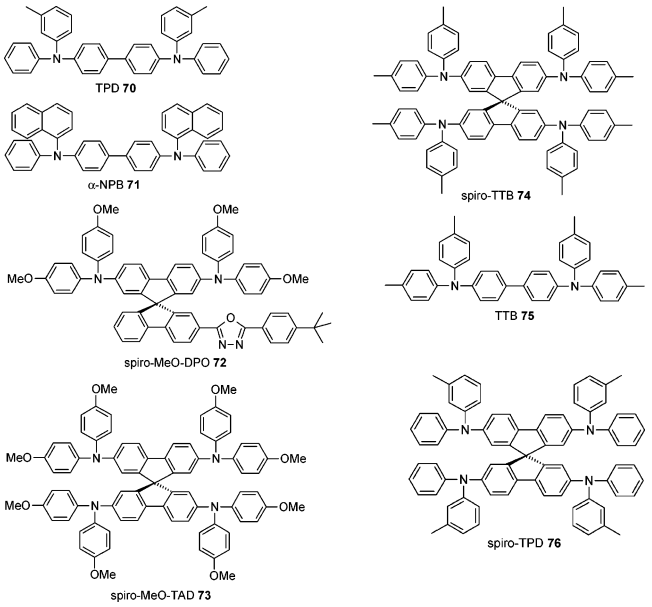

shown in Figure 5, together with the corresponding data for the parent compounds.

2.3.2. Oxadiazoles and Other Heterocyles

In contrast to arylamines, oxadiazoles are interesting for their electron-accepting properties. If only one *tert*-butylphenyl-oxadiazole substituent is attached to the spirobifluorene core in the 2-position (A1 **77**), the first reduction potential lies at −2.56 V (vs Fc/Fc^+, in THF). If a second

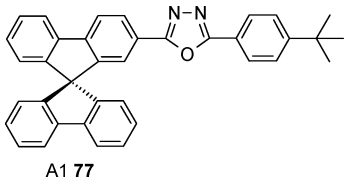

oxadiazole is applied at the same side in the 7-position of the spirobifluorene (A2 **78**), the value shifts to about −2.29

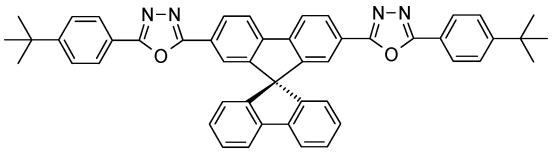

V, whereas the second reduction can be found at −2.61 V.[121] If the substituents are applied at different sides (2,2′-positions, spiro-PBD **28**), the first electron transfer is a merged wave for a formal two-electron transfer taking place at −2.46 V (in THF).[88] This corresponds to the reversible uptake of two electrons resulting in a stable bis(radical anion) as proved by spectroelectrochemistry measurements and differs only by 20 mV from the first reduction potential of its corresponding compound, 2-(4-biphenyl)-5-(4-*tert*-butylphenyl)-1,3,4-oxadiazole (PBD), under the same condition.[88] If the second half of the molecule is an arylamine, the reduction potential of the oxadiazole does not shift much (spiro-DPO **56**, spiro-MeO-DPO **72**, Figure 6). The reduction potentials of spiro-DPSP **58**, which does not contain an oxadiazole

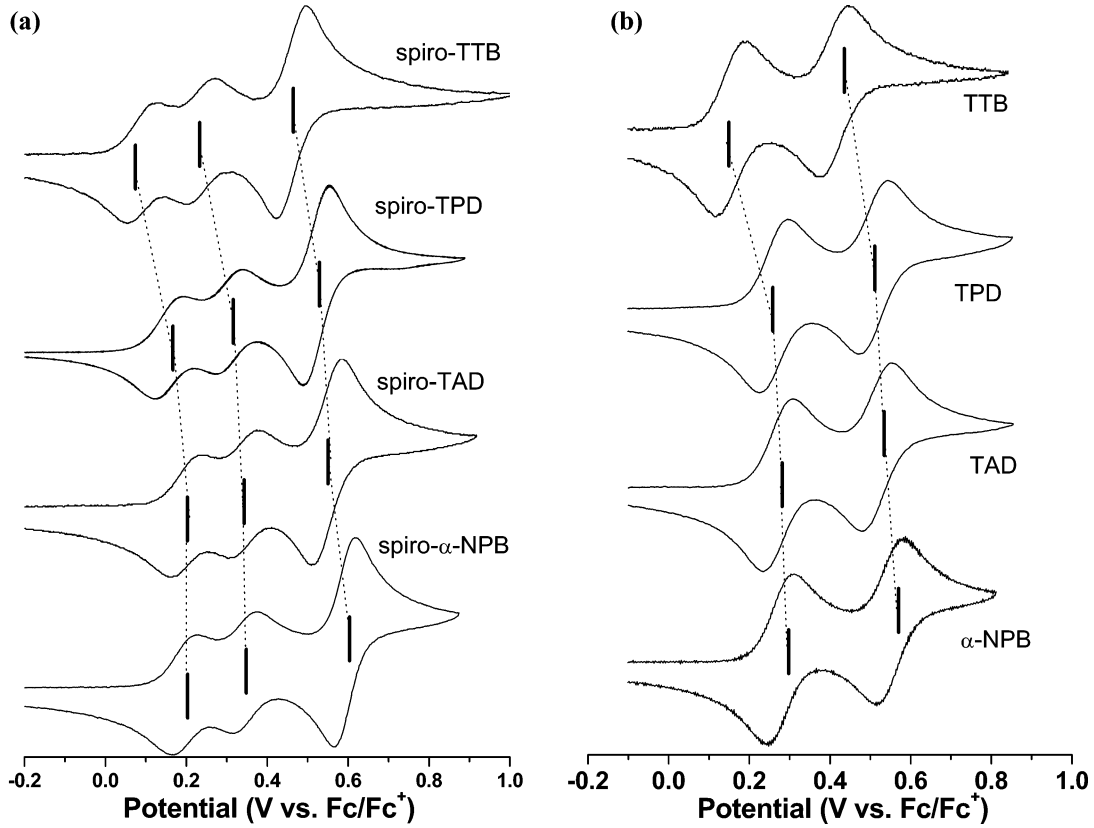

Figure 5. Cyclic voltammogram of (a) spiro-TAD **4**, spiro-TPD **76**, spiro-TTB **74**, and spiro-α-NPB **15** and (b) the parent compounds TAD **3**, TPD **70**, TTB **75**, and α-NPB **71**. The measurements were carried out in dichloromethane containing 0.1 M TBAHFP as supporting electrolyte: working electrode, platinum disc electrode; counter electrode, glassy carbon electrode; reference electrode, Ag/AgCl pseudo-reference electrode. The scan rate for all measurements was 50 mV/s performed at room temperature under nitrogen. The vertical bars indicate the values of half-wave potentials.

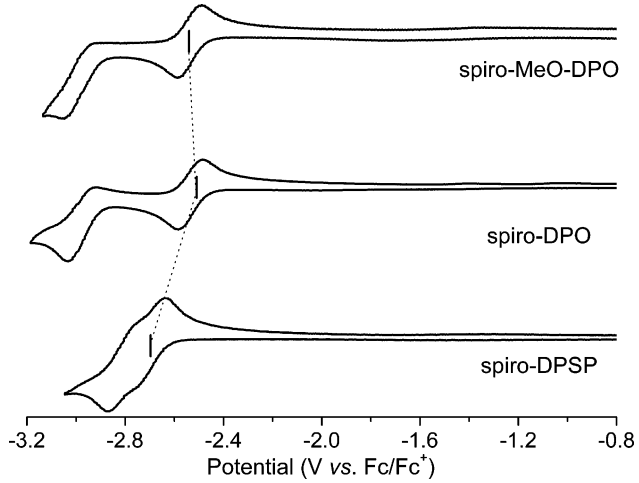

Figure 6. Reduction of spiro-DPSP **58**, spiro-DPO **56**, and spiro-MeO-DPO **72** containing oligophenyl or oxadiazole moieties. The measurement was carried out in THF containing 0.1 M TBAHFP as supporting electrolyte: working electrode, platinum disc electrode; counter electrode, glassy carbon electrode; reference electrode, Ag/AgCl pseudo-reference electrode. The scan rate for all measurements was 50 mV/s performed at room temperature under nitrogen. The vertical bars indicate the half-wave potentials.

moiety, are included in the figure in order to compare the reduction of the sexiphenyl chain with those of the oxadiazole moiety.

The electrochemical behavior of the pyrazoloquinolines spiro-PAQ-Me **65** and spiro-PAQ-Ph **66** was reported by Chen et al.[126] Spiro-PAQ-Me **65** and spiro-PAQ-Ph **66** exhibit reversible reductions with onset potentials vs Fc/Fc^+ in THF solution at −2.09 and −2.00 V, respectively. During the anodic sweep measured in dichloromethane, they undergo quasi-reversible oxidation processes with onset potentials at 0.87 V for spiro-PAQ-Me **65** and 0.86 V for spiro-PAQ-Ph **66**.

2.3.3. Oligophenyls and Oligofluorenes

The experiments on photoinduced charge transfer described above show that oligophenyls may act as electron acceptors. Indeed, reversible reduction and also oxidation steps can be detected for compounds of appropriate conjugation lengths. For a terfluorene containing three spirobifluorene units in a chain, both oxidation and reduction potentials were reported by Wong et al.[134] Two oxidation steps were detected at 1.32 and 1.56 V vs Ag/AgCl (CH_2Cl_2, 0.1 M n-Bu_4NPF_6), and two reduction steps at −2.01 and −2.21 V vs Ag/AgCl (THF, 0.1 M n-Bu_4NClO_4). Electrochemiluminescence was demonstrated for this compound.[118] For the compound spiro-DPSP **58**, containing biphenyl substituents instead of fluorene units at the spirobifluorene core, we measured first and second reduction potentials of −2.69 and −2.81 V vs Fc/Fc^+ in THF, respectively.[133]

For spiro oligophenyls with two identical chromophores, the question arises whether the doubly charged species have their charges on the same branch or on different branches. Crispin et al.[135] performed doping experiments with Li and Na in solid films and concluded that if spiro-4Φ **9** or spiro-6Φ **2** is doped with Li, dianions (bipolarons) are formed on the same spiro branch, whereas doping with Na leads to the formation of radical anions (polarons) on each branch.

The bisanthracene compound spiro-FPA **36** shows bipolar character, with a first oxidation potential at 0.76 V vs Fc/Fc^+ in CH_2Cl_2 and a reversible reduction at −2.42 V vs Fc/Fc^+ in THF.[111] The first oxidation and reduction potential of spiro-DPA **37** occur at 0.8 V (vs Fc/Fc^+, CH_2Cl_2) and −2.44 V (vs Fc/Fc^+, THF).[112]

2.3.4. Oligothiophenes

Most oligothiophene-functionalized spirobifluorenes exhibit reversible oxidation waves but show poor reversibility in reduction.[136,137] As is the case with arylamines, these materials have a higher effective conjugation length if bridged via a spiro atom with respect to the non-spiro linked compounds. This is manifested in smaller energy gaps and lower oxidation potentials. For a spiro compound containing a cyclohexyl-capped quaterthiophene chain (**79**), 0.18 V vs

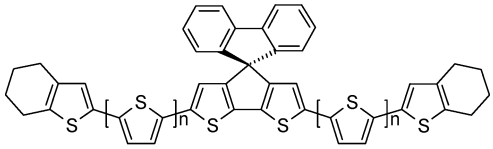

Fc/Fc^+ for the first oxidation and 0.57 V for the second oxidation were measured.[136] For the higher homologue with six thiophene rings in the chain (**80**), the values are 0.16 and 0.37 V, respectively. A third, quasi-reversible oxidation step was detected at 1.09 V. Reduction takes places at −2.58 and −2.78 V (irreversible) for **79** and at −2.32 and −2.43 V for **80**. Since the materials can also be reduced electrochemically, electrogenerated chemiluminescence is observable.[136]

For compounds based on the spirobifluorene core symmetrically functionalized with four mono- (**81**), bi- (**82**), and terthiophene (**83**) units, onset oxidation potentials of 1.20,

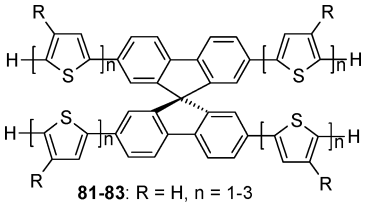

0.86, and 0.65 V vs SCE and sufficient stability of the radical cations were reported.[137] For the compounds **84**, **85**, and **86**, in which the thiophenes are substituted with alkyl chains in the 3-position, the onset potentials shift to 0.99, 0.88, and 0.85 V vs SCE, respectively. Electrochemical measurements have shown that radical cations of oligothiophene-functionalized 9,9′-spirobifluorene derivatives are more stable than those of non-spiro oligothiophenes. The oxidative peak potential shifts cathodically as the number of thiophene units increases due to a higher degree of π-delocalization. Simultaneously, the band gap energy can be varied between 2.18 and 2.98 eV.[137]

2.3.5. Other Compounds

The cyclic voltammograms of asymmetric spirosilabifluorene measured in CH_3CN/THF (9:1 v/v) show a single reduction and a single oxidation process.[109] Both processes are irreversible. Irreversible reduction may be due to extremely short lifetime of the corresponding radical anion. The onset potentials of oxidation and reduction for **33** were determined to be 1.11 and −2.42 V, respectively (vs Ag/AgCl), corresponding to 1.01 and −2.52 V (vs Fc/Fc^+).

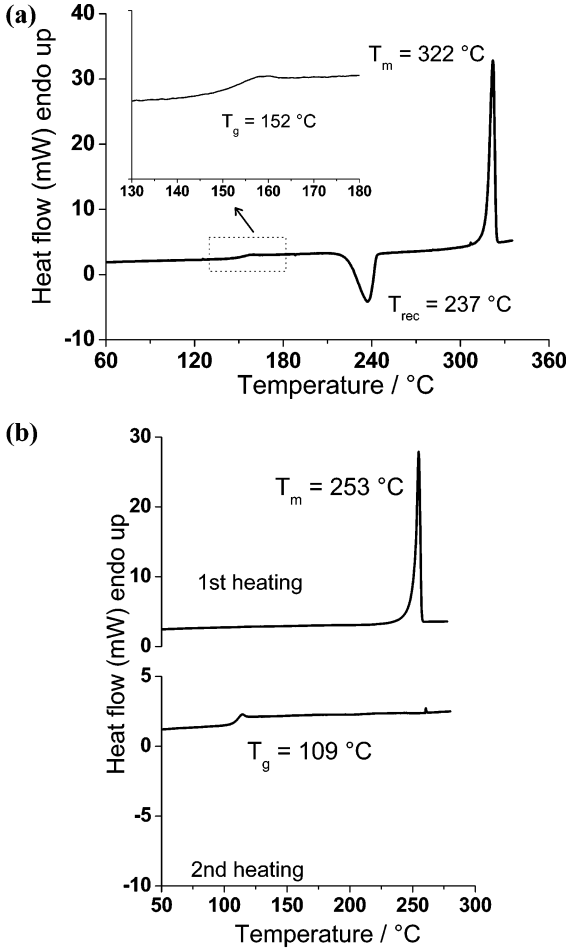

Figure 7. Differential scanning calorimetric curves for the molecular glasses (a) compound **90** (second heating curve) and (b) spiro-terphenyl **26** (first and second heating curve). The T_g is indicated by a characteristic step and the melting point by an endothermic peak. In panel a, recrystallization occurs above T_g, which manifests itself as an exothermic peak. The material in panel b forms a stable amorphous glass. The melting point from the first heating curve of a crystalline sample disappears in the second heating cycle. Only the glass transition is visible. All measurements were carried out under N_2 purging (20 mL/min) and at a rate of 10 K/min.

Thus the HOMO and LUMO levels for **33** are estimated to be −5.81 and −2.28 eV, respectively.

The cyclic voltammetry of dispirofluorene−indenofluorene compounds has been also measured. Compounds **67**, **68**, and **69** have the first and the second oxidation potentials at 1.03 and 1.47 V (irreversible), 0.96 and 1.48 V (irreversible), and 1.04 and 1.58 V (irreversible), respectively.[127] The measurement was carried out in acetonitrile, using ferrocene as an internal standard.

3. Solid-State Properties

3.1. Thermal Properties

As stated in the introduction, spiro compounds are generally characterized by a high glass transition temperature T_g due to their bulky shape. The crystallization kinetics above T_g can vary substantially, depending on the substitution pattern and is independent of the value of T_g. This means that in the typical time scale of a calorimetric experiment, recrystallization can be observed for some spiro compounds, whereas other compounds do not crystallize.[70] Figure 7a,b shows a typical calorimetric experiment for both cases. In

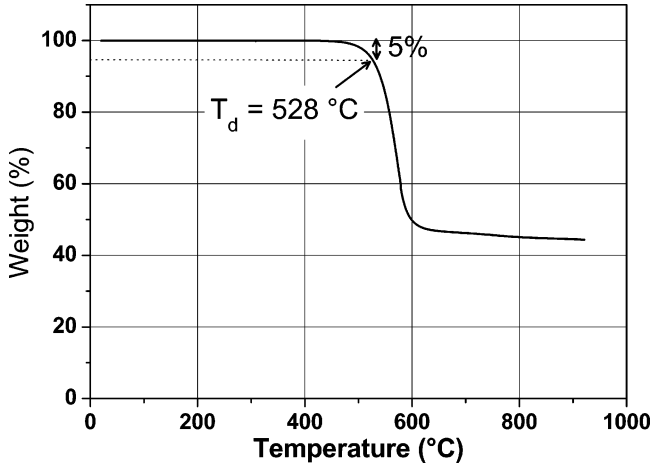

Figure 8. Thermogravimetric curve of spiro-α-NPB **15** measured at rate of 5 K/min under N_2 purging (200 mL/min).

Figure 8, a thermogravimetric curve for spiro-α-NPB **15** is displayed as example for the high thermal stability. The decomposition temperature, T_d, is defined as the temperature at which a 5% weight loss occurs during heating. For spiro-α-NPB **15**, this is the case at 528 °C.

In the series of the spiro oligophenyls, the T_g increases with increasing chain length in the order 184 °C (spiro-4Φ **9**), 212 °C (spiro-6Φ **2**), and 243 °C (spiro-8Φ **10**).[77,87,88,138] The melting point (T_m) also increases with lengthening of the molecules with additional phenyl rings. Further branching leads to even higher T_g's: Both spiro-octo-2 **24** and 4-spiro[2] **5** exceed the T_g of spiro-6Φ **2**, at 236 and 273 °C, respectively.[77,89,91,138] In contrast, the methoxy-substituted spiro-6Φ, spiro-6Φ(MeO)$_4$ **13**, has a reduced T_g of 191 °C with a melting point of 326 °C.[89] The T_g's of 4-Ph-spiro[2] **87**, 6-spiro[2] **88**, and 4-spiro[3] **12** are as high as 285, 258, and

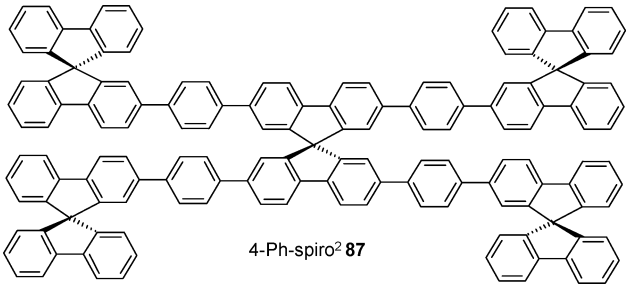

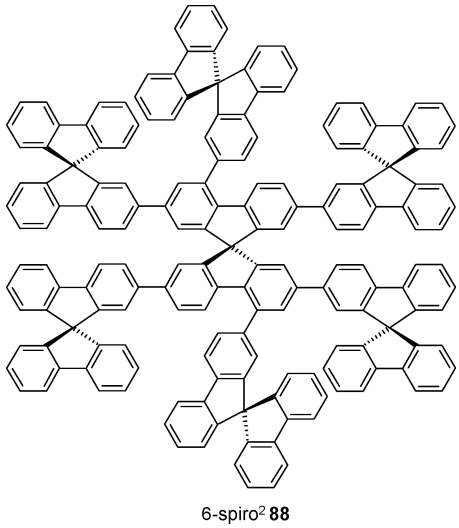

330 °C.[91,138] The calorimetric T_g of spiro-terphenyl **26** was measured at 109 °C and the melting point at 251 °C. No recrystallization was detected in the calorimetric scan after vitrification.[104] Among spiro compounds, the T_g of 4-spiro^3 **12** is the highest T_g, while 4-spiro^2 **5** shows the highest decomposition temperature at 620 °C.

Spiro oligophenyls containing alkoxy side chains, such as compound **62**, show very low T_g's (T_g = 70 °C).[124] Therefore, the introduction of alkoxy side chains in spiro oligophenyls serves only to improve the solubility of the compound at the cost of a significant reduction of the T_g with respect to spiro-6Φ **2**. The decomposition temperature is still high enough for applications (388 °C).

Spiro-linked oligofluorenes carrying *n*-octyl groups show significantly lower T_g's than those with *n*-propyl groups.[96] The strong interaction between *n*-octyl pendants seems to dominate over the effect of molecular weight, because both *n*-octyl-substituted spiro-terfluorene and spiro-pentafluorene exhibit $T_g \approx 60$ °C. Spiro-terfluorenes with both *n*-propyl and *n*-octyl pendants were found to crystallize upon heating beyond T_g.

An effective approach to high T_g terfluorenes has been successfully implemented in which all the fluorene units are spiro-configured to prevent interchromophoric interaction without disrupting π-conjugation.[139] Among these compounds, the highest T_g of 296 °C was obtained with dendritic pendants to a spiro-linked fluorene trimer (**89**), which was

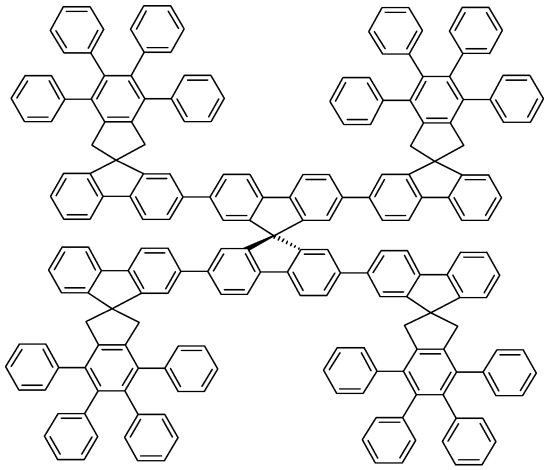

89

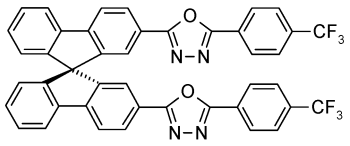

90

proven to stay amorphous even upon prolonged heating by means of polarizing optical microscopy and electron diffraction.

Arylamines such as TPD **70** and α-NPB **71** have found widespread application as hole transporter in OLEDs. However, the values of T_g of the corresponding compounds are not high enough to prevent thin films of the material from recrystallizing. The T_g's of the parent compound arylamines such as TAD **3**, TPD **70**, TTB **75**, and α-NPB **71** are 70, 62, 66, and 95 °C.[132] In contrast, the T_g's of their corresponding spiro compounds are 133, 115, 146, and 147 °C for spiro-TAD **4**, spiro-TPD **76**, spiro-TTB **74**, and spiro-α-NPB **15**, respectively.[77,87−89,132,138] Spiro-Carb **18** exhibits an even higher T_g (240 °C) and a remarkably high temperature stability (T_d = 570 °C) for an aromatic amine.

Usually the top-down asymmetric spiro compounds such as spiro-DPSP **58**, spiro-SPO **60**, spiro-DPO **56**, and spiro-MeO−DPO **72** exhibit T_g values between those of the corresponding symmetric spiro compounds.[107] Spiro-DPSP **58**, for instance, shows a T_g of 152 °C, which lies between the T_g's of spiro-6Φ **2** and spiro-TAD **4**. This also holds for spiro-DPO **56** and spiro-SPO **60**.

Calorimetric measurements for the left-right asymmetric spiro compounds, spiro-AMO-*t*-Bu **38**, spiro-AMPO-*t*-Bu **39**, spiro-AMO-CN **40**, spiro-AMPO-CN **41** and spiro-CN-PBD **29** gave high T_g's ranging from 165 to 212 °C.[107] These values are even higher than those obtained for the symmetric spiro compounds, spiro-TAD **4** and spiro-PBD **28**. This indicates that the spiro junction has a positive influence on the stability of the amorphous state of donor/acceptor-substituted spiro compounds. Note that no recrystallization was observed in the case of *tert*-butyl-substituted compounds, while the cyano-substituted compounds showed both recrystallization and melting signals in the time scale of the experiment. Obviously, the bulky *tert*-butyl groups reduce the kinetics of crystallization compared with the cyano group.[113]

Spiro compounds containing heterocyclic units, such as head-to-tail, regioregular oligothiophene-functionalized 9,9′-spirobifluorene, are interesting as charge-transporting materials in organic electronics.[137] It is well-known that unsubstituted α-oligothiophenes tend to crystallize. In contrast, oligothiophene-functionalized 9,9′-spirobifluorene derivatives without substituents were found to easily form amorphous glasses at ambient temperature. Compound **91** has the

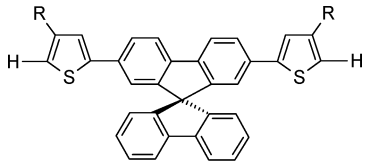

91 : R = *n*-C_6H_{13}

maximum T_g among these compounds at 205 °C.[137] Most of the compounds reported exhibit a stable amorphous glass in the solid state, as proven by thermal analysis. Increasing the number of thiophene units leads to improved thermal stability of these compounds.

Asymmetric spirosilabifluorenes show high T_g's between 203 and 228 °C, which similarly to the spiro carbon analogues can be attributed to the rigidity of the molecules.[109]

3.2. Thin Film Preparation and Optical Properties

Thin films of spiro compounds may be fabricated by means of thermal evaporation or by solution-based processes, such as spin coating. The spiro oligophenyls of lower to medium molecular weight can usually be thermally evaporated as well as spin-coated from various solvents, such as chloroform, chlorobenzene, toluene, or dichloromethane. In the former case, the molecular weight becomes the limiting factor; while for spin-coating decreasing solubility starts to limit the achievable film thickness. From chloroform solution, film thicknesses up to ~140 nm can be obtained for spiro-6Φ **2** using standard spin-coating techniques. The optical properties of spin-coated and evaporated films of the spiro compounds discussed herein are usually quite similar, and in some cases, such as the branched spiro-oligophenyl

spiro-octo-1 **23**, the optical constants, as obtained by variable angle spectroscopic ellipsometry (VASE), are hardly distinguishable, as shown in Figure 9.

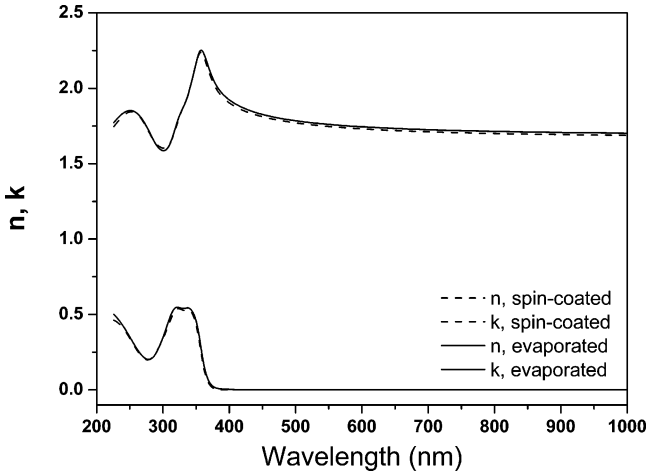

Figure 9. Optical constants dispersion of evaporated and spin-coated thin films of spiro-octo-1 **23** modeled with four Tauc−Lorentz oscillators.[140,141]

Table 1. Optical Data of Some Spiro Compounds Prepared by Vacuum Thermal Evaporation[89]

	α (10^{-2} nm^{-1})	
material	at 337 nm	at λ_{max}
spiro-TAD **4**	1.10	1.88
spiro-6Φ(MeO)$_4$ **13**	3.08	3.32
spiro-Carb **18**	1.90	2.30
spiro-DPVBi **19**	0.76	0.86
spiro-octo-2 **24**	1.45	1.56
spiro-PBD **28**	1.88	1.94
spiro-AMO-*t*-Bu **38**	0.90	1.70
spiro-AMPO-*t*-Bu **39**	1.09	1.36
spiro-SPO **60**	3.03	3.03

Table 1 shows the optical data of some spiro compound thin films prepared by vacuum thermal evaporation. The attenuation coefficient α is given for the pump wavelength of 337 nm and at the absorption maximum. Spectral data for absorption and emission can be found in Table 8 (section 6).

A crucial issue is the optical anisotropy of the resulting films,[142,143] which influences the optical and electrical properties of related devices such as OLEDs, for instance, quantum efficiency or charge transport. Anisotropic properties in vacuum-deposited spiro compounds were reported by Lin et al.[144] It was shown that both the real and imaginary parts of the refractive indices exhibit a significant uniaxial anisotropy with the optical axis being oriented along the surface normal. The in-plane extinction coefficient is substantially larger than the out-plane extinction coefficient.

In thin films, the shape of the absorption spectrum of 4-spiro^2 **5**, for example, remains identical to that measured in solution, showing the same vibronic splitting and only a slight red shift of the peak maxima of about 10 nm. These results indicate that the intermolecular interaction and aggregation of individual molecules in neat amorphous films of 4-spiro^2 **5** are effectively hindered by their sterically demanding structure. Accordingly, they behave like isolated molecules in highly dilute solution.[145] The fluorescence quantum yield of 4-spiro^2 **5** is 70% ± 10%, which is higher than that for spiro-6Φ. It is worth to mention that the quantum yield of spiro-6Φ **2** in the solid state increases from 38% to 58% from the amorphous to the fully crystalline state.[77,138]

The fluorescence lifetimes of the spiro compounds measured in thin films are 450−800 ps for spiro-4Φ **9**, 390−470 ps for spiro-6Φ **2**, and 380−450 ps for 4-spiro^2 **5**.

The second generation spiro-oligophenyl derivative spiro-octo-2 **24** has a solid-state photoluminescence quantum efficiency of 48%.[77] Even after thermal annealing, it has shown neither a decrease in the fluorescence intensity nor any detectable excimer emission. Even after the compound is melted at temperatures over 300 °C, the glassy solid still shows the same emission characteristics.

A very important characteristic, which holds for all spirobifluorene compounds discussed in this section, is that they do not exhibit a long wavelength emission beyond 500 nm, which is usually found in poly(fluorene)s after annealing and is attributed to chain defects by partial oxidation to fluorenone units.

The photoluminescence spectrum of the polar compound spiro-AMO-*t*-Bu **38** in thin films coincides with the spectrum measured in dilute solution.[107,113] It does not depend on the method used to fabricate the thin films (either through spin-coating or vapor deposition methods). The position of the emission peak, however, may differ by approximately 5 nm. The formation of excimers in the solid state can thus be excluded, because no additional bands at longer wavelength can be detected. Similar results were obtained for the cyano compound spiro-AMO-CN **40**. Again, these results confirm the effectiveness of the spiro concept to prevent intermolecular interaction and to stabilize the emission properties of the dyes in the solid state.

3.3. Surface Morphology

In this section, the surface morphology of vacuum-deposited thin films of spiro compounds grown on different substrates measured by tapping-mode atomic force microscopy (AFM) and optical microscopy is presented and compared with the surface morphology of the corresponding parent compounds. Time-dependent measurements are discussed as well.

Figure 10 shows the surface morphology change of spiro-TAD **4** thin films grown on a SiO_2/Si substrate. In Figure 10a, we see a very flat surface having a mean roughness of 1.56 nm. The peak-to-valley height is ∼9.8 nm. After spiro-TAD **4** thin films were stored for 5 weeks in ambient atmosphere and at room temperature (RT), the surface images of thin films were measured again, and the result is shown in Figure 10b. The as-deposited film underwent only negligible change; the mean roughness level slightly changed from 1.56 to 1.89 nm for films grown on SiO_2 substrates. The peak-to-valley heights of films after the samples have been stored for 5 weeks were 12.1 nm. Time dependent measurements of the surface morphology also showed that the films of spiro-TAD **4** did not change significantly after the samples were exposed to ambient atmosphere at RT for 5 weeks. The roughness values and average peak-to-valley heights did not change significantly either.

Figure 11a,b shows larger areas of spiro-TAD **4** thin films, after the samples have been stored for 9 months at RT in ambient atmosphere. The surfaces of spiro-TAD **4** thin films grown on SiO_2 substrate and *p*-Si substrate remained flat and smooth. In contrast, the films of TAD **3**, the corresponding parent compound of spiro-TAD **4**, underwent a distinctive

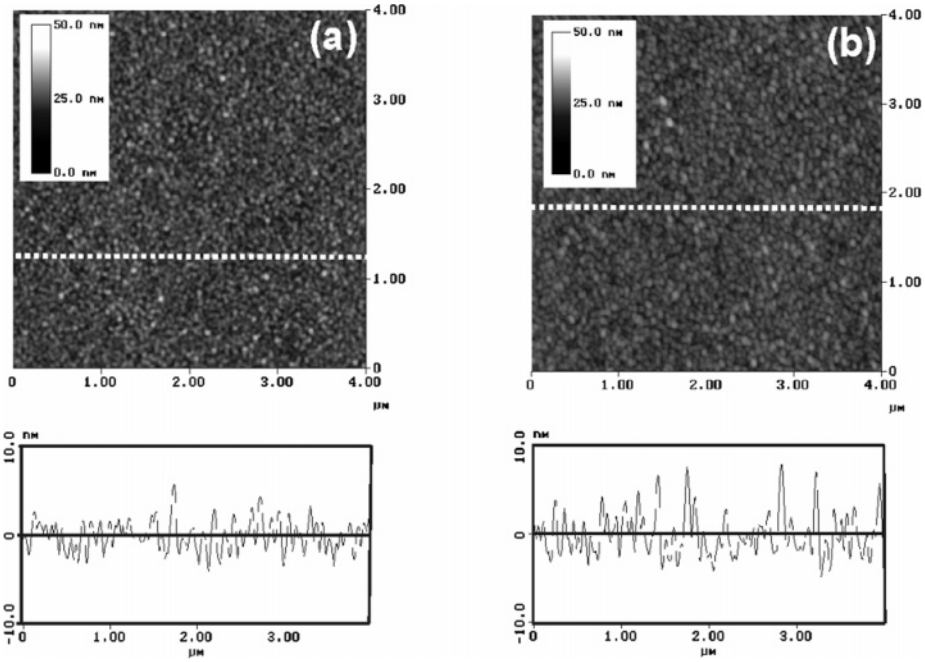

Figure 10. AFM topographical images of a spiro-TAD **4** thin film on a SiO_2/*p*-Si substrate ($4 \times 4\ \mu m^2$): (a) as deposited film in which the mean roughness, R_a, was 1.56 nm and the root-mean square roughness, R_q, was 1.96 nm; (b) sample after storage in ambient atmosphere at RT for 5 weeks in which the mean roughness, R_a, was 1.89 nm and the root-mean square roughness, R_q, was 2.41 nm.

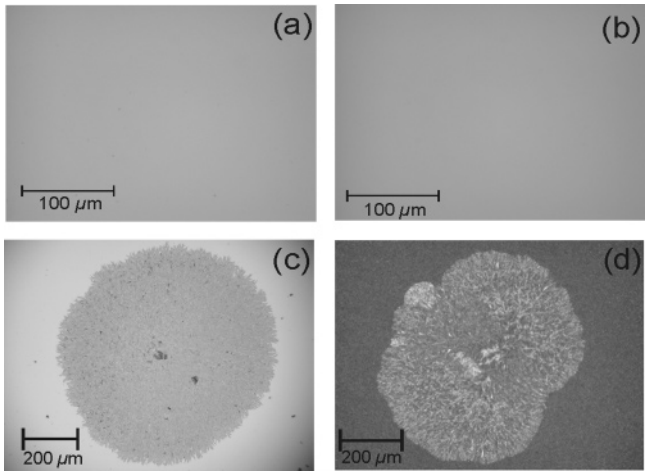

Figure 11. Optical microscopy images of spiro-TAD **4** thin films after the samples were stored in ambient atmosphere and at RT for 9 months. Spiro-TAD **4** thin films were grown on (a) SiO_2 substrate and (b) *p*-Si substrate. The optical microscopy images of TAD **3** thin films after the samples were stored in ambient atmosphere and at RT for 3 days. TAD **3** thin films were grown on (c) *p*-Si substrate and (d) SiO_2 substrate.

change in morphology, as shown in Figure 11c,d. The images were obtained after the samples were left in an ambient atmosphere at RT for 3 days. The films grown on *p*-Si substrate and SiO_2 substrate showed spherulite-type crystals and large voids. Crystalline domains with a radius between 500 and 900 μm were observed. The resulting crystals of TAD **3** films indicate that the films are not morphologically stable in ambient atmosphere and at RT. The optical microscopy data was supported by the data obtained from AFM measurements.[146]

The surface morphologies of as-deposited TAD **3**, TPD **70**, TTB **75**, α-NPB **71**, spiro-TAD **4**, spiro-TPD **76**, spiro-TTB **74**, and spiro-α-NPB **15** thin films grown on HMDS-treated SiO_2/*p*-Si have been studied.[132,146] The thin films of as-deposited parent compounds exhibited crystalline structures with different morphologies and large voids, which is not the case for the corresponding spiro compound films. No crystallization has been observed after up to 9 months.[146,147]

3.4. Patterning on a Mesoscopic Scale

There are also several approaches described in the literature aiming at controlling the morphology of thin films of spiro compounds on a micrometer scale. The first one is the application of azo substituents in order to write polarization gratings with large film thickness modulations. Surface corrugation gratings with a modulation depth of 320 nm were reported for 440 nm thick films of the compound spiro-ADA **92**.[148] The mechanism of this process, which was detected

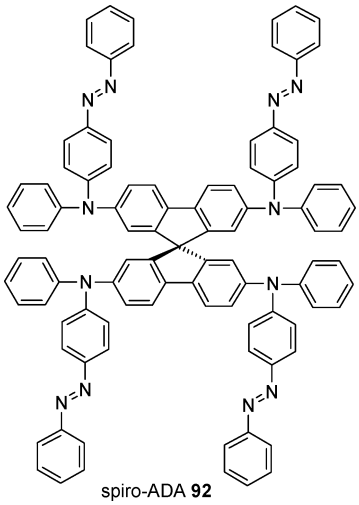

spiro-ADA **92**

for azo polymers in 1995[149,150] and later also applied for low molecular glasses,[151] is based on orientation redistributions of the azo chromophores. Due to photoselective isomerization cycles, the molecules tend to orient perpendicular to the laser polarization. Stress gradients then lead to mass transport and surface deformation. Since in spiro-ADA **92** four azo groups

are connected and therefore correlated in their orientation when irradiated with polarized light, one should expect a different degree of order when compared with molecules exhibiting only one,[152] two,[151] or three[153] chromophores. Data for comparison are lacking, though.

Another possibility to achieve surface patterns is a controlled relaxation of the intrinsic mechanical stress that occurs in evaporated or spin-coated multilayer structures. When this stress is allowed to relax by heating to the T_g of a layer covered by a solid deformable cladding, self-organized surface corrugations of defined spatial periodicities evolve. In films of spiro compounds, this effect was demonstrated, for example, for spiro-TAD **4** capped by silicon nitride,[154] spiro-6Φ **2** capped by silicon nitride,[155] and spiro-TAD **4** capped by spiro-6Φ **2** (Figure 12).[156]

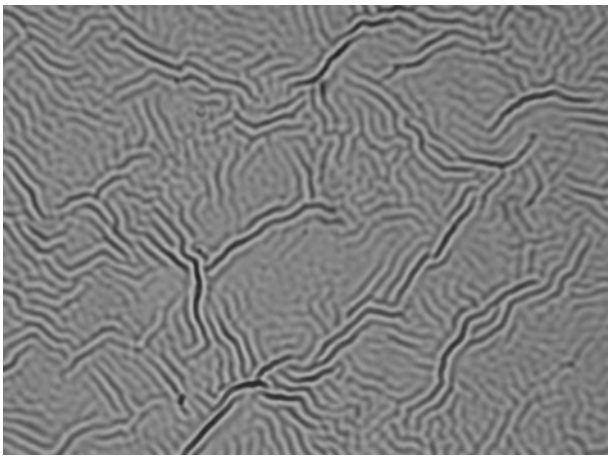

Figure 12. Periodic pattern formation in the system substrate/spiro-TAD **4**/spiro-6Φ **2**. The periodicity of the surface corrugation is 2 μm.

3.5. Waveguide Properties and Stimulated Emission

The suitability of thin films of spiro compounds for lasing can be evaluated either by pump and probe experiments to test for stimulated emission and quantification of the gain profile or with considerably lower demand on the equipment in so-called amplified spontaneous emission (ASE) experiments. Typically the films are a few hundreds of nanometers thick and form a slab waveguide on a low refractive index substrate. When the film is optically pumped, spontaneously emitted photons travel through the waveguide, where they are confined by total internal reflection. With increasing pump intensity, population inversion is attained, and the light traveling through the waveguide is amplified according to $I = I_0 \exp[(g - \alpha)l]$, where I_0 is the initial intensity, g and α are the gain and loss coefficients, and l is the distance traveled through the gain medium. The gain coefficient is strongly wavelength dependent, and thus the transitions with highest gain are amplified exponentially resulting in a narrowed output spectrum of the device. To derive the threshold of stimulated emission, we plot the full width at half-maximum (fwhm) of the emission spectrum versus the corresponding absorbed pump pulse energy on a logarithmic scale.[138]

The data points are then fitted to a sigmoidal curve and the intersection of the inflection tangent of the curve with the upper limit of line widths is defined as the threshold of ASE. To fit the data numerically, we use the function

$$\mathrm{FWHM} = \frac{A_1 - A_2}{1 + (x/x_0)^p} + A_2 \quad (1)$$

where x is the pulse energy, A_1 is the upper and A_2 the lower limit of line widths, and p corresponds to the slope of the function.[138] An alternative method leading to comparable values is a plot of emission intensity vs absorbed intensity, giving the threshold as sharp bend of the curve. ASE usually occurs near the maximum of the photoluminescence spectrum, but if the Stokes shift is small, reabsorption can shift the gain spectrum to longer wavelengths and lower values of the gain coefficient. Using guest−host systems with Förster transfer can significantly increase the separation of the emission and absorption spectra as well as decrease concentration quenching effects. ASE thresholds as low as ~200 nJ/cm^2 were demonstrated in a 130 nm thick film of 2.5% PV-spiro-4Φ **94** doped into spiro-6Φ **2** spin-coated

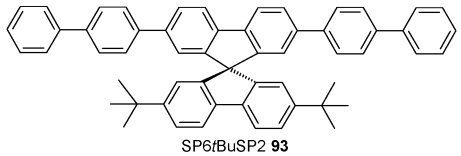

SP6*t*BuSP2 **93**

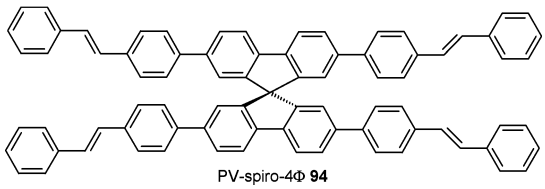

PV-spiro-4Φ **94**

from chloroform (see Figure 13).[157] ASE has been shown in several spiro compounds in neat and doped films (Table 2).[97,104,158−160]

Distributed feedback reflection (DFB) lasers,[162−166] which can be understood as a one-dimensional photonic crystal with a periodic variation of the (effective) refractive index along the propagation direction of the amplified light in a slab waveguide has been demonstrated featuring several low molecular weight spirobifluorene derivatives as the active gain medium, both in neat films and in guest−host systems.[89,97,104,158−161] This type of device is fabricated by spin-coating or vacuum-depositing a thin (50−500 nm) film on a low refractive index substrate with a surface grating of period Λ. Lasing occurs near the Bragg wavelength defined by $\lambda_{\mathrm{Bragg}} = 2n_{\mathrm{eff}}\Lambda/m$, where m is an integer referred to as the order and n_{eff} is the effective refractive index of the film, which is obtained by solving the Maxwell equations for the waveguide structure and which depends on the refractive indices of the film and the claddings as well as the thickness of the active material. Its numerical value (typically around 1.8−2) lies between those of the substrate and film refractive indices. Substrates with several regions of different grating periods are usually employed to test for the wavelength range accessible to DFB lasing with the material under consideration. Second-order DFB gratings are generally easier to fabricate because for a given material and wavelength the grating period is twice that of the corresponding first-order grating. Also, since first-order DFB lasers emit radiation out of the side (in plane) of the waveguide and second-order emission occurs also perpendicular to the surface, the latter is considerably less cumbersome to detect. On the other hand, lower losses due to waveguide scattering in first-order DFB lasers compared with second-order structures enable signifi-

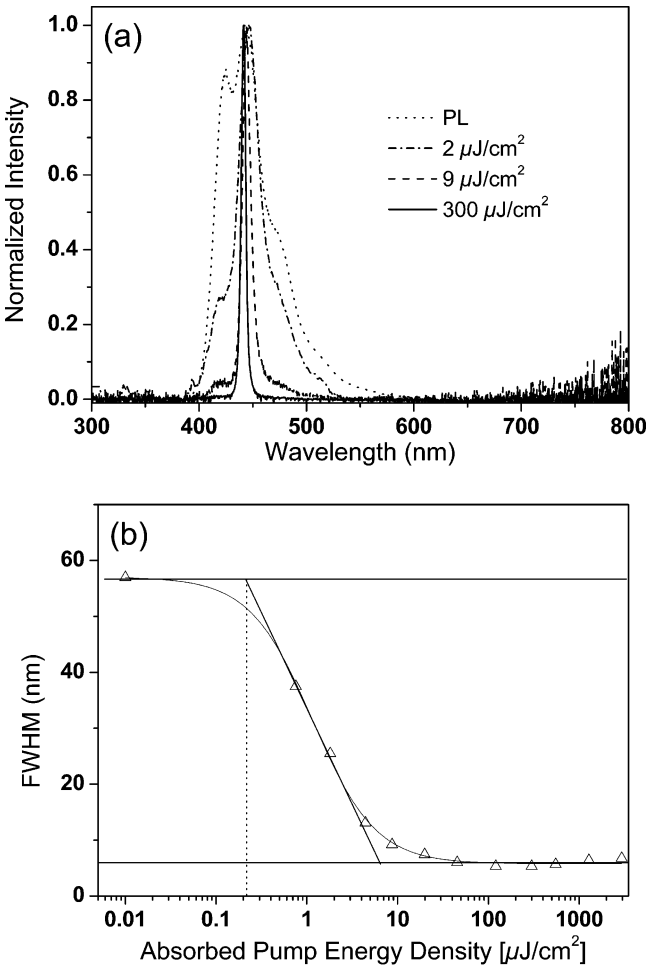

Figure 13. (a) ASE in a 130 nm thick film of a blend of 2.5% by weight PV-spiro-4Φ **94** in spiro-6Φ **2** spin-coated from chloroform and (b) the fwhm of the emission plotted versus the absorbed pulse energy per cm^2 fitted with a sigmoidal curve. The intersection of the inflection tangent of the fitted curve with the upper limit of line widths defines the threshold for stimulated emission.

Table 2. ASE Properties of Some Spiro Compounds

material	ASE threshold (μJ/cm^2)	λ_{ASE} (nm)	fwhm-ASE (nm)	ref
spiro-4Φ **9**			2.2	161
spiro-6Φ **2**	11	419	2.9	138, 161
4-spiro^2 **5**	3.2	428	3.2	138
4-spiro^3 **12**		443	3.9	138
spiro-6Φ(MeO)$_4$ **13**	30	427.5	9.3	89
spiro-octo-2 **24**	3	425.4	4.6	89
spiro-SPO **60**	1	419	5.4	89
spiro-Carb **18**	50	400.3	7.9	89
SP6*t*-BuSP2 **93**	111	412		160
2.5% PV-spiro-4Φ **94** doped in spiro-6Φ **2**	0.1	440	5.5	157

cantly lower thresholds. Schneider et al. have shown a 20-fold reduction in threshold for spiro-DPVBi **19** in 2,7-bis(biphenyl-4-yl)-2′,7′-di-*tert*-butyl-9,9′-spirobifluorene (SP6*t*-BuSP2 **93**) from 6 μJ/cm^2 for second-order DFB lasing down to 320 nJ/cm^2 in a first-order DFB laser.[158] DFB lasing with spiro compounds has been demonstrated covering wavelengths between 361.9 nm (spiro-terphenyl **26**) and 529.3 nm (spiro-DPVBi **19**) with only a small gap from 395 to 401.5 nm.[89,97,104,158−161] The lowest lasing threshold obtained for an undoped neat film of a spiro compound in a second-order DFB laser was 8.9 μJ/cm^2 in spiro-terphenyl **26** at a lasing wavelength of 383 nm on a 220 nm period grating. Table 3 shows the lasing properties of some spiro compounds.

Further challenges for organic semiconductors are the vertical cavity surface-emitting laser,[167,168] which is in principle a short path version of the Fabry−Perot cavity with distributed Bragg reflector (DBR) mirrors in a vertical stack of layers; the microring and disc lasers, where feedback is achieved by several round trips of the emitted radiation confined in the resonator by total internal reflection;[169−173] and 2D and 3D photonic crystal lasers.[162−166] Spiro compounds seem to be good candidates also for these laser types.

3.6. Charge Transport

An important parameter defining the charge transporting capabilities in thin films of semiconductors is the charge carrier mobility. The mobility μ is the proportionality factor between drift velocity and electric field as well as between conductivity and the charge concentration. In the characterization of organic semiconductor materials, time-of-flight (TOF) and field-effect transistor (FET) measurements have been widely used to extract the mobility of charge carriers. The basic principles of these methods can be found elsewhere.[174,175] The temperature dependence is interpreted within the terms of different charge transport models, for example, an Arrhenius-type model or the Gaussian disorder model.[174,176] In the latter, the charge carrier mobility is predicted to be proportional to the inverse square of the temperature ($\ln \mu \propto T^{-2}$) and to the square-root of the applied electric field ($\ln \mu \propto E^{1/2}$). The mobility is then given by

$$\mu(E,T) = \mu_0 \exp\left[-\left(\frac{2\sigma}{3kT}\right)^2\right] \exp\left[C_0\left(\frac{\sigma^2}{(kT)^2} - \Sigma^2\right)E^{1/2}\right] \quad (2)$$

where μ_0 denotes the prefactor mobility, σ is the energetic (diagonal) disorder, T is the temperature, k is the Boltzmann's constant, Σ is the degree of positional disorder (off-diagonal), C_0 is the empirical constant of 2.9×10^{-4} (cm/V)$^{1/2}$, and E is the applied electric field. The Arrhenius model describes the hopping transport as resulting from a single level of traps or an activation energy arising from polaron relaxation.[177] This model predicts that the mobility of charge carriers is logarithmically proportional to the reciprocal temperature ($\ln \mu \propto T^{-1}$).

Table 4 summarizes the charge transport properties of spiro arylamines measured by means of TOF technique. The hole mobilities (μ_h) are around 10^{-4} cm^2/(V s). Poplavskyy and Nelson[179] found that the temperature- and electric-field-dependent behavior of the TOF mobility within the Gaussian disorder (GD) model revealed higher prefactor mobilities (μ_0) and energetic (diagonal) disorder (σ) for the methoxy-substituted compound **73** than for the unsubstituted compound **4**. They explained their results by a higher negative charge density on the HOMO in the methoxy-substituted spiro compound that results in a greater intermolecular overlap integral and by a higher morphological disorder in solution-processed films than in evaporated films.

Recently, Kirkpatrick and Nelson[180] also reported that the effect of methoxy side groups on the spatial extent of the wave function may be able to explain why spiro-*m*-TTB **95** is found to have a smaller prefactor mobility than spiro-MeO-TAD **73**. The theoretical calculation has shown clearly

Table 3. Lasing Properties of Some Spiro Compounds

material	order	wavelength range (nm)	fwhm (nm)	threshold	ref
SP6*t*-BuSP2 **93**	2	401.5−434.2	0.11−0.40	83 μJ/cm^2 at 411.7 nm	159, 160
spiro-DPVBi **19**	2	457.8−529.3		26 μJ/cm^2 at 469 nm	158
spiro-DPVBi **19** in SP6*t*-BuSP2 **93**	2	435.3−498.9		6 μJ/cm^2 at 460 nm	158
spiro-DPVBi **19** in SP6*t*-BuSP2 **93**	1	478−530		320 nJ/cm^2 at 478 nm	158
spiro-4Φ -F_4 **14**	2	377.7−395	0.19−0.35	62 μJ/cm^2 at 382 nm	97
spiro-terphenyl **26**	2	361.9−393.8		8.9 μJ/cm^2 at 383 nm	104
PV-spiro-4Φ **94** doped in spiro-6Φ **2**	2	419−470		3.4 μJ/cm^2 at 440 nm	157

Table 4. Summary of the Charge Transport Properties Obtained by TOF Technique

material	μ_h[a] (cm^2/(V s))	μ_0 (cm^2/(V s))	σ (eV)	C_0 (cm/V)$^{1/2}$	Σ	ref
spiro-TAD **4**	5×10^{-4}	0.016	0.08	2.9×10^{-4}	2.3	178
spiro-*m*-TTB **95**	4×10^{-4}	0.010	0.08	2.9×10^{-4}	1.2	178
spiro-MeO-TAD **73**	2×10^{-4}	0.047	0.101	2.9×10^{-4}	2.3	179

[a] At an electric field of 2.6×10^5 V/cm and temperature of 300 K.

that the localization radius for spiro-MeO-TAD **73** is larger than that for spiro-*m*-TTB **95**. This will lead to a greater

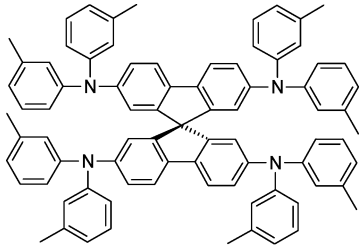

spiro-*m*-TTB **95**

overlap of wave functions on adjacent molecules and hence to a higher value of the transfer integral. The calculated values of the mean-square hole transfer integral at an intermolecular spacing of 12.7 Å are 237 meV^2, 98 meV^2, and 114 meV^2 for spiro-MeO-TAD **73**, spiro-*m*-TTB **95**, and spiro-TAD **4**, respectively.[180] Due to the strong localization of the wave function, the interaction between adjacent molecules and, hence, the local energetic landscape will be more sensitive to intermolecular geometry, thus leading to a larger energetic (diagonal) disorder.

TOF mobility data on ambipolar charge transport materials based on spiro compounds are still rare. One example for which data are available is spirobifluorene-derivative TDAF-1 **52**. A hole mobility of up to 4×10^{-3} cm^2/(V s) and an electron mobility of lower than 10^{-3} cm^2/(V s) were reported,[181] with reorganization energies of 182 and 279 meV for holes and electrons, respectively.[182] The electron and hole mobilities are in the range of 10^{-5} cm^2/(V s) for B4 **97**.[183]

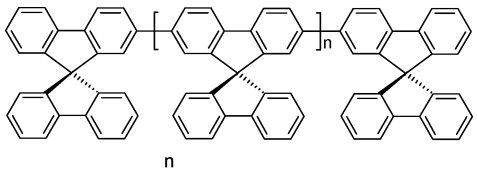

n

0	B2	**96**
1	TDAF-1	**52**
2	B4	**97**

In contrast, electron and hole mobilities in the range between 10^{-3} and 10^{-2} cm^2/(V s) can be obtained for B2 **96**.[183] Therefore, the mobilities of charge carriers decrease with increasing oligomer length. This can be attributed to the fact that longer oligomers can exhibit larger variations of molecular conformation of the corresponding molecule and, consequently, larger disorders, which may impede the corresponding charge carrier transport.

The charge carrier mobilities in thin films of spiro compounds and their corresponding parent compound have also been measured by the FET technique.[132,146,184] The calculated field-effect mobilities in thin films of spiro compounds are approximately 1 order of magnitude lower than those obtained by the TOF method. Figure 14 shows the field-effect mobilities of charge carriers in thin films of TPD **70** and spiro-TPD **76** as a function of temperature. The

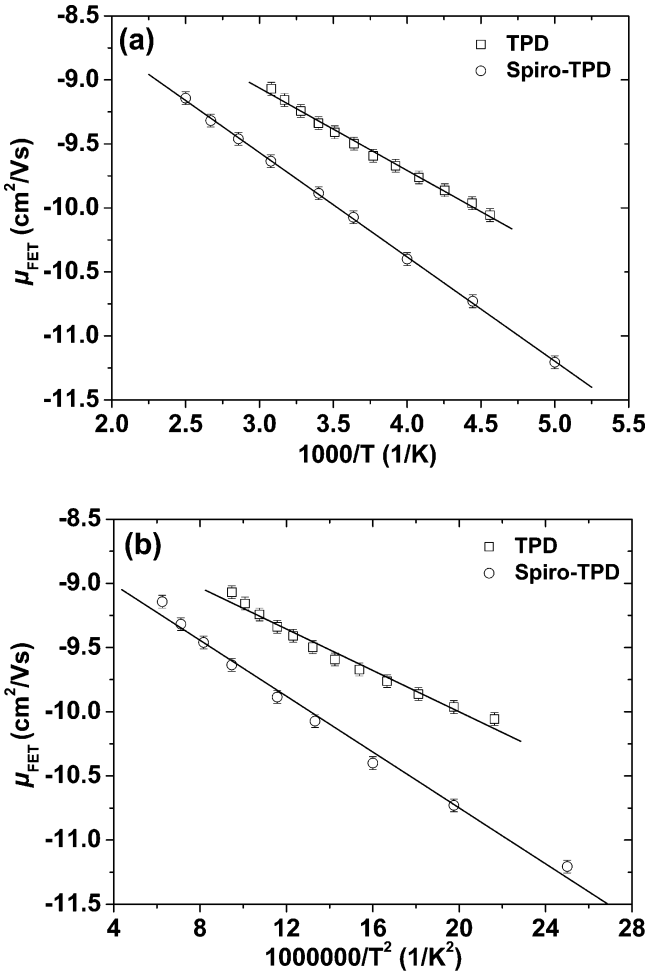

Figure 14. Field-effect mobilities of charge carriers in thin films of TPD **70** and spiro-TPD **76** plotted against (a) the reciprocal of the temperature in the Arrhenius representation and (b) the inverse square of the temperature in the GD model. Reprinted with permission from ref 132. Copyright 2006 WILEY-VCH Verlag GmbH.

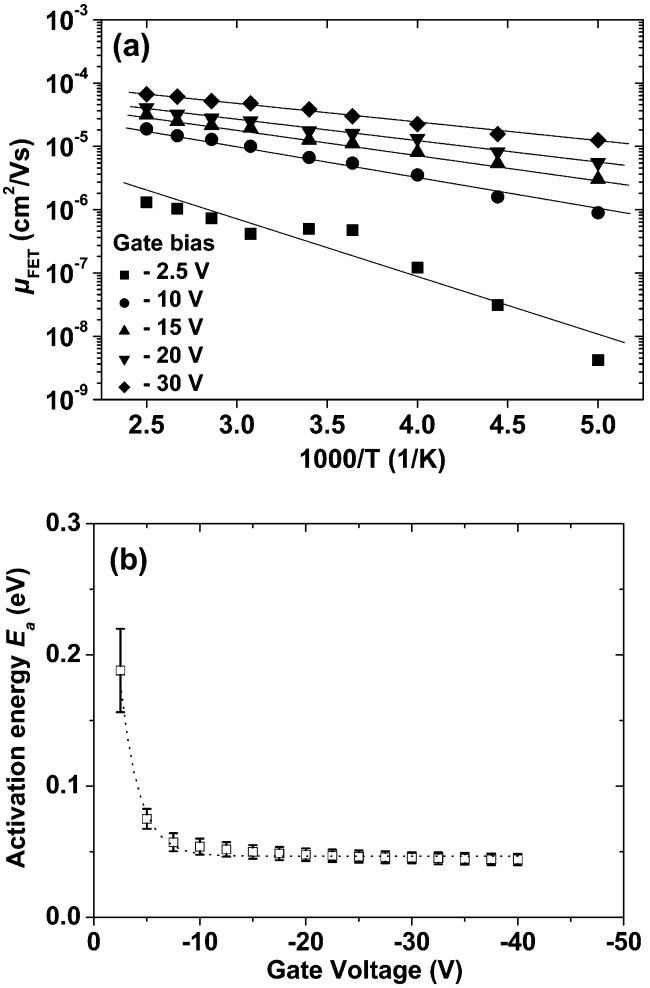

Figure 15. (a) Temperature dependence of field-effect mobility for a spiro-TPD **76** at gate biases of −2.5, −10, −15, −20, and −30 V and (b) the activation energy of field-effect mobility plotted against gate voltage. Reprinted with permission from ref 132. Copyright 2006 WILEY-VCH Verlag GmbH.

dependency of the field-effect mobility on the temperature can be plotted as mobility versus the reciprocal of the temperature (called the Arrhenius representation) and versus the inverse square of the temperature, according to the Gaussian Disorder (GD) model, respectively. The Arrhenius model has been found to fit our experimental data better than the GD model.[132,146] Prefactor mobilities in thin films of TPD **70** and spiro-TPD **76** of 8×10^{-4} and 2×10^{-4} cm²/(V s) were obtained for the Arrhenius and the GD model, respectively. Moreover, an activation energy E_a of 0.057 eV was obtained from the Arrhenius model for TPD **70**, which is in contrast with the result obtained from the TOF technique ($E_a = 0.12$ eV).[185]

Figure 15a shows the temperature dependence of the field-effect mobility for a spiro-TPD **76** FET at different gate biases, V_g ($V_g = -2.5$, −10, −15, −20, and −30 V). The lines are least-squares fits used to extract the activation energy. Figure 15b shows the dependency of the activation energy on the applied gate bias. The apparent activation energy decreased with increasing gate biases. At low gate biases, the activation energy is large, and as the gate bias is increased, it finally saturates at a value of 0.050 eV. The decrease of the activation energy with increasing the absolute gate bias value is probably a result of accumulated charges filling the lower-lying states. Therefore, any additional charge

Table 5. Transport Parameters Extracted from the FET Technique[132]

	Arrhenius model		GD model	
material	μ_0 (cm²/(V s))	E_a (eV)	μ_0 (cm²/(V s))	σ (eV)
TAD **3**	7.6×10^{-2}	0.220	4.4×10^{-3}	0.077
spiro-TAD **4**	4.0×10^{-3}	0.110	4.0×10^{-4}	0.057
TPD **70**	8.0×10^{-4}	0.057	2.0×10^{-4}	0.045
spiro-TPD **76**	8.0×10^{-4}	0.071	2.0×10^{-4}	0.051
TTB **75**	33	0.330	4.5×10^{-2}	0.092
spiro-TTB **74**	0.2	0.206	3.3×10^{-3}	0.076
α-NPB **71**	5.0×10^{-2}	0.174	2.0×10^{-3}	0.071
spiro-α-NPB **15**	8.0×10^{-2}	0.205	3.0×10^{-3}	0.077

carriers will occupy sites with a higher energy, and less energy will be required for jumping to neighboring sites.[186,187]

Table 5 summarizes all parameters extracted through the FET method.[132] The prefactor mobilities obtained from the Arrhenius model for TAD **3**, TPD **70**, TTB **75**, α-NPB **71**, spiro-TAD **4**, spiro-TTB **74**, spiro-TPD **76**, and spiro-α-NPB **15** cover a broad range of 8×10^{-4} and 33 cm²/(V s), which is rather unexpected. In contrast, the prefactor mobilities obtained from the GD model cover a range from 2×10^{-4} to 4.5×10^{-2} cm²/(V s), which is realistic for low molar mass amorphous thin films. The Gaussian distribution widths obtained from the Gaussian disorder model for all thin films are in the range of 0.051 and 0.092 eV. The discrepancy between a good data fit and a large deviation in the prefactor mobility value for the Arrhenius model is not fully understood yet. However, we find that the temperature dependencies of spiro arylamine compounds slightly differ from those of the parent compounds.

4. Applications

4.1. Field-Effect Transistors

In this section, organic field-effect transistors (FET) based on thin films of spiro compounds are reviewed. Figure 16 shows the schematic view of a typical bottom-contact and top-contact organic FET (OFET).

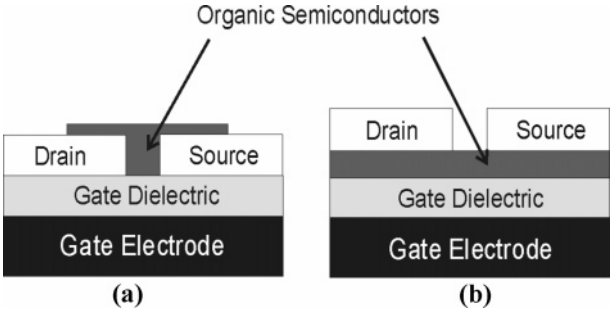

Figure 16. Schematic view of a bottom-contact (a) and a top-contact (b) OFET.

The output and transfer characteristics of a spiro-α-NPB **15** FET are given in Figure 17, as an example of spiro arylamines. The electrical characteristics are given for a fresh device measured in air and under vacuum. The drain current (I_{ds}) increases as the gate voltage (V_g) is increased toward a larger negative voltage, exhibiting an effective field-effect caused by the gate bias. The sign of the field-enhanced current ($I_{ds} < 0$ with $V_g < 0$) is consistent with an accumulation regime, owing to the p-type character of spiro-α-NPB **15**. At low drain bias (V_{ds}), the characteristics exhibit some nonlinearities that can be attributed to the nonohmic contact be-

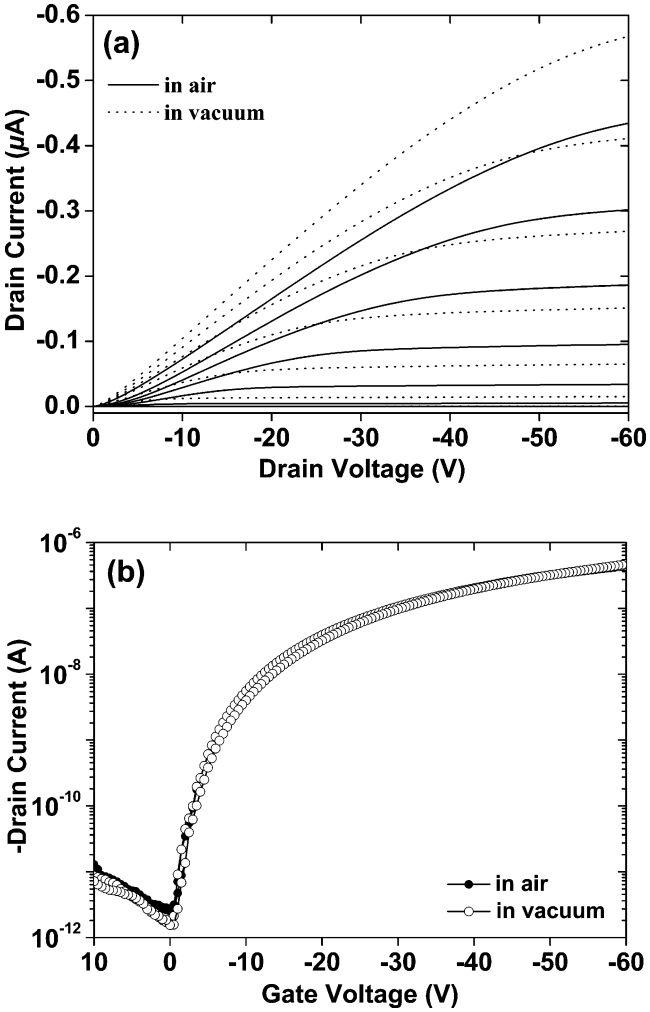

Figure 17. Output and transfer characteristics of a spiro-α-NPB **15** FET. Panel a provides the output characteristics measured in air and under vacuum. The gate bias was swept from +10 to −60 V in steps of 10 V. Panel b provides the transfer characteristics measured in air and under vacuum ($V_{ds} = -60$ V). Reprinted with permission from ref 132. Copyright 2006 WILEY-VCH Verlag GmbH.

tween spiro-α-NPB **15** and the gold electrodes. This behavior was found in all transistors based on thin films of spiro compounds and their corresponding parent compounds.[132]

The field-effect mobility of holes measured upon exposure to air was 2.9×10^{-5} cm^2/(V s). An on/off ratio of typically 1.8×10^5 for $V_{ds} = -60$ V can be obtained. In contrast, the saturated drain current (at $V_{ds} = V_g = -60$ V) measured under vacuum was 30% higher than the value measured in air. The field-effect mobility of holes was estimated to be 4.3×10^{-5} cm^2/(V s). The high on/off ratio in this device originates from the low drain current in the off state, a result of using material of high purity with no unintentional doping. In addition, the gate leakage current was relatively low in the devices.

Generally, thin film transistors based on spiro compounds are more stable compared with their corresponding parent compounds. As an example, Figure 18 shows the transistor characteristics of the same device, spiro-α-NPB **15** FETs, after being stored at room temperature in the dark in ambient atmosphere for 3 months. It has been found that the saturated drain current (at $V_{ds} = V_g = -60$ V measured under vacuum) decreased by 11% and the hole mobility decreased by only 4%. However, the switch-on voltage, V_{so}, of the transistor,

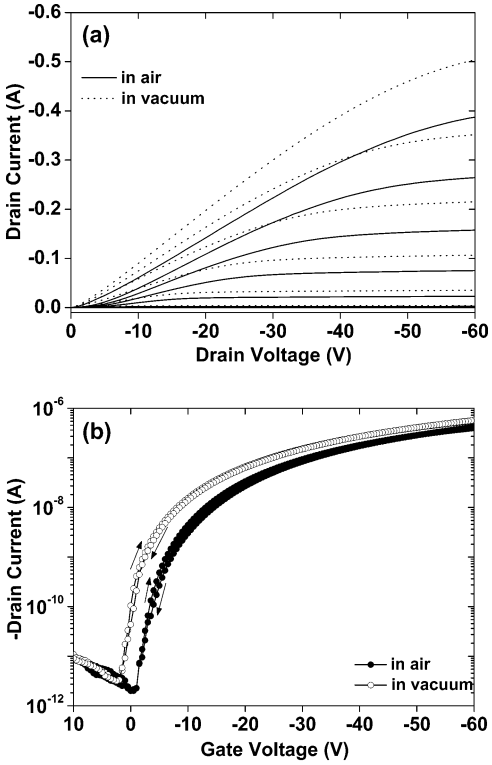

Figure 18. Output and transfer characteristics of a spiro-α-NPB **15** FET measured after the sample has been stored in ambient atmosphere for 3 months. Panel a provides the output characteristics measured in air and under vacuum. The gate bias was swept from +10 to −60 V in steps of 10 V. Panel b provides the transfer characteristics measured in air and under vacuum ($V_{ds} = -60$ V). The arrows show the direction of the gate bias being scanned during the measurement. Reprinted with permission from ref 132. Copyright 2006 WILEY-VCH Verlag GmbH.

which was 0 V for a fresh device, has slightly shifted toward positive bias after 3 months ($V_{so} \approx +1$ V). A similar result was also obtained for the fitted threshold voltage, which shifts from −4.2 to −4.8 V for in-air operation, after the sample was stored for 3 months. An on/off ratio of 2×10^5 (at $V_{ds} = -60$ V) was obtained for measurements performed in air. The measurement carried out under vacuum gave an ON/OFF ratio of 1.9×10^5 (at $V_{ds} = -60$ V), which is only slightly lower than the values measured for a fresh device. In contrast, the transistor action of corresponding parent compounds such as TAD **3**, TPD **70**, TTB **75**, and α-NPB **71** are not observable anymore after the devices have been stored for several days at ambient atmosphere or in a continuously evacuated vacuum chamber.[132,146]

A hysteresis in the transfer characteristics of a sample that was stored in ambient atmosphere for 3 months has also been observed. Probably, this hysteresis is due to the presence of trapped mobile charges introduced by the presence of moisture and oxygen as the sample was stored in ambient atmosphere.[132]

Table 6 summarizes the FET hole mobilities obtained for the spiro compounds. The hole mobility of spiro-α-NPB **15** is the lowest among the investigated compounds. Also, it was observed that spiro-TTB **74** is relatively prone to aging, as compared with the other spiro compounds. The hole mobilities in thin films of spiro-TAD **4** and spiro-TPD **76** appear to be independent of the ratio of channel width to channel length.[184] However, the mobilities computed from the linear regime are always lower than mobilities calculated

Table 6. Hole Mobilities in Thin Films of Spiro Compounds Extracted from FET Measurements

material	hole mobility (10^{-5} cm^2/(V s)) at RT	stability	ref
spiro-TAD **4**	6.7 ± 0.3	stable in air up to 9 months, mobility decreased by 2%	184
spiro-TPD **76**	6.9 ± 0.4	stable in air up to 9 months, mobility decreased by 3%	184
spiro-TTB **74**	5.7 ± 0.5	stable in air up to 4 months, mobility decreased by 13%	132
spiro-α-NPB **15**	4.4 ± 0.2	stable in air up to 3 months, mobility decreased by 4%	132

from the saturation regime of the characteristic curve for all transistors based on spiro compounds.[146]

4.2. Phototransistors and Solar Cells

4.2.1. Phototransistors

One key component of optoelectronic circuits is the phototransistor, allowing the detection of light and photoswitching. It is also interesting for light triggered amplification and high sensitive image sensors. In principle, phototransistors can be realized in the bipolar transistor geometry based on photoresponsive heterojunctions or as a unipolar device derived from the field-effect transistor. Whereas unipolar phototransistors based on inorganic semiconductors have been known for some time,[188] unipolar organic phototransistors (OPTs) have not been exploited widely. Examples of OPTs are based on poly(3-octylthiophene),[25] polyfluorene,[189] poly(phenylene ethynylene),[190] oligothiophene,[191] pentacene,[192] copper phthalocyanine,[192] and bifunctional spiro compounds.[122,123] In this section, the phototransistors utilizing spiro compounds as active thin films are reviewed. The photoresponsive materials are spiro-DPSP **58**, spiro-DPSP^2 **59**, spiro-DPO **56**, and coevaporated thin films of spiro-TAD **4** and spiro-6Φ **2**.

Figure 19 shows the schematic view of a bottom-contact OPT. Generally, the phototransistors can be operated as a *three-terminal* device with two electrical contacts (source and drain) and light as the amplifying gate or as a *four-terminal* device with an additional electrical gate, allowing additional biasing of the device by the electrical field-effect. Light works in the devices in a manner similar to the conventional field effect by increasing the number of mobile charge carriers in the channel. The underlying mechanism can be sufficiently explained by ultrafast photoinduced charge transfer (~430 fs) between an electron donor and an electron acceptor moiety upon illumination (see section 2.2.5).[121]

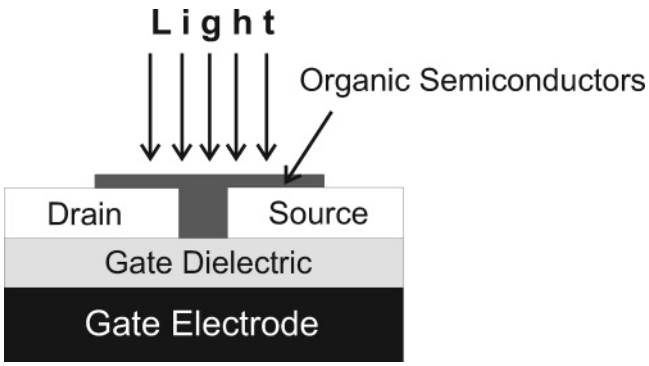

Figure 19. Schematic view of a bottom-contact OPT, where the light is used as a third or additional control parameter.

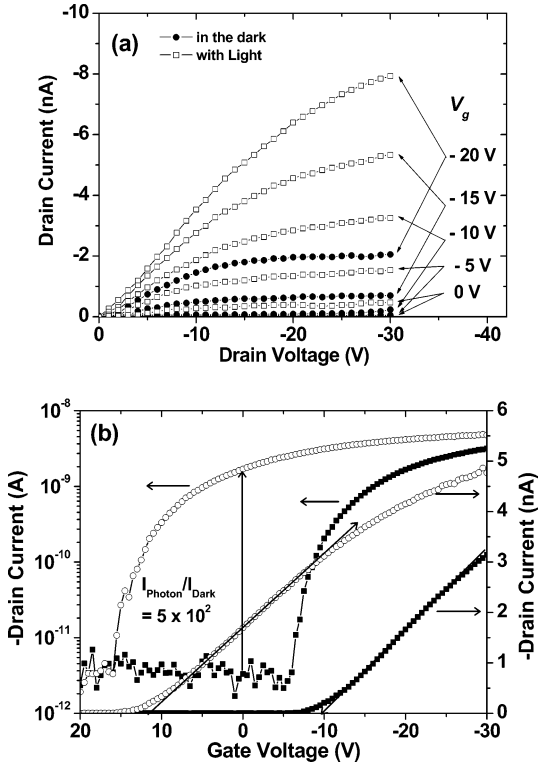

Figure 20. Panel a shows the output characteristics of spiro-DPSP **58** phototransistors at different gate voltages in the dark (●) and under illumination with 191 μW/cm^2 (□). The illumination of the device was done by using a Nichia NSHU590E UV light-emitting diode (λ_{max} = 370 nm, fwhm = 11 nm). Panel b shows the transfer characteristics (at $V_{ds} = -10$ V) measured in the dark and under illumination with 127 μW/cm^2. The drain current is plotted both logarithmically (left axis) and linearly (right axis).

Figure 20a displays the output characteristics of a spiro-DPSP **58** phototransistor measured in the dark and under an illumination of 191 μW/cm^2 at 370 nm. For measurements performed in the dark, the drain current clearly increases with increasing gate voltage toward a more negative value. The sign of the field-enhanced drain current ($I_{ds} < 0$ with $V_g < 0$) is consistent with an accumulation regime, owing to the p-type character of spiro-DPSP **58**.

A distinct increase in the current was observed under illumination. Without irradiation, the current is of the order of 10 pA, and it increases to several nanoamperes upon irradiation.[122] For a spiro-DPSP^2 **59** phototransistor, the current measured in the dark at $V_g = V_{ds} = -30$ V was −2.9 nA.[123] This current increased to −8.7 nA as the device was measured under illumination at 64 μW/cm^2.

Figure 20b shows the transfer characteristics of a spiro-DPSP **58** phototransistor. A ratio of photocurrent to dark current as high as 5×10^2 was obtained, which is comparable to amorphous silicon phototransistors.[188] It has been shown clearly that the $I_{ds}-V_g$ curves are not changed substantially in shape or magnitude but rather displaced by a shift in the fitted threshold voltage (from −9 V in the dark to +15 V at 127 μW/cm^2). The threshold voltage (V_{TH}) for OFETs in the accumulation regime is given by[175]

$$V_{TH} = -\frac{qn_0d}{C_i} + V_{FB} \quad (3)$$

where V_{FB} is the flat-band potential, C_i is the capacitance per unit area, d is the thickness of thin films, q is the ele-

mentary charge, and n_0 is the bulk carrier density. Assuming the flat-band voltage to be invariant, the charge carrier density is the only parameter which can be changed by illumination, causing the shift in the threshold voltage. From Figure 20b, it becomes clear that low light intensities could not be measured at zero gate voltage. Instead, the optimum working point can be adjusted by choosing a gate bias directly at the switch-on voltage (V_{so}) under dark conditions, in this case at −6 V. For low drain voltages, the OPT operates in the linear regime and allows the extraction of the charge carrier mobility.[175] A value of 1.3×10^{-6} cm^2/(V s) was obtained, independent of the illumination conditions. On the other hand, the hole mobility in thin films of spiro-DPSP[2] **59** measured in the linear regime was 2.7×10^{-7} cm^2/(V s). This compound has also been used as active materials in phototransistors.

OPTs based on spiro-DPO **56** have also been fabricated and characterized.[193] Ratios of photocurrent to dark current up to 1.9×10^3 (6.1 μW/cm^2) and 4.3×10^3 (11.5 μW/cm^2) can be obtained at $V_g = -10$ V, which is comparable to the values obtained for amorphous silicon phototransistors.[188] In this case, a responsivity of up to 16.1 A/W can be obtained at $V_g = -40$ V, which is higher than our previous results based on other spiro compounds[122,123] and polymer phototransistors.[25,189,190]

The time-resolved response of the phototransistor is shown in Figure 21. The time-resolved response behavior (for

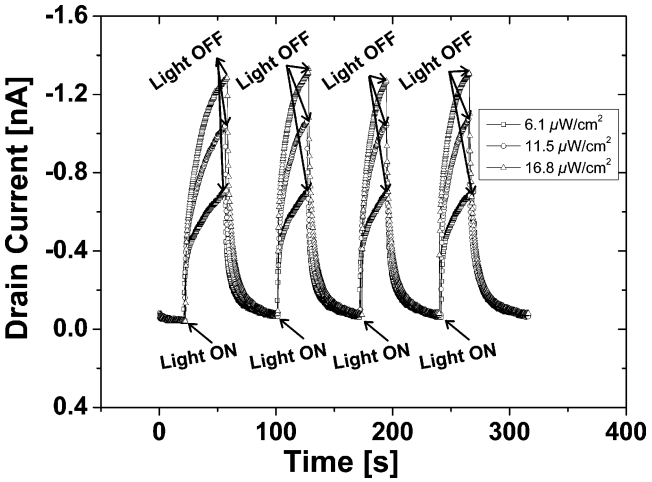

Figure 21. Time-resolved response of the spiro-DPO **56** phototransistor upon illumination with 6.1, 11.5, and 16.8 μW/cm^2 at $V_g = V_d = -20$ V.

instance, at an incident light intensity of 6.1 μW/cm^2) cannot be described by a single response time, but rather as a combination of a fast increase of photocurrent at the beginning and a second, slower process in the end. For the fast response, the time constant is approximately 2.9 s. On the other hand, the slower process has a rather long time constant of 20.5 s. The relaxation after switching the light off can be fitted by a single-exponential quite well, giving a time constant of 5.4 s. The relaxation time is related to the recombination of the photoseparated charges, which can be improved by an appropriate material design, thus allowing faster detection speed. A similar phototransistor, constructed with spiro-DPSP **58** as active material also showed a double exponential behavior, with a fast component of 1.5 s and a slow component of 10.3 s.[122]

In the following discussion, the photoeffect will be qualitatively explained as photoconductivity in a single-compound system. In the absence of any incident radiation, the charges injected by applying an appropriate gate bias (either positive or negative) remain located close to the active thin film/SiO_2 interface. In the bulk material, the molecules are in their neutral state. As light is absorbed in the film, an exciton is formed, which can eventually dissociate into electrons and holes. After dissociation (photoinduced charge transfer), a geminate pair of an electron at the donor and a hole at the acceptor is formed. These electron−hole pairs are bound by Coulomb interaction because of the low dielectric constant of the organic materials. Overcoming this Coulomb barrier, the charges may diffuse by hopping transport from donor to donor or acceptor to acceptor. In the transistor, the majority charge carriers participate in the overall transport, giving rise to the increased photocurrent. With the spiro concept, majority charge carriers and acceptors for the opposite charge can be combined in one material.

As mentioned previously, spiro-DPSP **58** consists of a sexiphenyl and a bis(diphenyl-amino)biphenyl moiety. In order to test the influence of linking both moieties in one molecule, a comparison experiment with an equimolar mixture of spiro-TAD **4** and spiro-6Φ **2** was made. The active layer was deposited by coevaporating the two materials.[146] Phototransistor action has also been observed in this device, but the performance was lower than that of spiro-DPSP **58**, probably because of domain formation and the corresponding distribution statistics.

4.2.2. Photodiodes

Recently, spiro compounds have also found use as active materials in diode-type organic UV photodetectors. The device structures employed in these studies are ITO/PEDOT−PSS (30 nm)/D2 **98** (25 nm)/A2 **78** (25 nm)/LiF (0.5 nm)/Al (150 nm) (device 1), ITO/PEDOT−PSS (30 nm)/

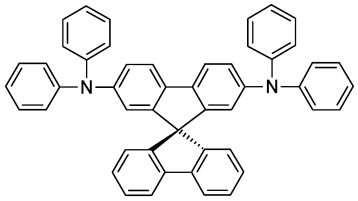

D2 **98**

D2 **98**−A2 **78** (mixture 1:1, 50 nm)/LiF (0.5 nm)/Al (150 nm) (device 2), and ITO/PEDOT−PSS (30 nm)/D2A2 **57** (50 nm)/LiF (0.5 nm)/Al (150 nm) (device 3).[194] Here, PEDOT−PSS stands for poly(ethylene dioxythiophene)−poly(styrene sulfonate), and ITO stands for indium tin oxide. All three devices displayed high external quantum efficiency at reverse biases, 30% electron/photon (0.09 A/W) for device 1 and approximately twice as much for devices 2 and 3 (62% (0.18 A/W) and 73% (0.22 A/W), respectively). The mechanism governing the device operation is taken to be an efficient photoinduced electron transfer with a quantum yield close to unity. It was also shown in a preliminary reliability test of the corresponding devices that the devices lose their photoresponse by 3−5% after being continuously illuminated for over 200 h with UV radiation (380 nm) of 1 mW/cm^2. A typical response time of approximately 400 ns was observed.[194]

4.2.3. Dye-Sensitized Solar Cells

Spiro compounds have found also applications as solid-state transport materials for the transfer of holes in dye-

sensitized solar cells, replacing the common I_2/I_3^- electrolyte system. The device, commonly referred to as a Grätzel cell, is based on the photoinduced electron transfer from a dye to mesoporous TiO_2.[195] The network of connected TiO_2 nanoparticles forms a large active surface area for light absorption and electron transfer. As the active material, ruthenium dyes such as $Ru(II)L_2(SCN)_2$ where L is 4,4′-dicarboxy-2,2′-bipyridyl ligands, are quite suitable because of the good adhesion of the carboxyl groups to the TiO_2 surface. If the dye is optically excited, electrons are injected into the conducting band of TiO_2, leaving a ruthenium(III) species.

$$[Ru(II)L_2(SCN)_2]^* \rightarrow [Ru(III)L_2(SCN)_2]^+ + e^-(TiO_2)$$

The electrons are collected by an F-doped SnO_2 electrode, and the electrical circuit is closed via a gold electrode by a mediator, which transports the charges needed for the back reduction of the dye (electrons are injected from the gold electrode to the LUMO of the dye or, in an equivalent picture, holes from the dye to the gold electrode). The original Grätzel cell suffers from the use of a liquid electrolyte with the redox system I_2/I_3^- as mediator, which causes some problems due to leakage and solvent evaporation unless properly sealed.

In order to avoid the problems associated with liquid electrolytes, all-solid-state variations of this cell have been developed by replacing the liquid electrolyte with hole-transporting spiro compounds.[196,197] The tetramethoxy derivative spiro-MeO-TAD **73** was used with $Ru(II)L_2(SCN)_2$ as sensitizing dye. Spiro-MeO-TAD **73** is a good hole transporter and penetrates the nanoporous TiO_2 network efficiently, and by introduction of methoxy substituents, the oxidation potential of the hole transporter was matched to that of the sensitizer. The structure and energy level diagram of this cell is displayed in Figure 22.

The incident-photon-to-electron conversion efficiency (IPCE) was determined to be 5%, which is still lower than that for comparable liquid cells. The IPCE is defined by the ratio of the number of electrons generated in the solar cell to the number of photons incident on the photoactive surface of the device at a given wavelength.[198]

$$\mathrm{IPCE}(\lambda) = \frac{n_{\mathrm{electrons}}(\lambda)}{n_{\mathrm{photons}}(\lambda)} = \frac{I(\lambda)hc}{P_{\mathrm{in}}(\lambda)e\lambda} \approx \frac{1239I(\lambda)}{P_{\mathrm{in}}(\lambda)\lambda} \quad (4)$$

where $I(\lambda)$ corresponds to the measured current in microamperes per square centimeter, $P(\lambda)$ is the input optical power in watts per square meter, and λ is the wavelength of the incident light in nanometers. Generally, the IPCE is measured under a short-circuit condition and is graphically displayed versus the corresponding wavelength in a solar cell's action spectrum. Therefore, the IPCE relates to the photoresponse or external quantum efficiency. By doping the hole transport material with $N(PhBr)_3SbCl_6$ and $Li[(CF_3SO_2)_2N]$, which increases the charge carrier concentration by partial oxidation, an IPCE of 33% was measured. The overall efficiency of the cell was 0.74% at white-light irradiation with 9.4 mW/cm^2. Under full sunlight (air mass 1.5, 100 mW/cm^2), short-circuit photocurrents of 3.18 mA/cm^2 have been achieved. In a later report,[199] the performance was improved by blending the hole conductor matrix with a combination of 4-*tert*-butylpyridine and $Li[(CF_3SO_2)_2N]$. The hole conductor matrix was applied by spin-coating a 0.17 M chlorobenzene solution of the hole conductor. Partial

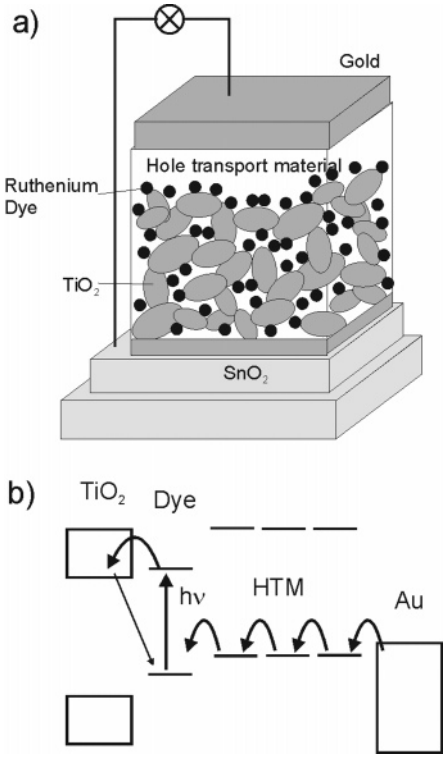

Figure 22. Panel a shows an organic solar cell with spiro-MeO-TAD **73** as solid-state hole transport material (HTM). The photosensitive ruthenium dye is attached as a monolayer to TiO_2 nanoparticles, thus forming a large active area for photoinduced electron transfer. Panel b shows the energy level scheme. Photoinduced electron-transfer takes place from the photoexcited ruthenium dye into the TiO_2 conduction band. The recombination directly back to the dye has to be suppressed. Instead, the current is directed through the circuit to the counter electrode and the hole transport layer, which brings the electrons back via hopping transport. Reprinted from ref 59. Copyright 2006. With kind permission of Springer Science and Business Media.

oxidation of spiro-MeO-TAD **73** by $N(p\text{-}C_6H_4Br)_3SbCl_6$ was used to control the dopant level and to increase the conductivity of the hole-conducting layer. Open circuit voltages of 910 mV and short-circuit currents of 5 mA were obtained, yielding a power efficiency of 2.56%.

This power efficiency has been improved to 3.2% by performing the dye adsorption step in the presence of silver ions at low concentrations in the dye solution. From spectroscopic evidence, it is inferred that the silver is mainly binding to the sensitizer via the amphidentate thiocyanate, allowing the formation of ligand-bridge dye complexes.[200]

Power efficiencies above 4% can be achieved by utilizing an organic indoline dye **99**, instead of the commonly used

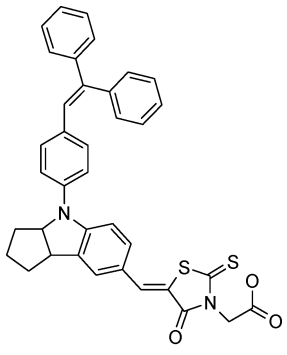

Indoline dye **99**

ruthenium dyes. The higher extinction coefficient makes it an ideal dye for solid-state dye-sensitized solar cells. This dye also shows light-harvesting properties superior to those of ruthenium dyes such as N719 **100** when applied as a sensitizer of mesoporous TiO_2 layer.[201]

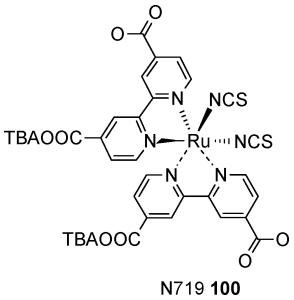

N719 **100**

An efficiency of 4% for the standard air mass 1.5 spectrum (100 mW/cm^2) can be obtained by using an amphiphilic dye with hydrophobic spacers (for example, Z907 **101**).[202,203] This

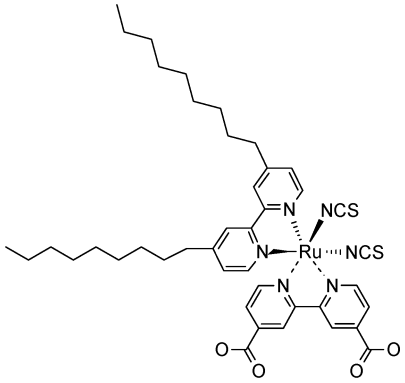

Z907 **101**

performance is attributed to the self-assembly of the dye to a dense layer on the TiO_2 surface with its carboxylate groups as anchors and with its hydrophobic isolating chains as a blocking layer between the hole conductor spiro-MeO-TAD **73** and TiO_2.

4.3. Light-Emitting Devices

Spiro compounds have been used in organic light-emitting diodes (OLED) in a variety of functions, as electroluminescent dye and as hole and electron transport material. The basic structure of an OLED is given in Figure 23. The structure is derived from a three-layer concept by Adachi, Tsutsui, and Saito,[204] who extended the original bilayer device of Tang and Van Slyke.[1] Light is generated in the central emission layer (or at one of its interfaces) by recombination of injected charge carriers being transported by mutual solid-state redox reactions. In OLED structures using electrophosphorent dyes for harvesting triplet excitons in addition to singlet excitons, additional charge and exciton blocking layers are used for an optimum perfomance.

One of the tasks for display applications is the combination of materials of different colors to produce white light and full color devices. For that reason, separate strategies aim at the development of blue-, green-, and red-emitting materials with suitable color coordinates. The color of the luminescence can best be described in the Commission Internationale de l'Éclairage (CIE) chromaticity diagram in which the color coordinates are defined as follows: The emission spectrum is weighted by the three given color matching functions for

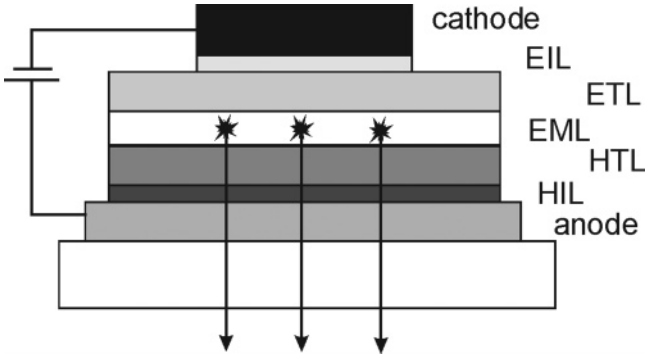

Figure 23. Structure of an OLED: HIL = hole injection layer (e.g., CuPc **102**, copper phthalocyanine); HTL = hole transport layer; EML = emission; ETL = electron transport layer; EIL = electron injection layer (e.g., LiF, lithium fluoride). The light generated by the recombination of holes and electrons is coupled out via the transparent anode (e.g., ITO, indium tin oxide). Typical cathode materials are Mg/Ag, Ca/Ag, Al. Reprinted from ref 59. Copyright 2006. With kind permission of Springer Science and Business Media.

the color perception of a standard observer and integrated, giving the tristimulus values x, y, and z with the normalization $x + y + z = 1$. In the diagram, usually given two-dimensionally by x and y, the white point is defined by the coordinates $x = y = z = {}^1/_3$.[205]

Blue electroluminescence based on a spiro compound single-layer device was reported in 1997. The active device consists of a vapor-deposited 60 nm thick layer of spiro-6Φ **2** sandwiched between the ITO anode and Al/Mg cathode. The color coordinates for the emitted blue light in photoluminescence and electroluminescence are at $x = 0.16$, $y = 0.08$ and at $x = 0.18$, $y = 0.15$, respectively.[88] In this device, a turn-on voltage of 9 V is measured. The turn-on voltage can be further reduced by combining spiro-6Φ **2** with the electron transporter Alq_3. In a two-layer device based on a 40 nm thick layer of Alq_3 **103** on top of a 40 nm thick layer

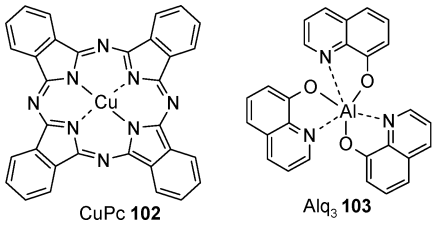

CuPc **102** Alq_3 **103**

of spiro-6Φ **2** sandwiched between the ITO anode and Al/Mg cathode on a glass substrate, the turn-on voltage is indeed reduced to 7.5 V.[88] A brightness of 900 cd/m^2 is measured at a voltage of 16 V. But the chromaticity values for the emitted light are shifted ($x = 0.31$, $y = 0.55$) closer to the emission of Alq_3 **103**. The reason for the color shift is that the emission zone is very near, partially inside, the Alq_3 **103** layers. A blue-light-emitting two-layer device based only on spiro compounds has been also fabricated by combining a 40 nm thick vapor-deposited spiro-PBD **28** layer on top of a 40 nm thick spin-coated layer of spiro-TAD **4** sandwiched between the ITO anode and Al/Mg cathode. A turn-on voltage of 2.7 V is measured. A brightness of 500 cd/m^2 was measured at a voltage of 5 V.

The issue of temperature stability of OLEDs was addressed by comparing the device performance of devices based on regular (non-spiro) OLED materials with that of devices made with spiro compounds.[206] By replacement of α-NPB

71 with spiro-TAD **4**, the thermal stability is greatly enhanced while the favorable electro-optical device properties are maintained. Moreover, these results have shown that OLEDs based on materials with high glass transition temperature are less prone to the occurrence of leakage currents during device operation. The investigation of blue OLEDs containing DPVBi **20** clearly showed that this material was the limiting factor for highly efficient devices. The low T_g of only approximately 64 °C can lead to an intermixing of adjacent layers even at temperatures as low as 80 °C, which may cause drastic spectral changes, whereas devices based on the morphologically stable compound spiro-DPVBi **19** ($T_g \approx 130$ °C) have shown robust emission behavior at temperatures above 120 °C.[206] Two different types of blue OLEDs have been also fabricated using spiro compounds. In this case, the device structures are (1) ITO/PEDOT−PSS **104** (∼30 nm)/NCB **105** (45 nm)/TBPSF **53** (30 nm)/Alq_3 **103** (20 nm)/LiF/Al and (2) ITO/PEDOT−PSS **104** (∼30 nm)/NCB **105** (45 nm)/TBPSF **53**−blue-emitting perylene (30 nm)/Alq_3 **103** (20 nm)/LiF/Al, respectively.[119] TBPSF

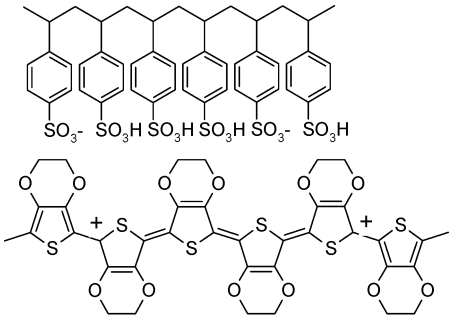

PEDOT-PSS **104**

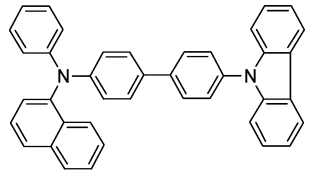

NCB **105**

53 and NCB **105** are 2,7-bis[2-(4-*tert*-butylphenyl)pyrimidine-5-yl]-9,9′-spirobifluorene and 4-(*N*-carbazolyl)-4′-(*N*-phenylnaphthylamino)biphenyl, respectively. The concentration of blue-emitting perylene was 1 wt %. A maximum brightness of >30 000 cd/m^2 (device 1) and ∼80 000 cd/m^2 (device 2) was obtained at an injection current of 5000 mA/cm^2. The electroluminescence efficiencies at a brightness of 100 cd/m^2 were about 2.3% photon/electron (1.6 cd/A) and 4% (5.2 cd/A) for devices 1 and 2, respectively. The nondoped device (device 1) showed pure blue electroluminescence from TBPSF **53**, while in the doped device (device 2), the electroluminescence was completely converted into that of perylene, indicating very efficient resonant energy transfer from TBPSF **53** to blue-emitting perylene.

Another spiro-type molecule for blue OLED applications is 2,2′-bis(10-phenylanthracen-9-yl)-9,9′-spirobifluorene, spiro-FPA **36**.[111] Devices with the configuration ITO/CuPc **102**/α-NPB **71**/spiro-FPA **36**−*x*% TBP **106**/Alq_3 **103**/LiF/Al have been fabricated and studied, where TBP **106** stands for 2,5,8,11-tetra-*tert*-butylperylene. With a 1.0 wt % TBP **106**-doped spiro-FPA **36** emissive layer (20 nm), a high luminescence efficiency of 4.9 cd/A (2.07 lm/W) with CIE coordinates of $x = 0.134$ and $y = 0.207$ at a current density of 20 mA/cm^2 and driving voltage of 7.4 V was obtained. A

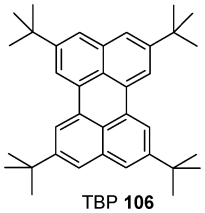

TBP **106**

maximum current efficiency of 4.9 cd/A and a maximum brightness of 9720 cd/m^2 was reported for a device with the structure ITO/CuPc **102** (15 nm)/α-NPB **71** (50 nm)/SDPF **51** (30 nm)/Alq_3 **103** (50 nm)/Mg/Ag, where SDPF **51** is 2,7-dipyrene-9,9′-spirobifluorene.[117] The emission peak of this device was at 472 nm, and the CIE coordinates (at 20 mA/cm^2) were $x = 0.17$ and $y = 0.27$.

Recently, a series of 2′,7′-di-*tert*-butyl-9,9′-spirobifluorene derivatives incorporating arylamine at the 2- or 7-position or both have been synthesized[207] and successfully employed as active materials in blue-emitting OLEDs. Double-layer devices with a narrow full width at half-maximum (fwhm) of less than 68 nm in the blue were demonstrated using these materials as hole-transporting and emitting material and TPBI **107**, 1,3,5-tris(*N*-phenylbenzimidazol-2-yl)benzene, as electron-transporting layer. ITO/**108**/TPBI **107**/Mg/Ag device emitted

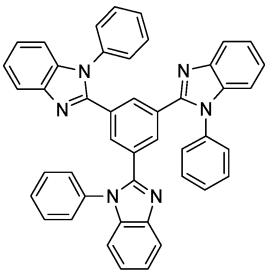

TPBI **107**

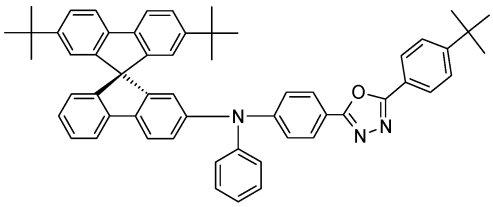

108

pure blue light with CIE coordinates at $x = 0.15$ and $y = 0.09$. A maximum luminescence of 8390 cd/m^2 (at 13.5 V), a maximum luminescence efficiency of 3.6 cd/A, and a maximum power efficiency of 2.1 lm/W were obtained.

Wong and co-workers also reported devices with bright blue electroluminescence based on spiro compounds.[134] The device structure used in this study was ITO/PEDOT−PSS **104** (30 nm)/TDAF-1 **52** (50 nm)/TPBI **107** (37 nm)/LiF (0.5 nm)/Al. This device exhibited pure blue electroluminescence with a turn-on voltage of ∼3 V. The electroluminescence spectrum of the device is similar to the photoluminescence spectrum of the corresponding active spiro compound. The device can be operated at low voltage, for instance, at 6 V (with a brightness of 100 cd/m^2) or at a bias 8 V (with a brightness of 1000 cd/m^2). High external quantum efficiency of 2.5−3% photon/electron and brightness of up to 5000 cd/m^2 were achieved in this device.

Efficient blue OLEDs based on spiro compounds have also been fabricated by employing double heterostructure devices

that provide effective double confinement of both carriers and excitons.[208] In a device structure consisting of ITO/PEDOT−PSS **104**/TDAF-1 **52**/LiF/Al, pure blue electroluminescence was achieved but with a low quantum efficiency (0.15% photon/electron). By addition of 50 nm 4,4′,4″-tris(*N*-carbazolyl)-triphenylamine (TCTA **109**)[56] be-

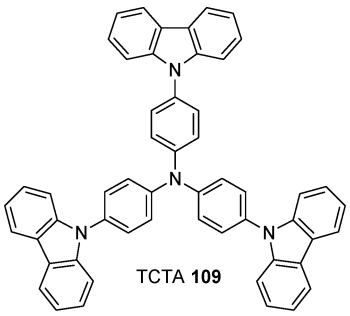

tween PEDOT−PSS **104** and the active compound, the quantum efficiency increased by a factor of 53. Moreover, the brightness is substantially enhanced in comparison to single-layer devices, indicating the positive effect of TCTA **109** on improved hole−electron balance. Addition of 30 nm of TPBI **107**, sandwiched between active material and cathode, without TCTA, resulted in a quantum efficiency of 2.5%. Finally, a quantum efficiency of 4.1% (1.1 cd/A) and brightness of 8000 cd/m^2 were obtained when the device structure was ITO/PEDOT−PSS **104**/TCTA **109** (40 nm)/TDAF-1 **52** (30 nm)/TPBI **107** (30 nm)/LiF/Al.

Blue electroluminescence was also demonstrated with spirobifluorene-based pyrazoloquinolines as emissive material[126] from devices with the configuration ITO/α-NPB **71** (40 nm)/CBP **110** (10 nm)/TPBI **107**−*x*% spiro-PAQ-Ph **66** (20 nm)/TPBI **107** (20 nm)/Mg/Ag, where CBP **110** denotes

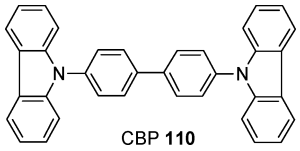

4,4′-dicarbazolyl-1,1′-biphenyl. As the concentration of the spiro compound in TPBI **107** was varied from 1.0 to 5.0 wt %, the electroluminescence peak with a maximum at 460 nm was maintained. The turn-on bias for devices with 1.0, 2.0, and 5.0 wt % spiro compound **66** in TPBI **107** remained almost constant (approximately 3.5 V). However, the highest external quantum efficiency was obtained for devices with 1.0 wt % spiro compound **66** in TPBI **107** (3.67% at a current density of 20 mA/cm^2). The CIE coordinates of this device were $x = 0.14$ and $y = 0.15$.

A spiro oligophenyl containing alkoxy side chains, 2,7-dibiphenyl-3′,6′-bis(octyloxy)-9,9′-spirobifluorene **62**, was used as active material in blue OLEDs.[124] The device structure was ITO/TPD **70** (60 nm)/**62** (40 nm)/Alq_3 **103** (20 nm)/LiF (1 nm)/Al (100 nm). The device showed a maximum luminance of 3125 cd/m^2 at a bias of 12.8 V. The power efficiency was 0.9 lm/W at a brightness of 100 cd/m^2. An external quantum efficiency of 2.8% was obtained at a brightness of 100 cd/m^2 with color coordinates $x = 0.14$ and $y = 0.12$.

OLEDs with an emission in orange-red region was reported by blending 2,7-bis{4-[2-(4-dodecyloxyphenyl)-1,3,4-oxadiazol-5-yl]phenyl}-spirobifluorene **111** with poly-[2-(2-methylethylhexyloxy)-5-methoxy-1,4-phenylene vi-

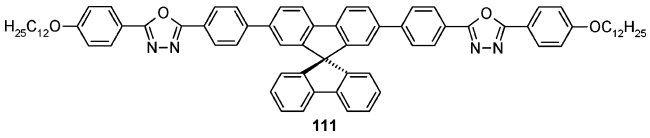

nylene] (MEH-PPV).[209] Two different types of devices have been used. The first device type was ITO/blend of MEH-PPV with **111**/Al (150 nm) and the second device type was ITO/PEDOT−PSS **104** (40 nm)/blend of MEH-PPV with **111**/Al (150 nm). The devices without PEDOT−PSS **104** exhibited an external quantum efficiency of 0.02% because the blend contains 50 wt % compound **111**. In those that use PEDOT−PSS **104**, an efficiency of 0.08% was obtained at a current density of 30 mA/cm^2. The external quantum efficiency also increased as the ratio of the spiro compound in the blend increases.

Chen et al. demonstrated red-light-emitting diodes based on spiro compounds.[116] The red-emitting materials used are designed and synthesized by combining a di(4-tolyl)amino (pTSPDCV **50**) or diphenylamino (PhSPDCV **49**) electron donor with a dicyanovinyl electron acceptor in a spiro compound. The device structure ITO/α-NPB **71** (10 nm)/pTSPDCV **50** (40 nm)/2,9-dimethyl-4,7-diphenyl-1,10-phenanthroline, BCP **112** (20 nm)/Alq_3 (30 nm)/Mg/Ag

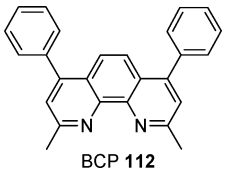

exhibited a maximum luminescence of 6080 cd/m^2. However, the operating voltage at a current density of 20 mA/cm^2 was 7.7 V. The maximum efficiency is 2.6%, and the corresponding current efficiency and power efficiency were 1.8 cd/A and 0.9 lm/W. The electroluminescence peak was centered at 652 nm with the CIE coordinates at $x = 0.66$ and $y = 0.33$. In contrast, a device with the same configuration but with PhSPDCV **49** as active material exhibited a maximum luminance of 11 380 cd/m^2. The operational voltage was 8.1 V at a current density of 20 mA/cm^2. The maximum efficiency of the corresponding device was 3.6% (3.5 cd/A, 1.8 lm/W), and the electroluminescence peak was at 638 nm. The CIE chromaticity coordinates of this device were $x = 0.65$ and $y = 0.35$.

An important approach toward reducing the internal resistance of OLED devices was presented by Leo and coworkers by controlled redox doping of the charge transporting material. Controlled redox doping of the transport layer is beneficial for two reasons: high conductivities are achieved by the increased number of charge carriers, and thin space charge layers created by doping (near to the electrode) lead to low contact barriers and quasi-ohmic contacts. For this purpose, spiro-TAD **4** was chosen as a hole-transporting material with high stability. Several results have been reported showing significant improvements in OLED performance.[210] One example is a highly efficient deep-blue OLED with an n-doped electron transport layer and a p-doped hole transport layer. By incorporation of the spirobifluorene-substituted anthracene 9,10-bis(9,9′-spirobi-[9*H*-fluorene]-2-yl)anthracene **113** or 4P-TPD **114**, 4,4′-bis-(*N*,*N*-diphenylamino)-tetraphenyl, as emitting layers in a p−i−n-type OLED structure, a luminance of 100 cd/m^2 at an operating voltage of 2.9 V and 1000 cd/m^2 at 3.4 V was

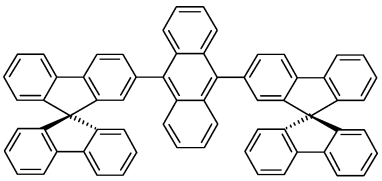

spiro-Anthracene **113**

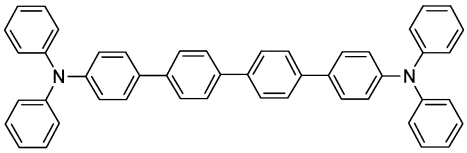

4P-TPD **114**

obtained.[211] In an optimized device structure, a satisfactory color coordinate ($x = 0.14$ and $y = 0.14$) was achieved with **113** as emitter. High current efficiencies of 4.5 cd/A and quantum efficiencies of 3% at a brightness of 100 cd/m^2 were demonstrated. Spiro-TAD **4** was also used in a very highly efficient, low-voltage phosphorescent OLED based on a p−i−n junction.[212−214] By incorporation of MeO-TPD **115**, Bphen **116**, spiro-TAD **4**, F_4-TCNQ **117**, TCTA **109**, Ir(ppy)$_3$ **118**, Cs, TAZ **119**, and TDATA **120**,[52] utilizing ITO as anode and aluminum as cathode, a power efficiency of approximately 77 lm/W and an external quantum efficiency of 19.3% was achieved at a brightness of 100 cd/m^2 with an operating voltage of only 2.65 V. More importantly, the efficiency decayed only weakly with increasing brightness, and a power efficiency of 50 lm/W was still obtained even at 4000 cd/m^2.

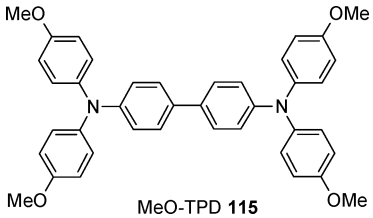

MeO-TPD **115**

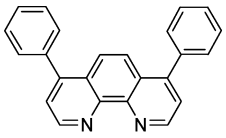

BPhen **116**

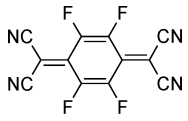

F_4-TCNQ **117**

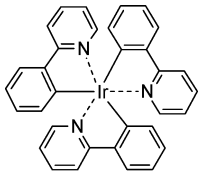

Ir(ppy)$_3$ **118**

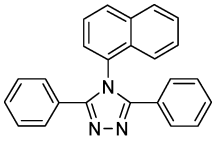

TAZ **119**

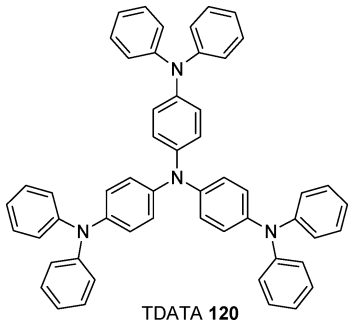

TDATA **120**

Doping of an emissive oligophenyl with a dye emitting at longer wavelengths offers the possibility of obtaining almost any desirable mixed color by fine-tuning the dopant concentration. Preferred for various display applications is white light emission. If an emitting host is doped, the color coordinates follow a trajectory in the CIE diagram with increasing dopant concentration. This is shown in Figure 24

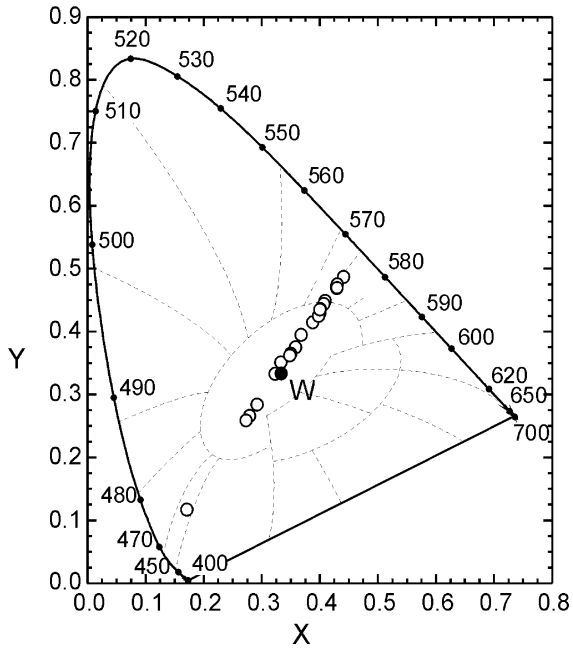

Figure 24. CIE color diagram for electroluminescent devices, consisting of anode/spiro-TAD **4**/spiro-4Φ **9**−rubrene **121**/Alq$_3$ **103**/cathode with different concentrations of rubrene. The spectrum shifts from blue to yellow, crossing the white point (W). Reprinted from ref 59. Copyright 2006. With kind permission of Springer Science and Business Media.

for a series of electroluminescent devices based on spiro materials as hosts. White light emission from OLEDs utilizing doped spiro compounds as emissive layers has been also reported. Two series of white-light-emitting devices using exclusively high T_g materials have been fabricated. They are ITO/spiro-TAD **4**/spiro-octo-2 **24**−rubrene **121**/Alq$_3$ **103**/Mg/Ag (device A) and ITO/spiro-TAD **4**/spiro-4Φ **9**−rubrene **121**/Alq$_3$ **103**/Mg/Ag (device B).[215] Without rubrene **121** dopant, devices A and B emit blue light. Optimized correspondence with the white point (CIE 0.33, 0.33) has been achieved with a rubrene concentration of 0.58 wt % for both types of devices (CIE 0.32, 0.33 for device A, CIE 0.30, 0.36 for device B). At these points, a luminous efficiency of 2.4 cd/A and a maximum luminance as high as 11 800 cd/m^2 were attained at a voltage of 15 V for device A. An efficiency of 1.6 cd/A and a maximum luminance of 4100 cd/m^2 were achieved for device B.

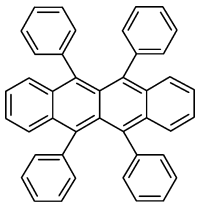

Rubrene **121**

Recently, white OLEDs have been also fabricated by utilizing blue-emitting DPVSBF **122**, 2,7-bis(2,2′-diphenylvinyl)-spirobifluorene, lightly doped with DCJTB **123**,

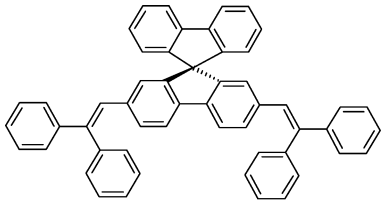

DPVSBF **122**

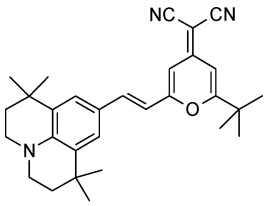

DCJTB **123**

4-(dicyanomethylene)-2-*t*-butyl-6(1,1,7,7-tetramethyljulolidyl-9-enyl)-4*H*-pyran, as the source of the emission and α-NPB **71** and Alq_3 **103** as the hole and electron transporter, respectively.[216] The device displayed a luminous efficiency of 8 cd/A, a power efficiency of 5.35 lm/W, and an external quantum efficiency of 3.31% at a driving current of 20 mA/cm^2 (at 4.7 V). The brightness under such conditions is 1575 cd/m^2, while up to 66 000 cd/m^2 is feasible at a driving bias of 15 V. The CIE coordinates remain nearly constant, changing only from 0.35, 0.36 to 0.32, 0.34 as the voltage increased from 6 to 12 V. It was also found that the relative device lifetime increased by a factor of ∼20 with respect to a similar device with 4,4′-bis(2,2-diphenylvinyl)-1,1′-biphenyl (DPVBi **20**) as the active material for blue emission. The extended half-lifetime of this device can be attributed to the higher morphological stability of the spiro compound.

Extending the emission of OLEDs into shorter UV wavelengths is still a big challenge. Recently, highly efficient UV OLEDs have been fabricated by utilizing **107** and **108**.[105,106] The OLED device structure was ITO/PEDOT−PSS **104** (30 nm)/TCTA **109** (40 nm)/B2 **96** (30 nm)/TPBI **107** (30 nm)/LiF (0.5 nm)/Al. Electroluminescence maxima were observed at 374 and 392 nm. The turn-on voltage was very low with a value of only 2.5 V. The maximum brightness and external quantum efficiency were 4890 cd/m^2 (at 11 V) and 3.6%. UV OLED based on other spiro-compounds were also reported.[105] The corresponding OLED device structure was ITO/PEDOT−PSS **104** (30 nm)/TCTA **109** (40 nm)/SSS **27** (30 nm) (device A) and TST **124** (30 nm)/TPBI **107** (30 nm)/LiF (0.5 nm)/Al (device B). Device A exhibited an emission below 400 nm with two distinct electroluminescence peaks at 373 and 393 nm. These UV-emitting devices showed high quantum efficiency (2.6% for device A and 3.1% for device B) with a low turn-on voltage

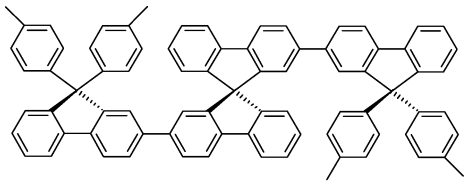

TST **124**

of 3 V. The brightness of these device were 4020 cd/m^2 at a voltage of 13.5 V for device A and 3600 cd/m^2 at 12 V for device B.

Spirobifluorene derivatives have been also investigated as host materials for red-phosphorescent devices with the device structure of ITO/PEDOT−PSS **104** (30 nm)/TCTA **109** (30 nm)/8 wt % $Btp_2Ir(acac)$ **125** doped in SSS **27** (device C)

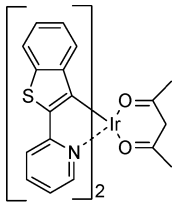

$Btp_2Ir(acac)$ **125**

or TST **124** (device D) (30 nm)/BCP **112** (10 nm)/Alq_3 **103** (60 nm)/LiF (0.5 nm)/Al.[105] In this case, the emitting layer consists of spirobifluorene derivatives, SSS **27** and TST **124**, doped with 8 wt % of the red phosphor bis(2-(2′-benzo[4,5-α]thienyl) pyridinato-N,C$^{3'}$) ($Btp_2Ir(acac)$ **125**). A thin layer of BCP **112** was inserted between the emitter and the electron transporter as hole-blocking and exciton-blocking layer in order to provide exciton and carrier confinement. The brightness of the device was 4060 cd/m^2 (device C) and 4330 cd/m^2 (device D). The operational turn-on voltages were between 2.5 and 3.0 V. The maximum quantum efficiency of the device was 8.6% at a current density of 0.3 mA/cm^2 for device C and 10% at 0.07 mA/cm^2 for device D. Both devices exhibited maximal power efficiency of 4 lm/W.

Recently, a spiro compound was also used as the active material for studying the spin injection in OLEDs.[217] The OLED structure is nickel/spiro-TAD **4**/Alq_3 **103**/$Ni_{0.81}Fe_{0.19}$. An increase in intensity for antiparallel configuration of magnetic electrodes of up to 0.3% was observed, which corresponds to a spin polarization of electrons and holes of ∼4%. However, this increase is not evident for spin injection but seems to be a consequence of the magnetic dependence of the electroluminescence intensity combined with magnetic stray fields from the electrodes.[217]

5. Synthesis of Spiro Compounds

5.1. General Synthetic Routes to the Spirobifluorene Core

The common feature of many spiro compounds synthesized so far is the central core of spirobifluorene **126**, which can be substituted in each position to build up the final compounds. The core can conceptually be considered to be constructed either from two biphenyl moieties with an additional carbon atom or from two fluorene moieties sharing a common carbon atom. The numbering in the final compound originates from the fluorene nomenclature. The fluorene moieties share their carbon atom number 9, which

leads to the full name of 9,9′-spirobi[9*H*-fluorene], also denoted as 9,9′-spirobifluorene.

Most spiro-linked compounds are synthesized from this central spirobifluorene with equal or different substituents in one or more positions. The choice of an adequate pathway for a product depends on the desired substitution pattern. Some products can be derived directly from the spirobifluorene core, while for others the substituents need to be introduced in the precursors before linkage of the central spirobifluorene core. Compounds that are identically substituted in the four *para*-positions—2,2′,7,7′—are usually synthesized from spirobifluorene **126** itself (Figure 25). The

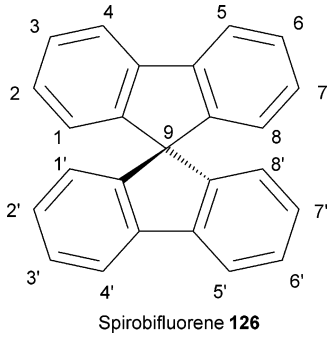

Figure 25. Structure of spirobifluorene **126** and the corresponding numbering of the ring system.

same strategy is also used for 6-fold substitution in the 2,2′,4,4′,7,7′ positions. Compounds featuring functional groups only in the 2 and 7 positions, for example, cannot be prepared by the same strategy. Selective 2,7-substitution such as halogenation is not possible due to the higher reactivity in the 2′-position as compared with the 7-position. 2,2′-Substituted spirobifluorene derivatives can be obtained directly by disubstitution of spirobifluorene if deactivating substituents are used. An alternative way is the introduction of the 2,7- or 2,2′-substituents via the precursors, prior to the spiro linkage.

5.2. Synthesis of Spirobifluorene

The unsubstituted 9,9′-spirobifluorene **126** was synthesized first by Clarkson and Gomberg in 1930 (Scheme 1).[218] They

Scheme 1

started with 2-iodobiphenyl, which was obtained through Sandmeyer's reaction from 2-aminobiphenyl. The intermediate 9-(biphenyl-2-yl)-9-fluorenol was obtained in 70% yield by adding the Grignard reagent from 2-iodobiphenyl to 9-fluorenone.

In the final step, a catalytic amount of hydrochloric acid is added to a boiling solution of the carbinol in acetic acid, which leads to a ring-closure reaction, whereupon most of the formed 9,9′-spirobifluorene precipitates on cooling from the solution. For this step, Clarkson and Gomberg reported a yield of 84%. The overall yield starting from 2-iodobiphenyl was 59%.

Several modifications in the synthetic procedures have been added since the first synthesis. Recently, commercially available 2-bromobiphenyl is mostly used, although the Grignard reaction between 2-bromobiphenyl and magnesium proceeds more slowly.[219−222] Wu et al. reported the use of 2-chlorobiphenyl in the synthesis of spirobifluorene, which was metalated by using *n*-butyllithium instead of magnesium. The overall yield of the corresponding synthesis was 84%.[223] Tour et al. used *tert*-butyllithium for the metalation of 2-iodobiphenyl achieving nearly the same yield for the formation of the carbinol and reported 98% for the synthesis of spirobifluorene.[219] Poriel et al. compared the Grignard and the lithiation pathways and reported higher yields for the milder Grignard variant.[221] Overall yields starting from 2-halogeno-biphenyl reported by other groups cover a large range from 19% to 90%.[219,221−224] Our group obtained a yield of 67%.[107]

5.3. Synthesis of Precursor Compounds

Most identically 2,2′,7,7′-tetrasubstituted spiro compounds are derived from the tetrahalogenated derivatives of spirobifluorene, 2,2′,7,7′-tetrabromo-9,9′-spirobifluorene **127** and 2,2′,7,7′-tetraiodo-9,9′-spirobifluorene **128**. Halogenated compounds are versatile candidates for further substitution like cross-coupling and amination. Of these two precursors, the tetrabromo derivative **127** is used more often because of its easy preparation in high yields and good processability. In contrast to **127**, the tetraiodo derivative **128** is hardly soluble in common organic solvents. However, the main advantage of **128** is its higher reactivity during cross-coupling reactions and aminations.

Compound **127** can be synthesized according to the procedure proposed by Tour and co-workers, who reported a yield of 100%, utilizing a stoichiometric amount of bromine and ferric chloride as catalyst in chloroform at 0 °C.[219,220] This procedure has been confirmed by Pei et al. with a slightly lower yield of 87%.[225] Chun et al. prepared **127** catalyst-free with an excess of bromine in DMF at room temperature in a yield of 71%.[148]

Our group has also implemented a catalyst-free bromination using dichloromethane as solvent with a yield of 91% (Scheme 2).[91] We found that an excess of bromine without

Scheme 2

the addition of a Lewis acid catalyst allows for the selective 4-fold bromination in the 2,2′,7,7′-positions of spirobifluorene, whereas the addition of ferric chloride combined with an excess of bromine resulted in 2,2′,4,4′,7,7′-hexabromo-9,9′-spirobifluorene **129** in good yields (78%).[91]

2,2′,7,7′-Tetraiodo-9,9′-spirobifluorene **128** has also been synthesized by several groups. Tour and co-workers used a mixture of concentrated sulfuric acid, iodic acid and iodine in acetic acid and reported a yield of 84%.[220] Lützen and co-workers used periodic acid instead of iodic acid and reported a lower yield of 51%.[222] Wu and co-workers used iodochloride in refluxing acetic acid and reached a yield of 75%.[223] In our group, we applied the bis(trifluoroacetoxy)-iodobenzene/iodine system as described by Merkushev[226] to prepare **128** with a yield of 95%.[91]

5.3.1. Precursors with 2-Mono- or 2,7-Disubstitution

The synthesis of 2-halogeno- or 2,7-dihalogeno-9,9′-spirobifluorenes can be achieved by using 2-halogenofluorenone or 2,7-dihalogenofluorenone instead of unsubstituted fluorenone. The corresponding dibromo derivative can easily be synthesized by bromination of fluorenone in water.[227] In our group, we synthesized the monobromo derivative in an analogous manner.[228]

Alternatively, 1- or 2-fold halogenations of fluorene and following oxidation with potassium dichromate or chromium trioxide in acetic acid[229] or tetrabutylammonium hydroxide and air in pyridine[225] was applied. Tao et al. used *N*-bromosuccinimide and methanesulfonic acid with commercially available fluorenone to get the bisbrominated product.[117] The halogenated fluorenone compound can then be coupled with the metalated biphenyl. Subsequent intramolecular condensation yields the corresponding spirobifluorene derivatives.

Diederich and co-workers reported the synthesis of 2-bromo-9,9′-spirobifluorene **130** in 78% yield.[230] The 2,7-dibromo-9,9′-spirobifluorene **131** was prepared by several groups with yields between 62% and 86%.[91,117,225,231] 2-Iodo-9,9′-spirobifluorene **132** was synthesized in our group with a yield of 34%, starting from 2-iodo-fluorenone.[91] Some groups reported the use of 4,4′-di-*tert*-butyl-2-bromobiphenyl and mono- or dihalogenofluorenone to yield the 2,7-bisalkylated monobromo and dibromo derivatives **133**[232,233] and **134**,[234] respectively.

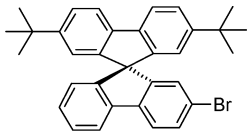

133

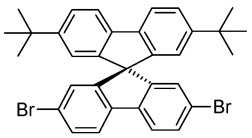

134

Compound **133** has been synthesized by Kim et al. in an overall yield of 51%.[232] Shin et al. reported a slightly better yield of 59% using the same procedure.[233] In 2005, Kim et al. also reported on the synthesis of the bisbrominated derivative **134** in 40% yield using an analogous procedure.[234]

Another important precursor is the 2,7-dibromo-2′,7′-diiodo-9,9′-spirobifluorene **135**, prepared by Pudzich[107] using the Merkushev procedure[226] from 2,7-dibromo-9,9′-spirobifluorene **131** as precursor (Scheme 3). Pudzich showed that

Scheme 3

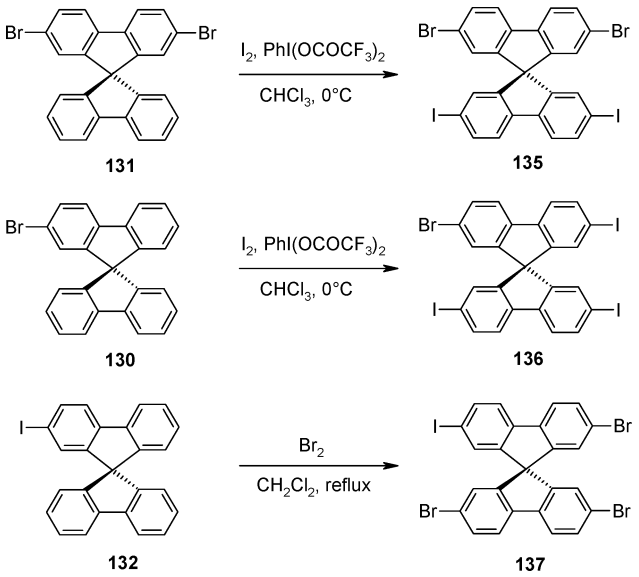

it is possible to carry out reactions such as cross-coupling or amination reactions selectively with the more reactive iodine substituent without affecting the bromine substituents.[107] In a second step, the bromine substituents can be used for further reactions.

Applying the same strategy, Weissörtel was able to synthesize 2-bromo-2′,7,7′-triiodo-9,9′-spirobifluorene **136** in 75% yield starting from 2-bromo-9,9′-spirobifluorene **130**.[91] The inverted halogenated precursor 2-iodo-2′,7,7′-tribromo-spirobifluorene **137** was also synthesized by Weissörtel in a yield of 86% starting from **132**.[91] In this case, the bromination was done by using bromine in dichloromethane without Lewis acid catalyst. These compounds were utilized as precursors in the synthesis of spiro starburst compounds, for example, 4-spiro[3] **12**.[91]

The 2-mono- and 2,7-dihalogeno-9,9′-spirobifluorenes can be converted into boronic acids or esters to achieve a complementary partner in Suzuki coupling reactions.[105,134,222]

5.3.2. Precursors with 2,2′-Disubstitution

The corresponding 2,2′-dihalogeno-9,9′-spirobifluorene precursor is not easy to prepare in an analogous manner to the 2,7-derivatives. The first and seemingly simplest synthesis is the direct electrophilic aromatic substitution. The direct bromination in 2- and 2′-positions was first described by Sutcliffe et al.,[235] who reported a yield of 70% of the desired product 2,2′-dibromo-9,9′-spirobifluorene **138** by using bromine in dichloromethane at room temperature and ferric chloride as catalyst. This and similar procedures were confirmed by other groups. Pei et al. and Park et al. reported the synthesis with a yield of 88%[225] and 81%,[229] respectively.

Repeating this procedures in our group, we always found 2-mono- **130** and 2,7-dibromo-9,9′-spirobifluorene **131** as byproducts. The monobromo compound **130** can be separated by recrystallization, but the 2,2′- and 2,7-dibrominated products were hardly separable by recrystallization or conventional chromatography. Only by HPLC we were able to separate the 2,2′-isomer **138** and the 2,7-isomer **131**.

Chiang et al.[114] also reported on the problems with the purification of **138** synthesized by direct electrophilic

Scheme 4

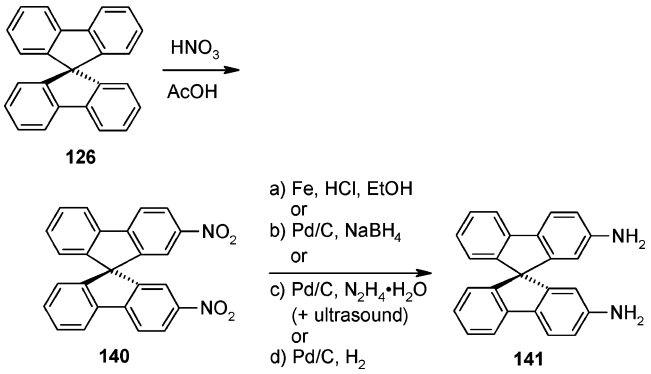

aromatic substitution. They reported that the ^{1}H NMR spectrum of **138**, stated in ref 225, shows unusually broad signals in contrast to the spectra of **131**, **130**, and **127**. This could be attributed to an impurity or an isomer mixture of **138** and **131**. The spectra of the pure isomers are very similar and thereby a mixture could generate such broadened signals. Other analytic methods such as elementary analysis reported by Sutcliffe et al.[235] and mass spectrometry reported by Pei et al.[225] cannot distinguish between these isomers either.

A preferable way to get pure 2,2′-bishalogenated 9,9′-spirobifluorene is to use a more selective electrophilic reagent first and then convert the intermediate 2,2′-disubstituted product in one or more steps into the bishalogenide. A good example for 2-fold selective electrophilic substitution on spirobifluorene **126** is the nitration, which was investigated by Weisburger and co-workers.[236] They used concentrated nitric acid in refluxing acetic acid for nitration and found that careful control of reaction times and conditions permits the formation of either 2-nitro-9,9′-spirobifluorene **139** or 2,2′-dinitro-9,9′-spirobifluorene **140** as the main products.

We found that the dinitration of spirobifluorene **126** can also produce byproducts, which however can be separated much more easily than halogen byproducts from each other. The yields range between 60% and 70%.[222,235−237] Dinitrospirobifluorene **140** can be reduced to the bisamine **141** by several pathways (Scheme 4). Weisburger et al. used iron and hydrochloric acid in ethanol to get **141** in quantitative yield.[236] Chou et al. reported only 64% using the same procedure.[237] The palladium on charcoal/hydrazine hydrate system was applied by Sutcliffe et al. reporting a yield of 89%.[235] Lützen and co-workers also used palladium on charcoal but replaced hydrazine hydrate with sodium borohydride and used methanol instead of ethanol to get **141** in 76% yield.[222] As a further modification Wong et al. used hydrogen and palladium on charcoal to yield 98% of the bisamine **141**.[238] In our group, we also used palladium on charcoal/hydrazine hydrate in ethanol for reduction and additionally applied ultrasound, obtaining pure **141** in quantitative yield.[239]

The bisamine **141** can be converted into 2,2′-dihalogeno-9,9′-spirobifluorenes using the Sandmeyer reaction and modifications. Wu et al. used copper(II) bromide and *tert*-butylnitrite in dry acetonitrile following the procedure Doyle et al.[240] to prepare **138** in 58% yield.[241] Wong et al. also attempted the Doyle procedure and found a mixture also containing excessively brominated compounds. Nevertheless, the target compound **138** could be isolated in a low yield (<30%) by recrystallization from toluene.[238]

Recently, Thiemann et al. described a copper-free Sandmeyer reaction with aqueous alkali iodide solution to get the 2,2′-diiodo-9,9′-spirobifluorene **142** and reported a yield of 72%.[222] Utilizing the procedure proposed by Moore et al.[242] via the diethyltriazenyl derivative **143**, Wong et al. reported a yield of 96% for **142** (Scheme 5).[238]

Recently, Chiang et al. reported a new synthesis of 2,2′-dibromo-9,9′-spirobifluorene **138**, based on selective ipso substitution of trimethylsilyl (TMS) groups by bromine.[114] The acid-labile TMS groups cannot sustain the dehydratation conditions during spiro formation. Thus, the TMS groups have to be substituted before condensation to the final spiro compound. Furthermore Chiang et al. avoided the fluorenone compound by reaction of two molecules of (2′-bromobiphenyl-4-yl)-trimethylsilane with dimethyl carbonate (Scheme 6).[114] The 2-bromobiphenyl derivative was obtained by Suzuki coupling of 1,2-dibromobenzene and 4-(trimethylsilyl)benzeneboronic acid. The overall yield of 36%, starting from (2′-bromobiphenyl-4-yl)-trimethylsilane, appears low, but the overall yield of the synthesis of **138** starting from 2-bromobiphenyl and fluorenone is not higher using the Sandmeyer pathway to get pure **138** in multigram amounts. Nevertheless, in case of 2,2′-diiodo-9,9′-spirobifluorene **142**, which can substitute **138** in most reactions, the overall yield is even higher according to the report of Wong et al.[238] (80% when starting from spirobifluorene **126**).

Another often used 2,2′-substituted starting compound is the 2,2′-diacetyl-9,9′-spirobifluorene **144**. Similar to the nitration, the 2-mono- and 2,2′-diacetylation works well, being even more selective than the dinitration. By Friedel−

Scheme 5

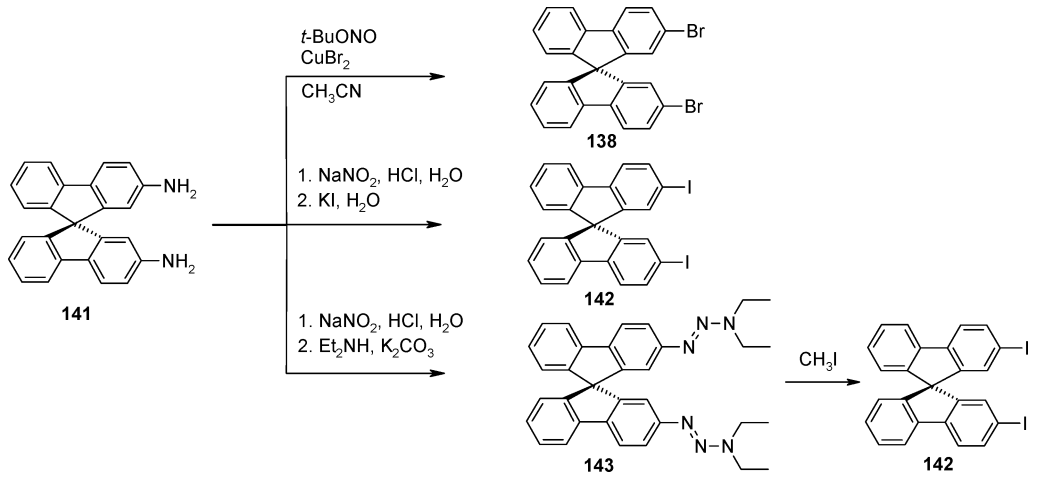

Scheme 6

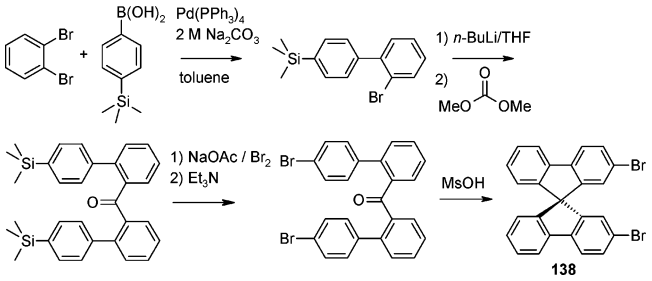

Crafts acylation with acetylchloride and aluminum chloride in carbon disulfide, the bisacetylated product **144** can be synthesized in 89% yield (Scheme 7).[81,243] Monoacetylated

Scheme 7

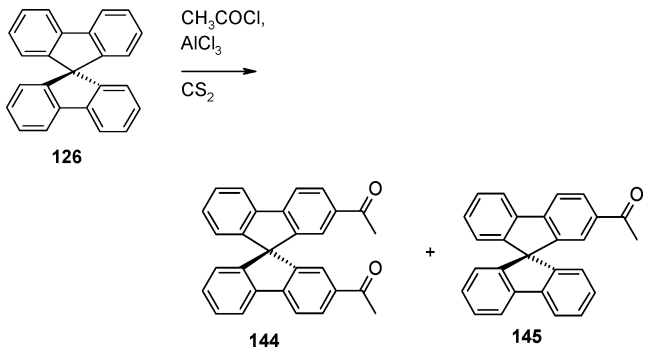

byproduct **145**, in some cases also traces of spirobifluorene **126**, 2,2′,7-triacetyl-9,9′-spirobifluorene **146**, and 2,2′,7,7′-tetraacetyl-9,9′-spirobifluorene **147** were found.[81,243] The ratio of mono- to bisacetylation can be controlled by stoichiometry. The occurring byproducts can easily be separated from the main product by chromatography. Recrystallization, as described in the literature,[243] does not work properly according to our experience.

Compound **144** can be easily converted into heterocycles, for example, oxadiazole derivatives.[113] On the other hand, it is also possible to halogenate the 7,7′-positions by direct electrophilic aromatic substitution, because the 2,2′-positions are already blocked. Using this procedure, the 2,2′-diacetyl-7,7′-dibromo-9,9′-spirobifluorene **148** was first prepared by Alcazar et al. in 77% yield.[244] Derivative **148** is a good precursor for the synthesis of "left-right asymmetric" spiro compounds.[113] Compound **144** can also be converted into the ditriflate **149** in few steps with a high overall yield (Scheme 8).[222,239] The procedure is similar to that reported by Cheng et al. for the synthesis of 9,9′-spirobifluoren-1,1′-ditriflate **150**.[245] The aryltriflates possess a reactivity similar to arylbromides during Suzuki coupling reaction[246] and can therefore replace the halogenides in some cases.

Applying Baeyer−Villiger oxidation with *meta*-chloroperbenzoic acid, one can convert the bisacetyl derivative **144** into the bisacetoxy-spiro compound **151** in yields between 73% and 91%.[222,239,243] The 2,2′-dihydroxy-9,9′-spirobifluorene **152** can then be prepared nearly quantitatively by following alkaline saponification of the ester functions.[81,222,239]

When spirobifluorene is identically substituted only in the 2- and 2′-positions, the symmetry is C_2, and the corresponding compounds exist in two enantiomeric forms. The described pathway leads to a racemic mixture of both enantiomers.[222] Toda et al. separated the (+)-enantiomer, (+)-**152**, in 90% yield and 100% ee from the racemic mixture

Scheme 8

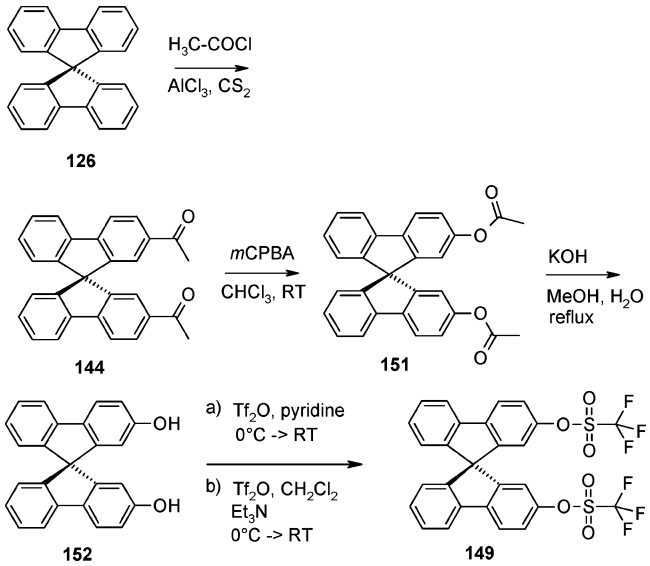

by clathrate formation with (*R*,*R*)-(+)-2,3-dimethoxy-*N*,*N*,*N*,*N*-tetracyclohexylsuccindiamide.[247]

The absolute configuration, hitherto unknown, was determined recently by Lützen and co-workers using X-ray crystal structure analysis of the clathrate.[222] They found that the (+)-enantiomer, (+)-**152**, has the (*R*)-configuration applying the rules for central chirality.[248−251] They were also able to isolate the (*S*)-configured (-)-enantiomer, (−)-**152**. The spiro-bistriflates (*rac*)-**149**, (+)-**149**, and (−)-**149** can then be prepared in high yields from racemic or enantiomerically pure spiro-diols (*rac*)-**152**, (+)-**152**, and (-)-**152**. Our group prepared (*rac*)-**149**[239] using trifluoromethane sulfonic acid anhydride in pyridine.[252] Lützen and co-workers used a slightly modified procedure from Abad et al.[253] to synthesize both enantiomeres of **149**, starting from the enantiomerically pure spirodioles (±)-**152** or (−)-**152**.[222] The main advantage of the triflate pathway is the possibility of separation of the enantiomers on the spiro-diole step, thereby enabling the synthesis of enantiomerically pure final compounds.

5.3.3. Precursors with Other Substitution Patterns

In recent years, spirobifluorenes with new substitution patterns have been reported by several groups.[124,245,254,255] Common to all these syntheses is that the starting materials are methoxy-substituted biphenyl derivatives. Lee et al. reported the synthesis of a spirobifluorene core with ether groups in the 3′ and 6′ positions, while the positions 2 and 7 in the second spiro-half are substituted with either bromide **153** or boronic acid functions **154**.[124]

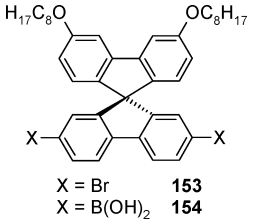

Cheng et. al described a new synthesis for the 1,1′-substitution pattern.[245,254] The methoxy groups in 1,1′-dimethoxy-9,9′-spirobifluorene **155** were cleaved to hydroxy functions using boron tribromide. They obtained both enan-

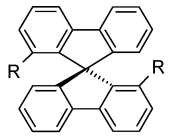

R = OMe **155**
OH **(rac)/(+)/(-)156**
OTf **(+)/(-)150**

tiomers of the 9,9′-spirobifluorene-1,1′-diol **156** in 99% e.e. by inclusion resolution with 2,3-dimethoxy-*N*,*N*,*N*′,*N*′-tetracyclohexylsuccinamide. The enantiomerically pure compounds (+)-**156** and (−)-**156** were converted into bistriflates (+)-**150** and (−)-**150** for further reactions in the 1,1′-positions.

Fournier et al.[255] were able to prepare 3,3′,6,6′-tetrasubstituted spirobifluorenes. After spiro linkage from a fluorenol derivative, the 3,3′,6,6′-tetramethoxy-9,9′-spirobifluorene **157**

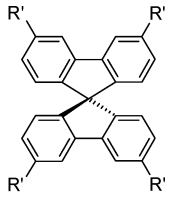

R' = OMe **157**
OH **158**
OTf **159**

was obtained, cleaved to the tetraphenol **158** by a similar procedure as for **156**, and then converted to the tetratriflate **159**.

5.4. Spiro Compounds Containing Oligoaryls

It is well-known that with increasing number of phenyl units, the solubility of *para*-oligophenyls decreases drastically, along with a growing tendency to crystallize.[77] Spiro-linked *para*-oligophenyls up to a chain length of 10 phenyl rings exhibit considerably higher solubility than their corresponding parent compounds.[77,88,256]

The synthesis of spiro-4Φ **9** and spiro-6Φ **2** involves Suzuki coupling[257] of phenyl- or biphenylboronic acid with the tetrabromo compound **127**.[59] Compounds **9** and **14** can be iodinated selectively to **160** and **161** and further coupled with phenyl- or biphenylboronic acid yielding spiro-8Φ **10** and spiro-10Φ **11** (Scheme 9).[59]

The spiro-linked *para*-terphenyl 2,2′-diphenyl-9,9′-spirobifluorene (*rac*)-**26**, as the first member of spiro-linked oligophenyls with an odd number of phenyl rings along the chains, has been synthesized in our group starting from the racemic bistriflate (*rac*)-**149** in 94% yield (Scheme 10).[239]

Recently, Thiemann et al. synthesized some derivatives of spiro-terphenyl **26**, starting from the enantiomerically pure spirodiols (*R*)-**152** and (*S*)-**152** applying the same synthetic strategy.[222]

To enhance the morphologic stability of these spiro-linked oligophenyls, we used two further modifications. On one side, additional substituents in the 4- and 4′-positions result in spiro-oligophenyls with an octahedric, globular structure, increasing not only the glass transition temperature and therefore the stability of the amorphous state but also the solubility of the compounds. These so-called "spiro-octahedric" compounds spiro-octo-1 **23** and spiro-octo-2 **24** have been synthesized with starting compound 2,2′,4,4′,7,7′-

Scheme 9

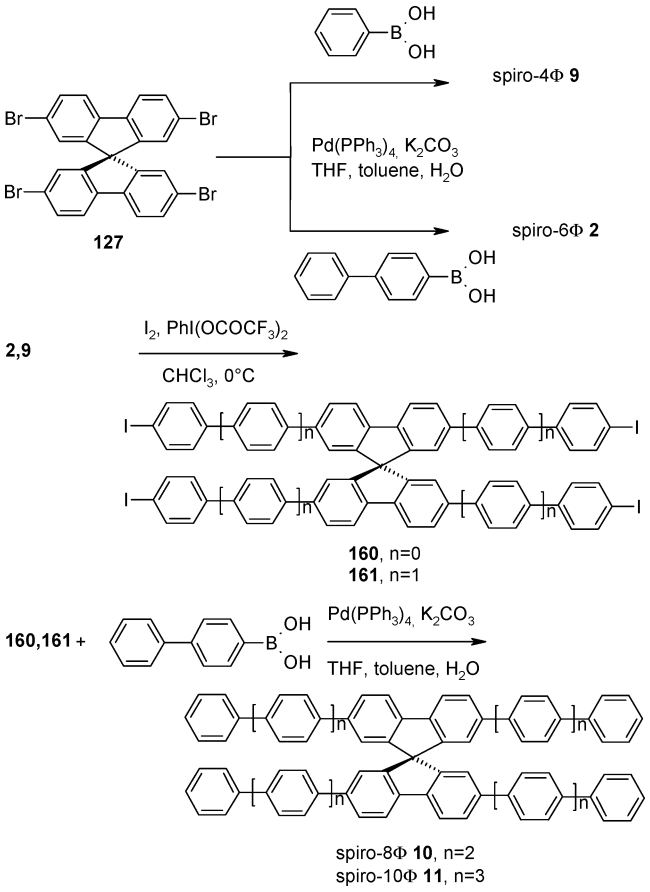

Scheme 10

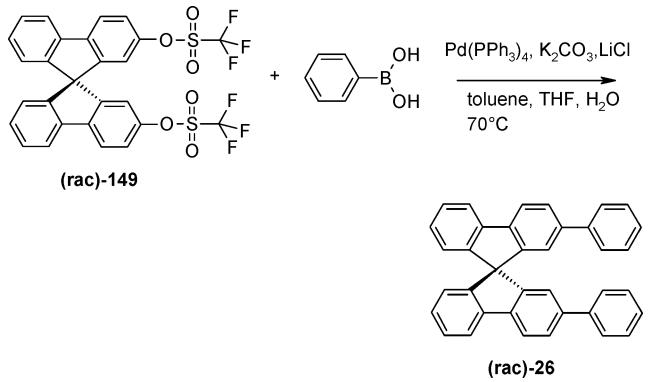

(rac)-149

(rac)-26

hexabromo-9,9′-spirobifluorene **129** through 6-fold Suzuki coupling.[59,77,88] Compound **23** was selectively tetraiodinated and then Suzuki coupled with biphenylboronic acid to yield spiro-octo-3 **25** (Scheme 11).

On the other side, a decrease of rotational freedom of the oligophenyl system was expected to enhance the optical properties, especially the fluorescence quantum yield in neat films, and also the morphologic stability. This led to the development of the "starburst" spiro-oligophenyles 4-spiro[2] **5**, 4-spiro[3] **12**, 4-Ph-spiro[2] **87**, and 6-spiro[2] **88**.[59,145] Moreover, the terminal fluorene units in these compounds act as spacers, which prevent interaction between the main oligophenyl chains of adjacent molecules in the solid state. In the case of **12**, the molecular periphery around the central pentafluorene chains leads to an energetic gradient, in which excitation energy can be transferred radiationlessly from the outer fluorene units via the intermediate sexiphenyl to the central deciphenyl chains (photonic funnel).

Scheme 11

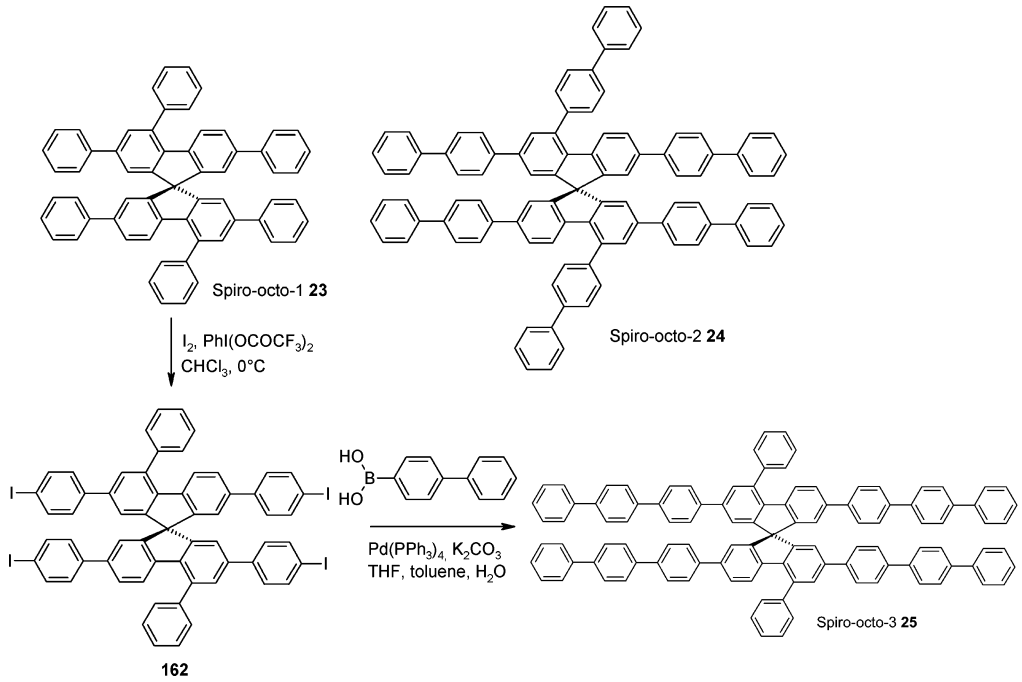

Scheme 12

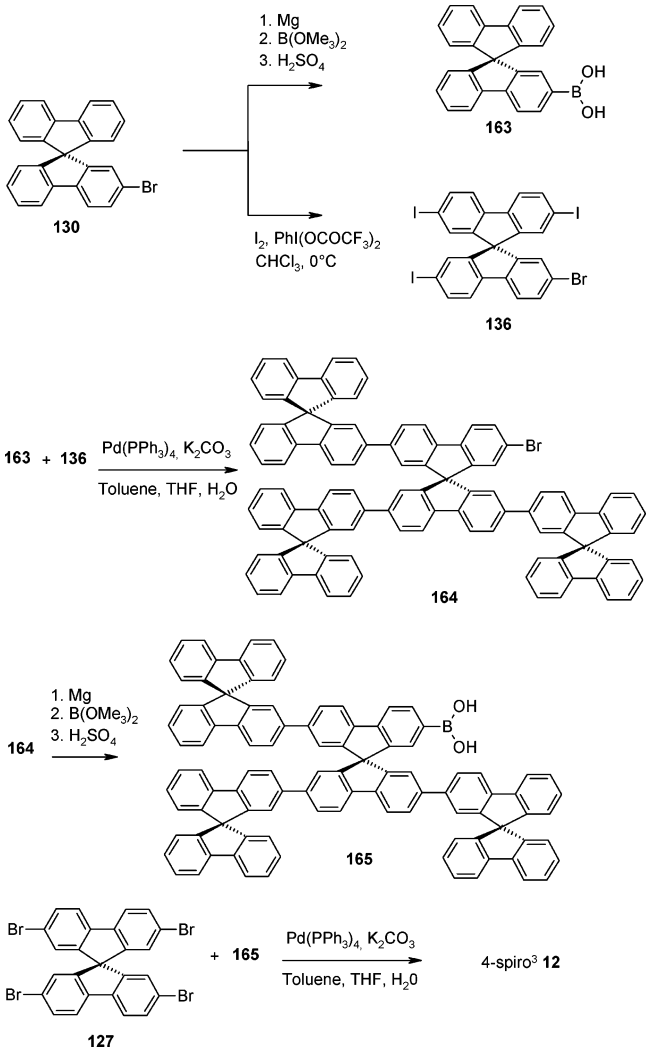

All mentioned "starburst" spiro-oligophenyls are finally synthesized by coupling 9,9′-spirobifluorene-2-yl-boronic acid **163** with halogenated spirobifluorene precursors. The syntheses of 4-spiro[2] **5** and 6-spiro[2] **88** start from the tetra-**127** and hexabromospirobifluorene **129**, respectively, while the halogeno compound in the synthesis of 4-Ph-spiro[2] **87** consists of a 4-fold iodinated spiro-quaterphenyl **166**, which was prepared similarly to **162**.[59] The synthesis of 4-spiro[3] **12** is shown in Scheme 12.

Further oligo spirobifluorenes and oligo(9,9-diarylfluorenes) were reported by Wong and co-workers.[105,106,134] The synthesis of 2,7′-bisfluorenyl-substituted spirobifluorenes TDAF-1 **52**, **168**, **169**, and **170** started from spirobifluorene-2,7-diboronic ester **167**, which was subsequently Suzuki-coupled with either 2-bromo-spirobifluorene **130** or different 2-bromo-9,9′-diaryl-fluorenes (Scheme 13).[134] Syntheses of bis-(9,9′-spirobifluorene) B2 **96** and quater-(9,9′-spirobifluorene) B4 **97** also have been reported.[106,134,183]

The synthesis of 2,2′-bisfluorenyl-substituted spirobifluorenes started from 2,2′-diiodo-9,9′-spirobifluorene **142** with subsequent Suzuki coupling employing diarylfluorene boronic esters **171** or **172** to yield the target compounds SSS **27** and TST **124** (Scheme 14).[105]

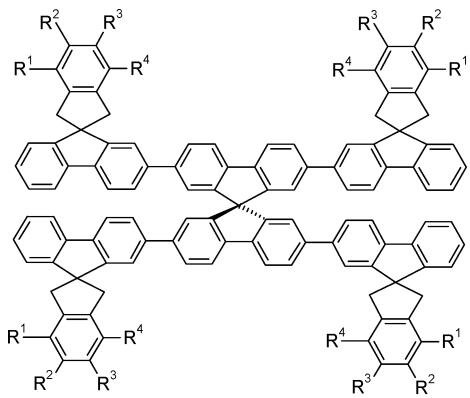

173, $R^1=R^2=R^3=R^4=H$
174, $R^1=R^2=Ph$, $R^2=R^3=H$
89, $R^1=R^2=R^3=R^4=Ph$

Scheme 13

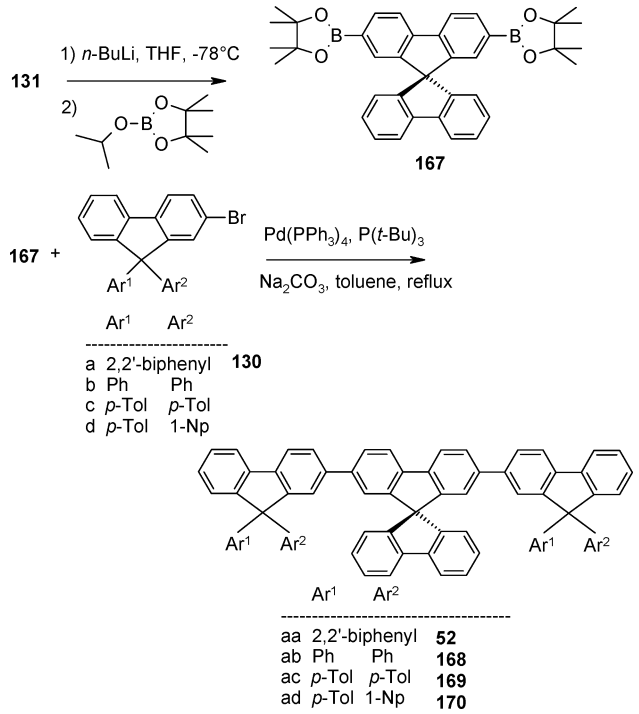

Scheme 14

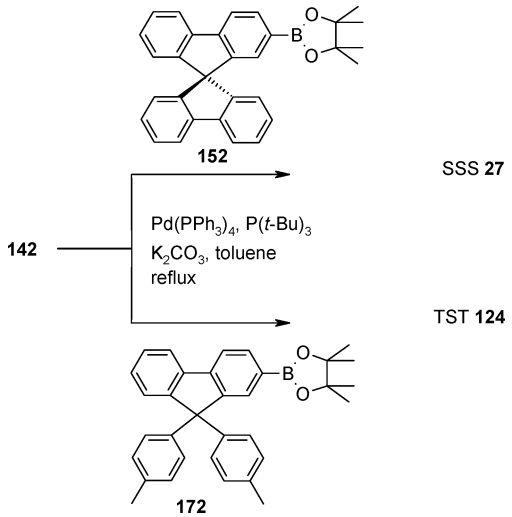

Rothberg and co-workers reported spiro-linked terfluorenes **89**, **173**, and **174**[139] and spiro-linked ter-, penta-, and heptafluorenes with alkyl side chains **175**−**179**.[96]

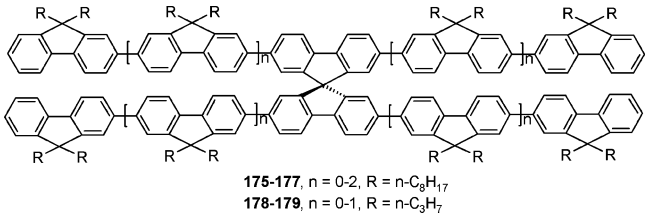

Several other groups have also prepared spiro compounds containing oligoaryl moieties. Kim et al. synthesized TBSA **180** by Suzuki coupling of 2-bromo-(2′,7′-di-*tert*-butyl)-9,9′-spirobifluorene **133** and anthracene-9,10-diboronic acid.[233] Other anthracene-containing spiro compounds have been described by Shen et al. (spiro-FPA **36**)[111] and Gerloff et al. (spiro-DPA **37**).[112]

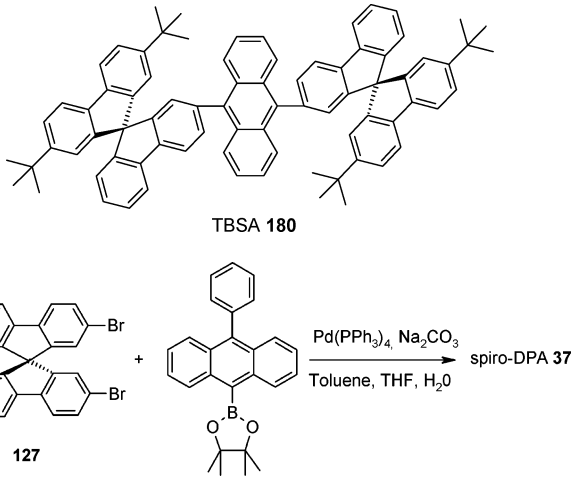

Tao et al. prepared the 2-fold 2,7-pyrene-substituted spiro compound SDPF **51**.[117] Cao et al. prepared the spiro-bridged bistruxene derivative **64** and compared it with compounds containing other bridges.[125]

Recently, Horant et al. reported the synthesis of dispirofluorene−indenofluorenes (DSFIF) **67**, **68**, and **69**, for which three different synthetic approaches have been described in the literature (Scheme 15).[127] The double spiro connection starting from different fluorenol precursors was achieved by using the original procedure taken from Clarkson and Gomberg.[218]

Kimura et al. reported the synthesis of the trispirocyclic compounds **181** and **182** (Scheme 16).[258] The corresponding synthesis was similar to that of dispirofluorene−indenofluorene **67**.[127]

Reports of compounds with substitution patterns other than in the 2,2′,7,7′-positions of spirobifluorene are rare. Lee et al. used octyloxy groups in the 3′- and 6′-positions to increase the solubility, varying the length of the *para*-oligophenyl chain in the other molecular half, **61**−**63**.[124]

5.5. Spiro Compounds with Stilbene and Azobenzene Units

A spiro-compound with stilbene units is spiro-DPVBi **19**, which was synthesized in 52% yield by Suzuki-coupling of 2,2-diphenylvinylboronic acid and 2,2′,7,7′-tetrabromo-9,9′-spirobifluorene **127**, as shown in Scheme 17.[206] The synthesis of the 2,7-substituted derivate DPVSBF **122** has been reported by Wu et al.[259] Spiro-ADA **92**, which contains four phenylazodiphenylamine groups, was synthesized by Hartwig−Buchwald coupling of 4-(phenylazo)diphenylamine and **127** in 89% yield.[148]

5.6. Spiro Compounds Based on Arylamines

Aromatic amines are widely studied and used as hole transport materials in organic electronics. The electronic characteristics like energy levels (redox potentials) and charge carrier mobilities can be adjusted by the substitution pattern of the aryl substituents. Spiro-linked arylamines can be prepared in high yields, either by Hartwig−Buchwald coupling[260] of secondary amines and halogenated spiro-precursors or by copper-promoted Ullmann coupling reaction. The synthesis of spiro-linked tetraamines is outlined in Scheme 18. The corresponding spiro arylamino compounds are spiro-TAD **4**, spiro-α-NPB **15**, spiro-PhOx-TAD **16**, spiro-PhTh-TAD **17**, spiro-Carb **18**, spiro-MeO-TAD **73**,

Scheme 15

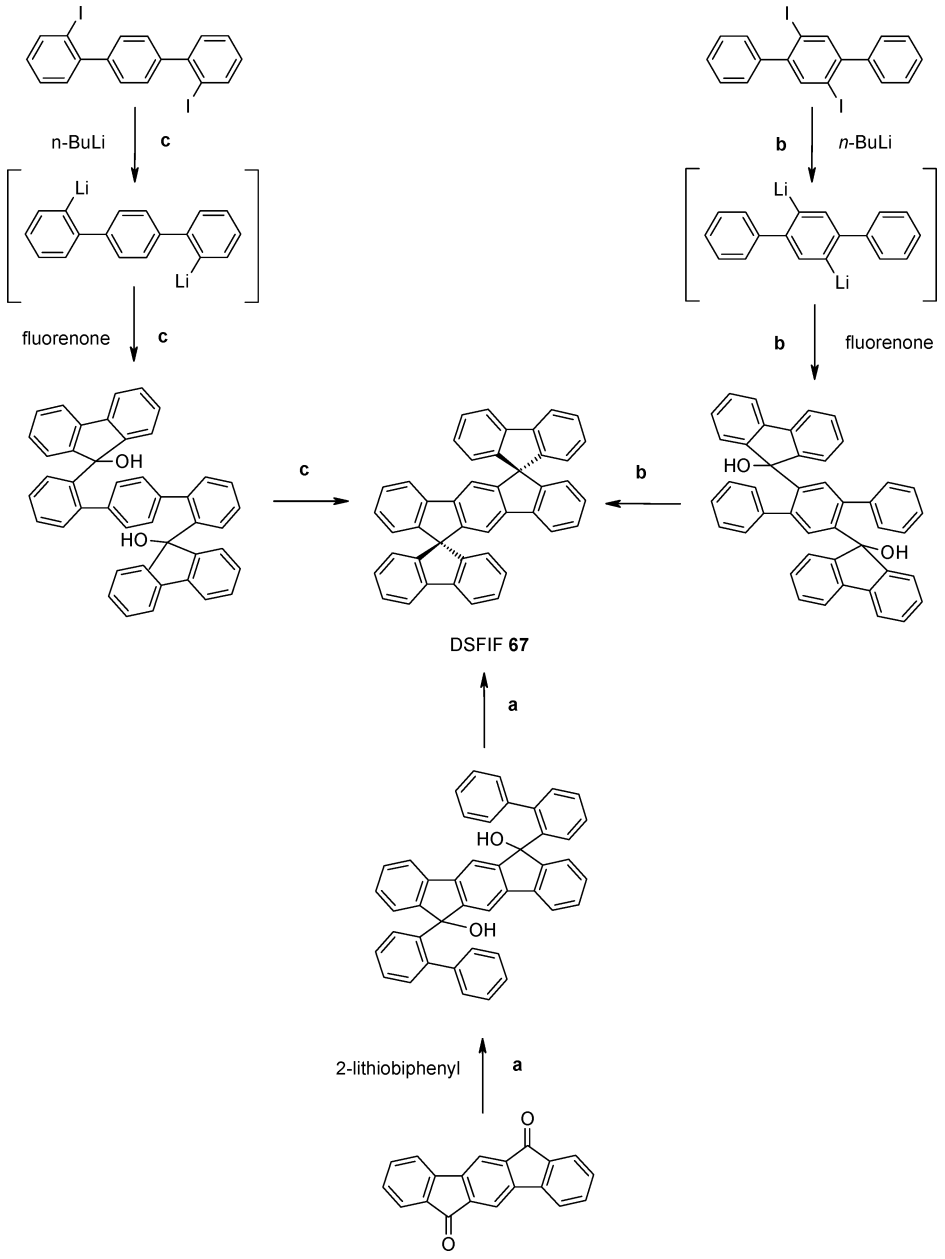

Scheme 16

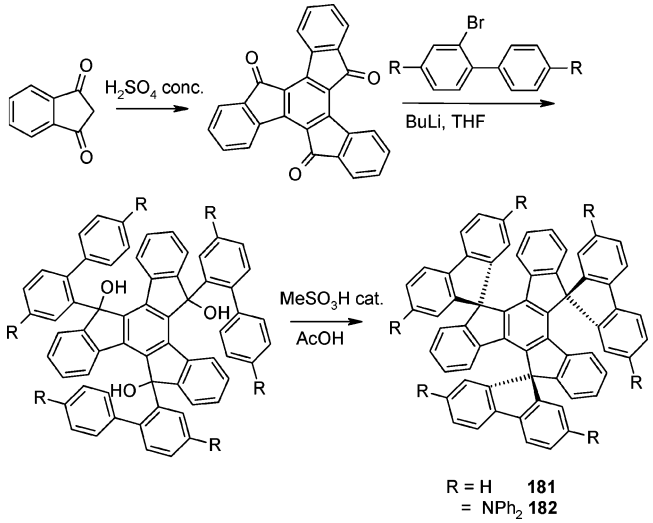

spiro-TTB **74**, spiro-TPD **76**, spiro-*m*-TTB **95**, spiro-*β*-NPB **183**, spiro-MeO-TPD **184**, and spiro-MeMeO-TAD **185**.[91]

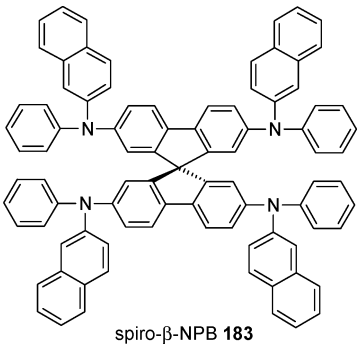

spiro-β-NPB **183**

Recently, Shen et al. reported on several 2,7-di-*tert.*-butyl-9,9′-spirobifluorene substituted arylamino derivatives (compounds **108** and **186**−**199**, Chart 1).[207]

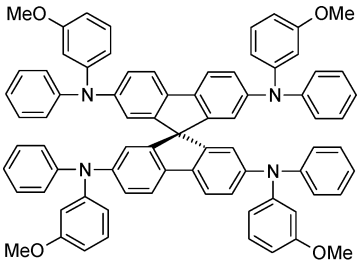

spiro-MeO-TPD **184**

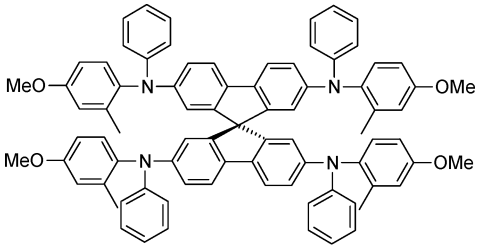

spiro-MeMeO-TAD **185**

The precursors [(2′,7′-di-*tert*-butyl)-9,9′-spirobifluoren-2-yl]-phenyl-amine **200** and *N*,*N*′-diphenyl-[(2′,7′-di-*tert*-butyl)-9,9′-spirobifluorene]-2,7-diamine **201** were synthesized through Hartwig−Buchwald coupling of **133** and **134**, respectively (Scheme 19).

All syntheses used Hartwig−Buchwald coupling except that of compound **199**, in which Stille coupling was utilized (Scheme 20).

5.7. Thiophene Compounds

In general, there are two synthetic pathways to build up heterocyclic spiro compounds. First, cross-coupling reactions like the Negishi, Kharash, Stille, Suzuki, or Sonogashira coupling reactions can be utilized to connect the heterocyclic subunit to the spirobifluorene core.[137] On the other hand, the heterocyclic compounds can be built up from spiro precursors containing heteroatoms. The first spiro compounds comprising oligothienylene or oligo(thienylene ethinylene) subunits as branches connected to a central core of spirobifluorene were reported by Tour and co-workers.[220,261] These compounds were synthesized by Stille and Sonogashira coupling reactions from thienylene precursors and a tetrahalogenated spiro core, as shown in Scheme 21.

Scheme 17

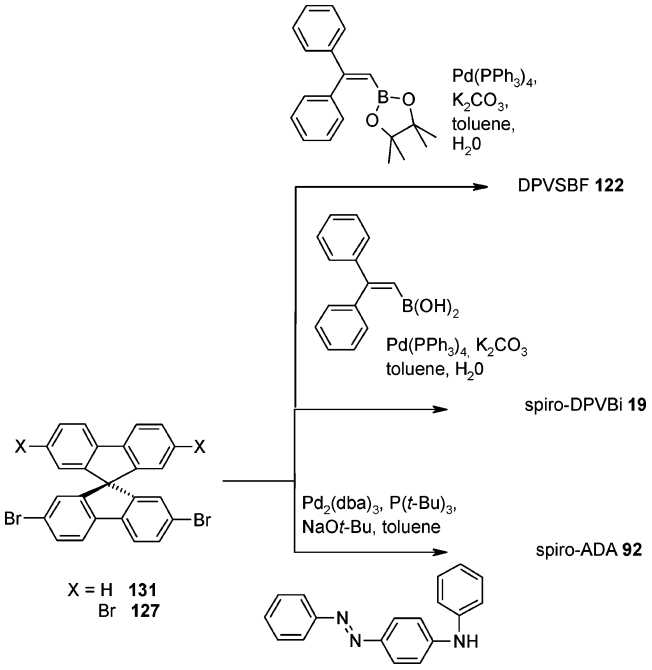

Scheme 18

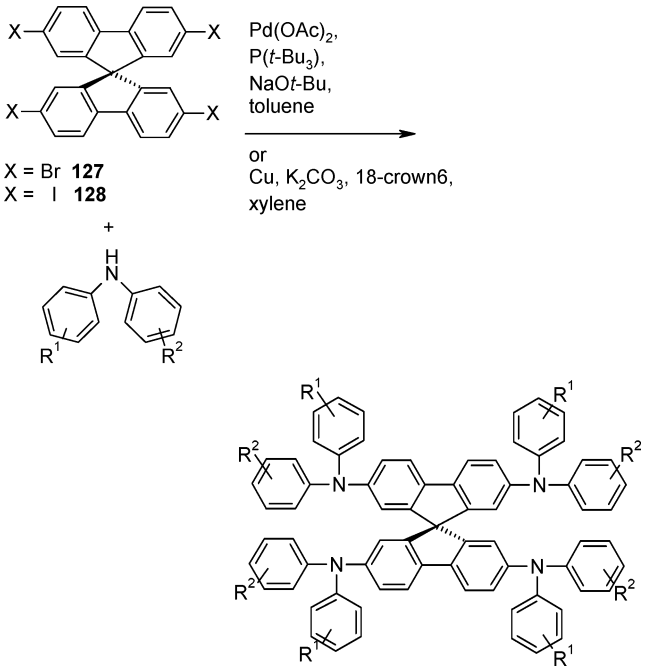

The spiro-oligothiophenes, compounds **81**−**86**, **91**, and **204**−**220**, are similar to **202**. These compounds were reported by Pei and co-workers.[137,225] They utilized the Suzuki coupling reaction to connect oligo(hexylthiophenes) and Negishi coupling to connect unsubstituted oligothiophenes to the halogenated spiro cores.[225]

5.8. Oxadiazole Compounds

Another class of compounds for use in organic electronics consists of substances containing oxadiazole units. Oxadiazole derivatives are well-known for their excellent electron-transporting capabilities, while often suffering from low glass transition temperatures and thus poor morphological stability. In contrast to the spiro compounds containing thiophene units, the oxadiazole-containing moieties were not introduced via a coupling reaction but directly built up by heterocycle synthesis between spirobifluorene-2,2′-biscarboxylic acid chloride **222** and tetrazole derivatives (or vice versa). This reaction was utilized for the preparation of the spiro-linked version, spiro-PBD **28**, of the electron-transporting compound PBD (Scheme 22).[59,87,88]

Compound **111** (Scheme 23) was recently published by Oyston et al.[209] In contrast to spiro-PBD **28**, the oxadiazole moiety was synthesized separately and then coupled by 2-fold Suzuki coupling with spirobifluoren-2,7-diboronic ester **167**.

5.9. Other N-Containing Heterocycles

The blue-emitting, pyrimidine-containing compound TBPSF **53** was synthesized by Wu et al. through Suzuki coupling of 2,7-spirobifluorene diboronic ester **167** and 5-bromo-2-(4-*tert*-butylphenyl)-pyrimidine in the presence of $Pd(PPh_3)_4$ and $P(t\text{-}Bu)_3$.[119]

The spiro-bridged bis(phenanthroline) ligand **30** for the synthesis of transition metal complexes was reported by Wu

Chart 1

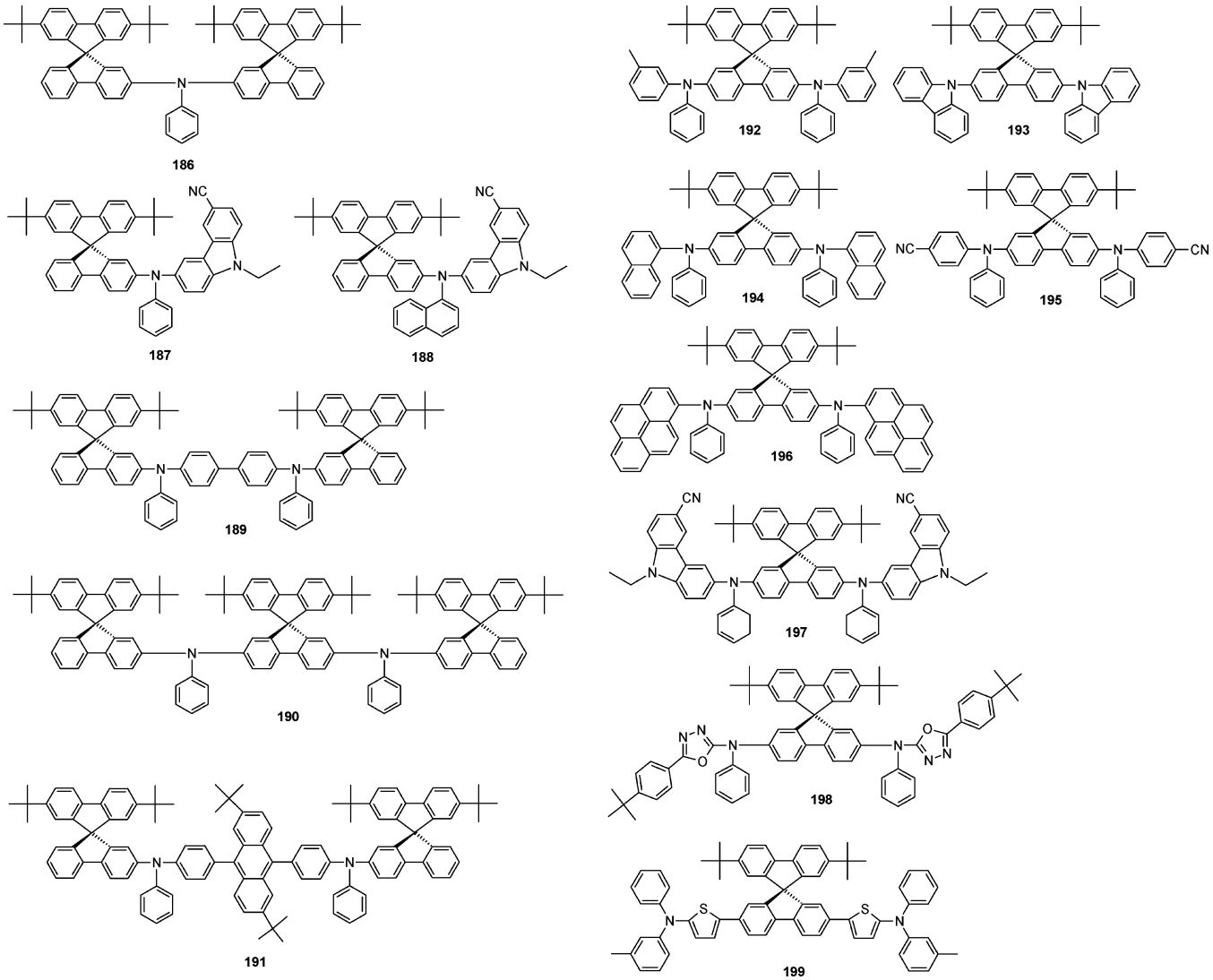

Scheme 19

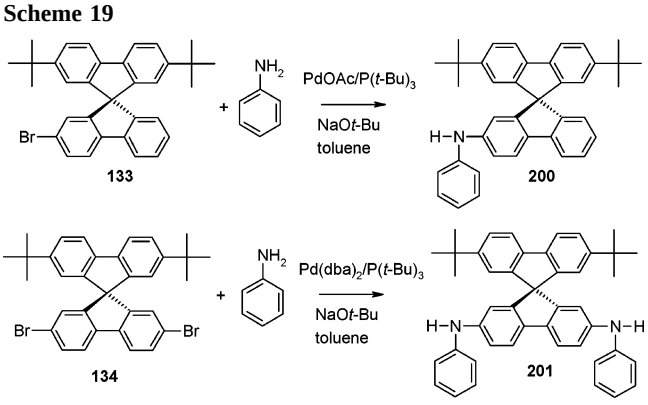

et al.[108] and Juris et al.[262] The synthetic route involves the Friedländer condensation of 2,2′-diacetylspirobifluorene **144** and 8-amino-7-quinolinecarbaldehyde, as outlined in Scheme 22. Condensation of **144** with phenylhydrazine yielded 88% of **223** (Scheme 24). To obtain **31**, the bisphenylhydrazone **223** was heated in polyphosphoric acid.[108] In addition, di- and tetra-9,9′-spirobifluorene porphyrines have been synthesized by Poriel et al.[221] as well as the corresponding manganese and iron complexes.[263,264] These compounds are promising materials as catalysts for the oxidation of alkenes

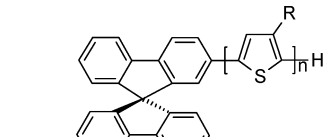

204-206: R = H, n = 1-3
207-209: R = *n*-C_6H_{13}, n = 1-3

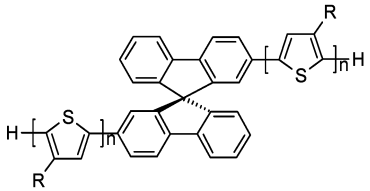

210-212: R = H, n = 1-3
213-215: R = *n*-C_6H_{13}, n = 1-3

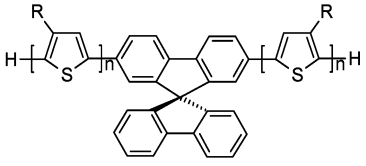

216-218: R = H, n = 1-3
219-220: R = *n*-C_6H_{13}, n = 2,3

Scheme 20[a]

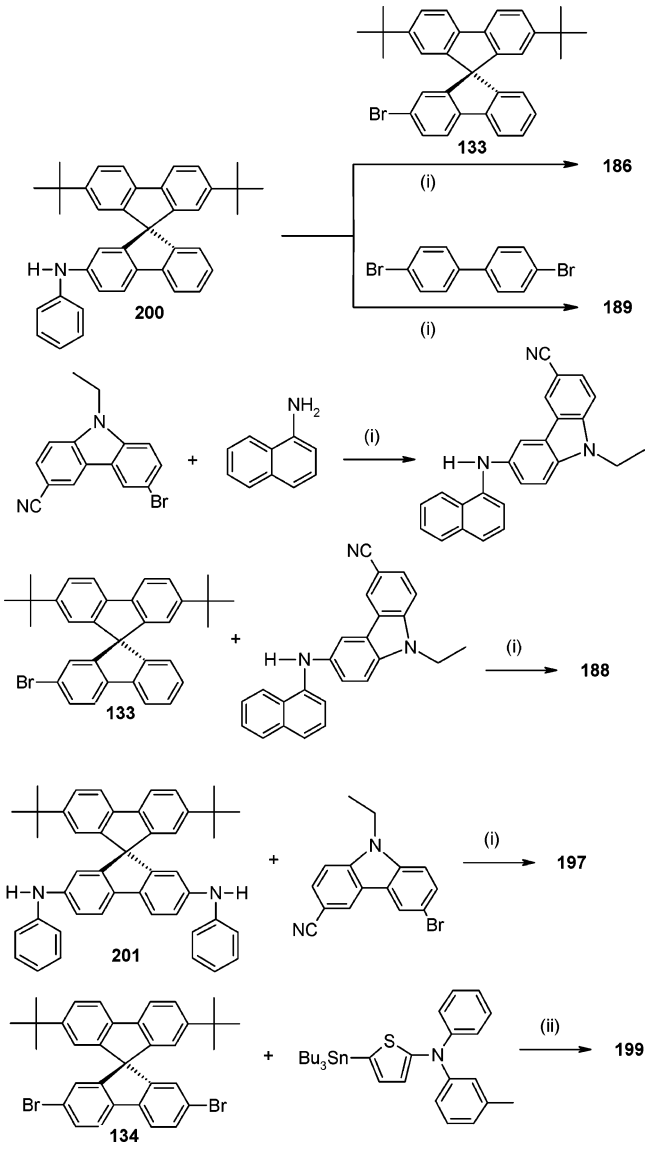

[a] Reagents and conditions: (i) 2 mol% $Pd(OAc)_2$, 2 mol% P(*t*-Bu)$_3$, NaO*t*-Bu; (ii) 2 mol% $PdCl_2(PPh_3)_2$, DMF.

by hydrogen peroxide and iodosylbenzene as oxygen atom donors.

Spiro compounds based on pyrazoloquinolines were described by Chiang et al.[265] and Chen et al.[126] The synthesis started from 2,2′-dinitro-9,9′-spirobifluorene **140** and is outlined in Scheme 25.

Fournier et al. attached aminotriazine groups in the 3-, 3′-, 6-, and 6′-positions, starting from the tetratriflate **159**, to yield **226** and **227**.[255]

5.10. Spiro Compounds with Mixed Chromophores

Mixing different chromophore units in one molecule not only gives new functional materials featuring unique properties but also enables one to learn about the interplay of the physicochemical properties of the corresponding chromophores. One possibility of connecting different chromophores with one another is through a spiro center. The combination of an electron donor and an electron acceptor group in the same molecular half is expected to influence the optical and electrical properties of the parent compounds. This leads to the general structure for vertical or "left-right" asymmetric spiro compounds with a 2,2′-A,7,7′-B substitution pattern, as shown in Figure 26.

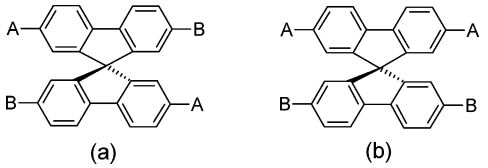

Figure 26. General structure of "left-right" 2,2′-A,7,7′-B-substituted (a) and "top-down" 2,7-A,2′,7′-B-substituted (b) asymmetric spiro compounds.

The other class of mixed spiro compounds with a horizontal or "top-down" asymmetric 2,7-A,2′,7′-B substitution pattern, is intriguing because it gives rise to the possibility of combining different functions (i.e., emitting and charge transporting properties) in one molecule, potentially reducing the necessary number of separate functional layers in an OLED.[59,107,113]

5.10.1. "Left-Right" Asymmetric (2,2′-A,7,7′-B-Substituted) Spiro Compounds

Based on the concept of "left-right" asymmetric substitution, a series of spiro-bridged emitters equipped with electron-donating arylamine groups and electron-accepting oxadiazole moieties has been reported by Pudzich et al.[59,107,113] The synthesis starts from 2,2′-diacetyl-7,7′-dibromo-9,9′-spirobifluorene **148**, which was first prepared by Diederich and co-workers.[244]

Scheme 21

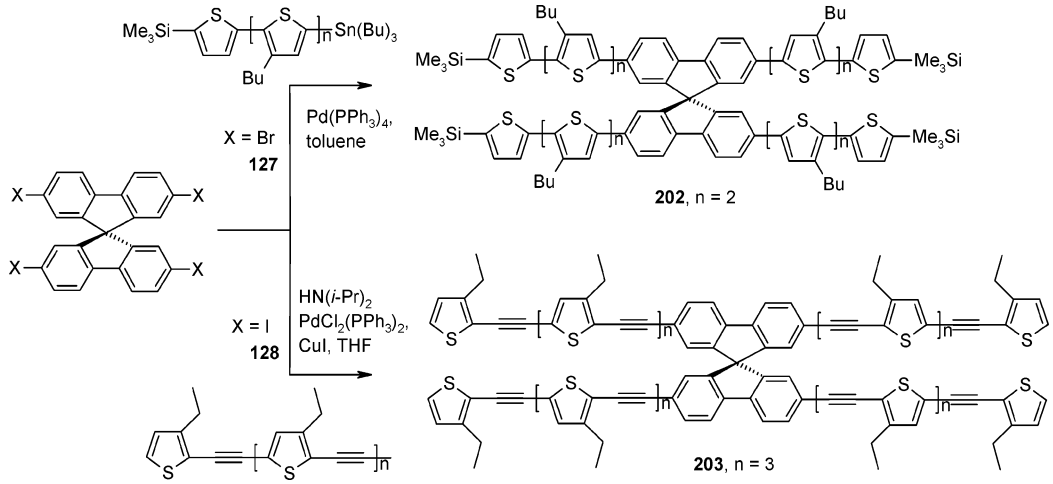

Scheme 22

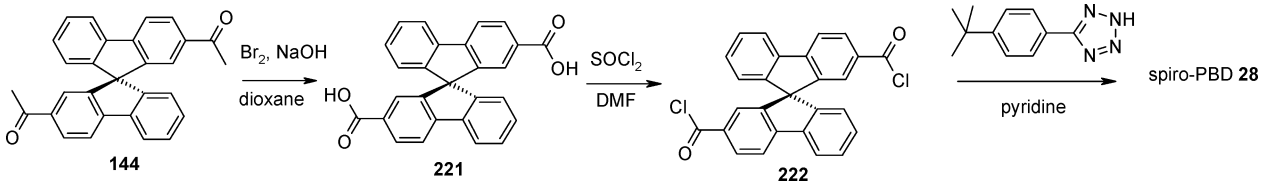

Scheme 23

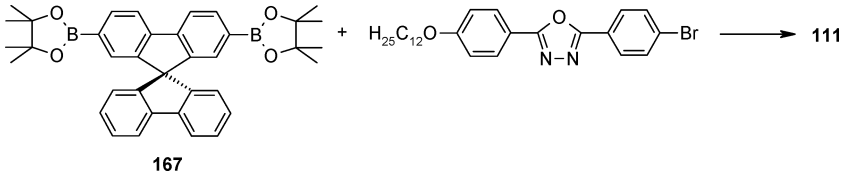

Scheme 24

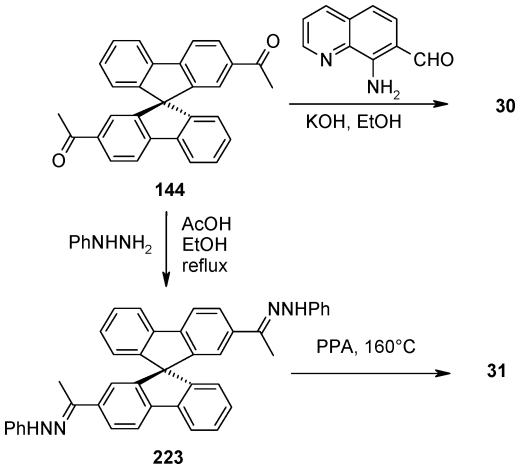

Scheme 25

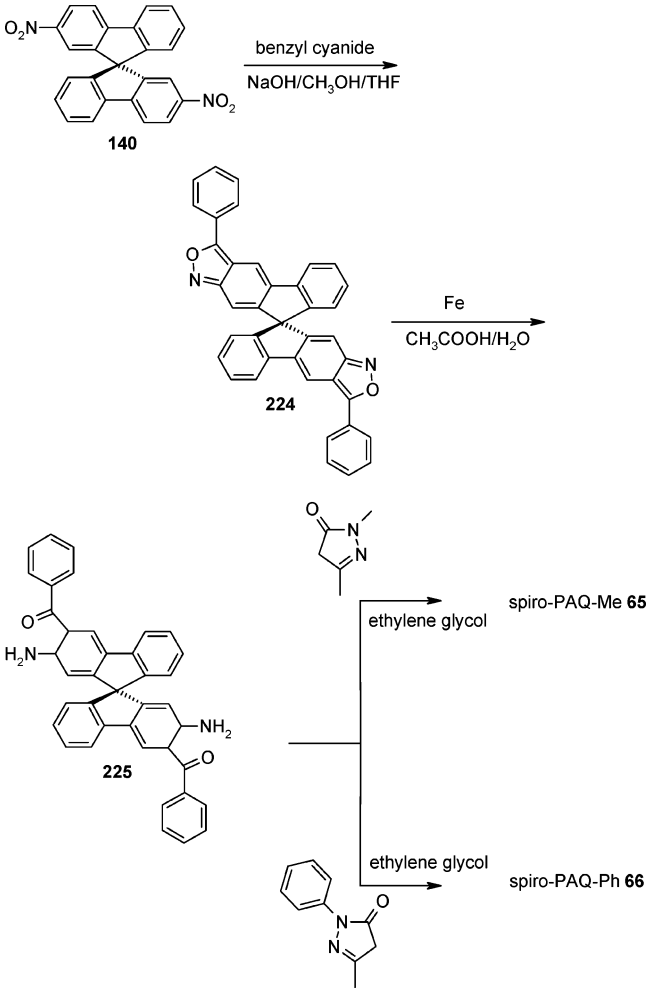

Several asymmetric spiro compounds containing oxadiazole and diphenylamine moieties have been synthesized from **148** in a similar way as spiro-PBD **28** (Scheme 26).[59] The target compounds spiro-AMO-*t*-Bu **38** and spiro-AMO-CN **40** were synthesized via the Hartwig−Buchwald reaction,[260] while spiro-AMPO-*t*-Bu **39** and spiro-AMPO-CN **41** have been prepared by the Suzuki coupling reaction.[257]

The cyano derivative spiro-CN-PBD **29** of spiro-PBD **28** was prepared in a similar way as for compound **230**, starting from 2,2′-diacetyl-spirobifluorene **144** (Scheme 22) instead of **148**.[107]

Chiang et al. recently reported a series of new spiro compounds containing donor and acceptor groups with the substitution pattern 2,2′-donor-7,7′-acceptor-9,9′-spirobifluorene.[114] DPASF **42** and CHOSF **44** were synthesized through Hartwig−Buchwald coupling of diphenylamine onto 2,2′-dibromo-9,9′-spirobifluorene **138** or its bisformylated derivative **231** (Scheme 27).

The final products BTSF **45**, BTCNSF **46**, and CNSF **47** were synthesized from the starting compound CHOSF **44** (Scheme 28). These compounds were generated in 51−69% yields under Knoevenagel conditions (basic Al_2O_3 in dry toluene). DPVSF **43** was synthesized in 87% yield from **44** using a 2-fold Horner−Wadsworth−Emmons reaction.

In addition to CNSF **47**, Chiang et al. have also prepared the half-substituted spiro compound PhSPDCV **49** and its *para*-tolyl derivative pTSPDCV **50**.[116] The synthesis started with 2,7-dibromo-9,9′-spirobifluorene **131**. After a single lithiation with a stoichiometric amount of *n*-butyllithium at −78 °C, followed by reaction with dimethylformamide and subsequent acidic hydrolysis, compound BrSPCHO **232** was obtained. Hartwig−Buchwald reaction of **232** with diphenylamine or ditolylamine yields the compound PhSPCHO **233** or pTSPCHO **234**, respectively. The final products

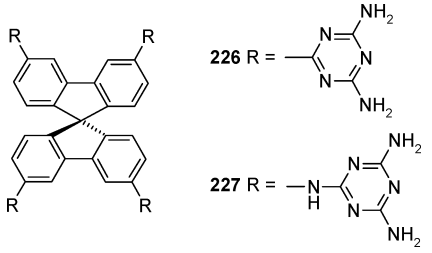

Scheme 26

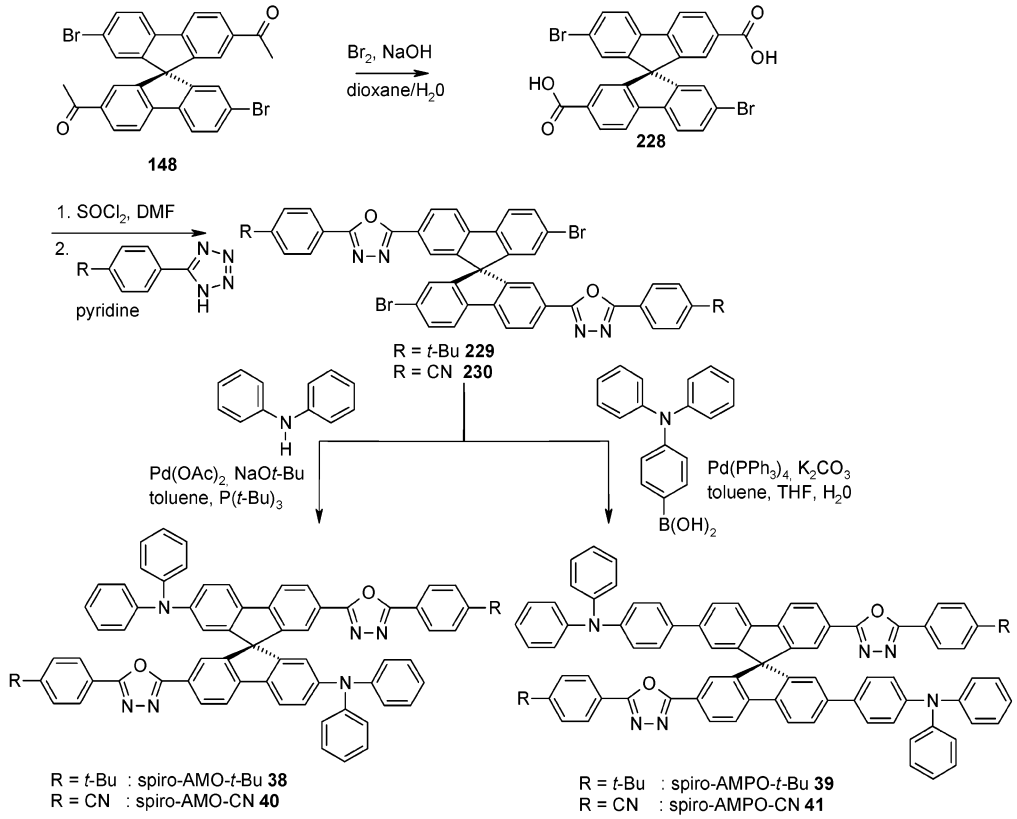

Scheme 27

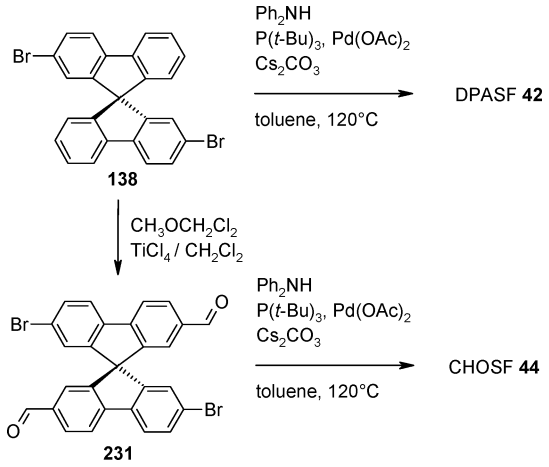

Scheme 28

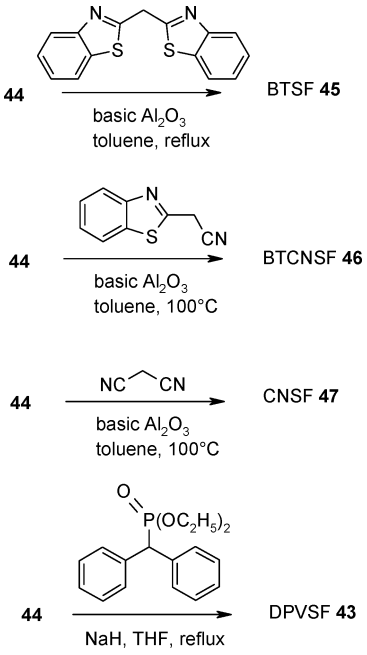

PhSP-DCV **49** and pTSPDCV **50** were obtained through Knoevenagel condensation with malononitrile (Scheme 29).

5.10.2. "Top-Down" Asymmetric (2,7-A,2′,7′-B-Substituted) Spiro Compounds

Spiro compounds based on a "top-down" asymmetric substitution pattern were initially intended to combine independent emitting and charge-transporting moieties in one molecule. A series of compounds containing combinations of hole-transporting arylamine with an oligophenyl chain as chromophore (spiro-DPSP **58** and spiro-DPSP[2] **59**), electron-transporting oxadiazole with an oligophenyl chromophore (spiro-SPO **60**), and hole-transporting arylamine with electron-transporting oxadiazole moieties (spiro-DPO **56** and spiro-MeO-DPO **72**) were synthesized by Pudzich et al.[59,107]

The precursor **235** of spiro-DPSP **58** was synthesized by selective coupling of biphenylboronic acid with **135** (Scheme 30). In the final step, spiro-DPSP **58** was obtained by Hartwig−Buchwald coupling of compound **235** with diphenylamine.[260] Using 9,9′-spirobifluorene-2-yl-boronic acid instead of biphenylboronic acid, the second generation spiro derivative of **235**, compound spiro-DPSP[2] **59** was also synthesized in our group.

The synthesis of spiro-SPO **60**, spiro-DPO **56**, and spiro-MeO-DPO **72** starts from 2,7-dibromo-spirobifluorene **131**, which was monoacetylated to obtain 2′-acetyl-2,7-dibromo-

Scheme 29

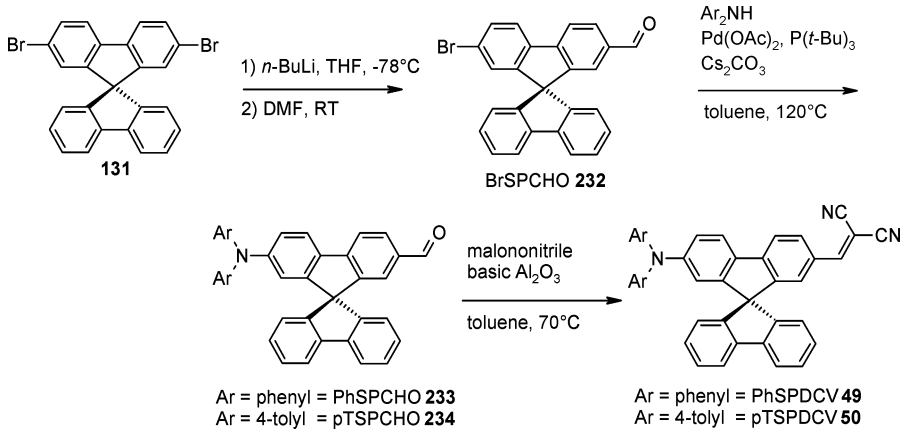

Scheme 30

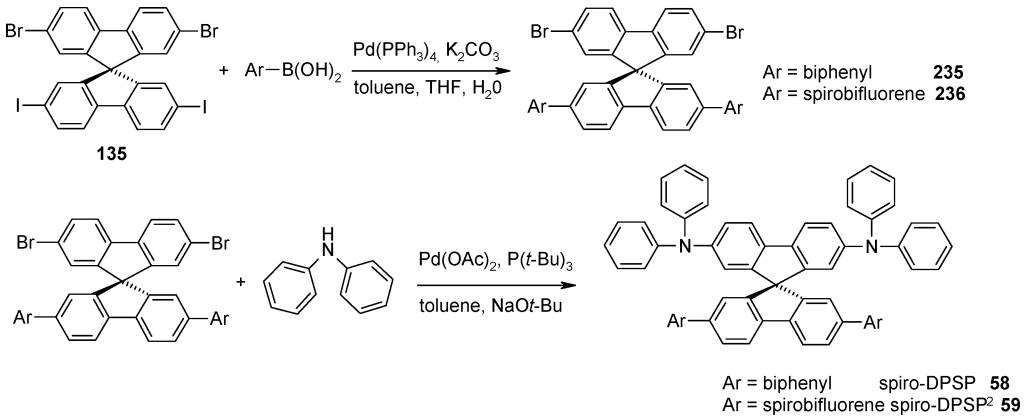

Scheme 31

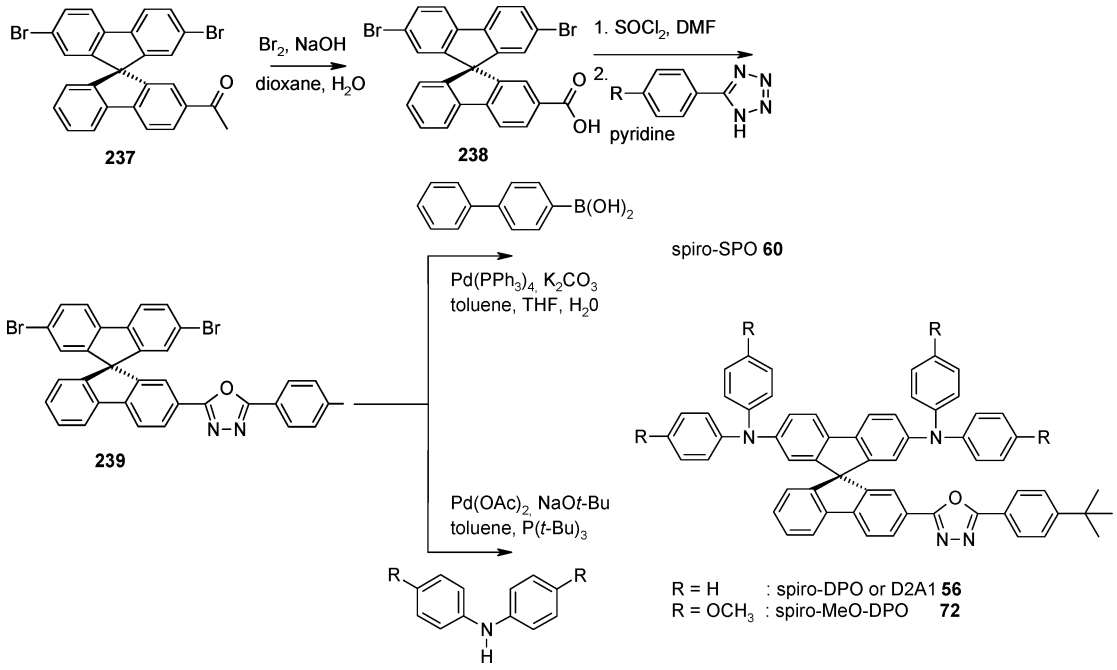

9,9′-spirobifluorene **237**. After haloform oxidation of the acetyl group, the resulting carboxylic acid **238** was used to form the oxadiazole compound **239** by reaction with *tert*-butylphenyltetrazole. Using Suzuki coupling with biphenylboronic acid, spiro-SPO **60** was obtained. Spiro-DPO **56** and spiro-MeO-DPO **72** were synthesized through coupling with diphenylamine and ditolylamine, respectively (Scheme 31).

Wong and co-workers also reported on the synthesis of mixed compounds containing a combination of electron transporter and hole transporter. Compound D1A1 **54** contains a diphenylamino moiety in one half and an oxadiazole in the other half,[120] while D2A2 **57** is composed of two diphenylamino units in one and two oxadiazole units in the other half.[120] D1A2 **55** is similar to D2A2 **57**, but it contains only

Scheme 32

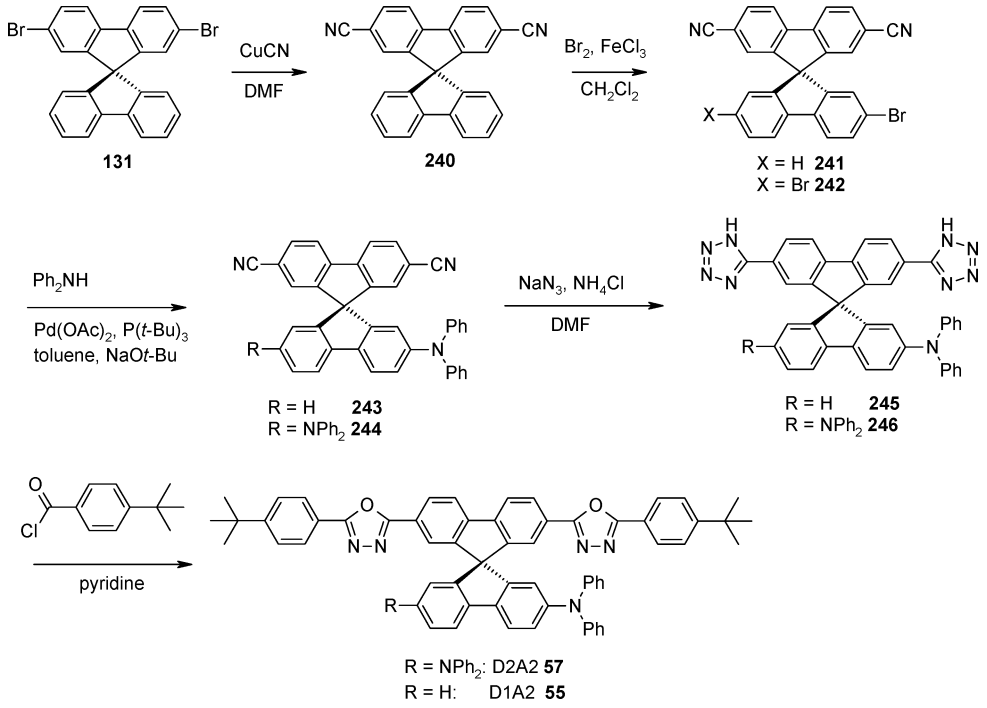

Scheme 33

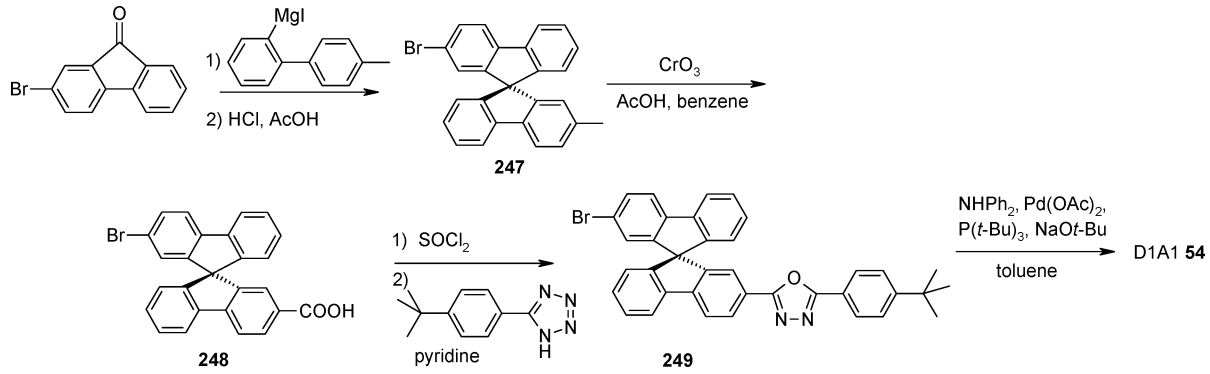

one diphenylamino unit in one half. D2A1 is, according to this nomenclature, a synonym of Spiro-DPO **56**.

In the synthesis of the "double" oxadiazoles D2A2 **57** and D1A2 **55**, Wong and co-workers used a different strategy. Instead of introducing two carboxylic acid moieties, they formed the bistetrazoles **245** and **246** from the corresponding dicyano precursors **243** and **244**, respectively (Scheme 32).[120,121]

Another pathway was used to synthesize D1A1 **54**.[121] By introducing a methyl and a bromine group in the precursors before spiro linkage, Wong et al. prepared the bromo methyl spirobifluorene **247**. After oxidation of the methyl group to the carboxylic acid **248**, the oxadiazole **249** was generated as usual, and in the last step, amination yielded D1A1 **54** (Scheme 33).

The model compounds D1 **250** and D2 **98** were simply synthesized by Hartwig−Buchwald reaction of diphenylamine with **130** or **131**, respectively. Compounds A1 **77** and A2 **78**, which were used for comparison, also started from **130** or **131**, respectively, and were synthesized via a similar pathway described in Scheme 32.

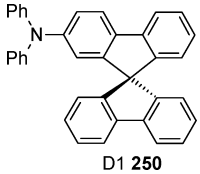

D1 **250**

5.11. Spirosilabifluorenes

Replacing the central carbon atom in spirobifluorene with silicon results in 9,9′-spirobi(9*H*,9-silafluorenes) or 5,5′-spirobi(dibenzosiloles). The synthesis of the neat core 9,9′-spirobi(9*H*,9-silafluorene) **251** was first reported 1958 by

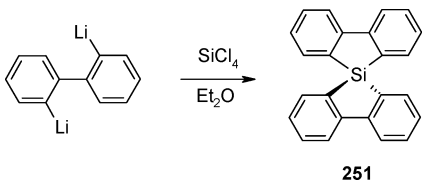

251

Gilman et al. yielding 56% starting from 2,2′-dilithiobiphenyl.[266] Starting from 2,2′-dibromobiphenyl several groups reported yields for **251** between 63% and 85%.[267−269]

A similar strategy was used by Lee et al. to prepare the aryl-substituted asymmetric spirosilabifluorene derivatives

32−**35**, starting from substituted 2,2′-dibromobiphenyl derivatives.[109,270]

6. Tables of Properties

For comparison, the thermal, optical, and electrical properties of the spiro compounds reported so far are summarized comprehensively in Tables 7−11.

7. Conclusion

By the spiro concept, morphologically stable amorphous glasses are obtained. With respect to the parent compounds that consist of only one half of the spiro compounds, the glass transition temperature is significantly increased. The comparatively high solubility is advantageous in many processing steps, for example, chemical purification and film deposition from solution. The perpendicular arrangement of chromophores via a spirobifluorene core retains the ground-state properties of the chromophores to a large extent, but for asymmetric spiro compounds in the excited state, interesting features such as photoinduced charge transfer have also been demonstrated. As far as the electrical properties are concerned, the oxidation and reduction potentials, especially the second ones, may be strongly influenced by the second half of the molecule. In this review, we presented a comprehensive overview of the basic physicochemical properties of spirobifluorene-based compounds in solution and in the solid state and their applications in optoelectronics. The range of potential applications based on these materials spans the whole field of thin film devices from organic transistors, photodetectors, and solar cells to organic light-emitting diodes and lasers. Important synthetic pathways to precursors as well as target compounds were also presented.

8. Acknowledgment

We would like to acknowledge our colleagues and coworkers K. Onken, J. Londenberg, I. Suske, and T. Ebert for their comments, support, and discussion.

Table 7. Absorption (λ_{Abs}), Fluorescence Maxima (λ_{Em}) and Fluorescence Quantum Yield (Φ_F) of Spiro Compounds in Dilute Solution

compounds	solvent	λ_{Abs} (nm)	λ_{Em} (nm)	Φ_F (%)	ref
spiro-6Φ **2**	CH_2Cl_2	342	385, 406	95	77, 87, 88
	C_6H_{12}	340	381	98	89
spiro-TAD **4**	CH_2Cl_2	375, 306	403		91
	CH_2Cl_2	378	402		87, 89
	C_6H_{12}	379	394, 413	42	89
4-spiro[2] **5**	CH_2Cl_2	353, 309, 298[a]	396, 418		91
	C_6H_{12}	350	393, 413	96	89
spiro-4Φ **9**	CH_2Cl_2	332	359, 378		87
	$CHCl_3$	334	362, 378	92	92
spiro-8Φ **10**	CH_2Cl_2	344	395, 416	95	77, 87
spiro-10Φ **11**	CH_2Cl_2	344	402, 420[a]	95	77, 87
4-spiro[3] **12**	CH_2Cl_2	358, 309, 297[a]	413, 435		91
spiro-6Φ$(MeO)_4$ **13**	CH_2C_{l2}	353	392, 412		89
	C_6H_{12}	343	387, 405	87	89
spiro-α-NPB **15**	CH_2Cl_2	378, 350,[a] 291,[a] 270	485		91
spiro-PhOx-TAD **16**	CH_2Cl_2	387,[a] 335,[a] 310, 266[a]	491		91
spiro-PhTh-TAD **17**	CH_2Cl_2	330,[a] 312, 300	511		91
spiro-Carb **18**	CH_2Cl_2	340, 290	372		91
	CH_2Cl_2	340	372		89
	C_6H_{12}	347	363, 380	83	89
spiro-DPVBi **19**	CH_2Cl_2	377	453		89
	C_6H_{12}	375	452	82	89
spiro-octo-2 **24**	CH_2Cl_2	345	397, 412		89
	C_6H_{12}	343	396	95	89
spiro-octo-3 **25**	CH_2Cl_2	277, 348	401, 421[a]		88
SSS **27**	$CHCl_3$	310, 333	367, 387		105
spiro-PBD **28**	CH_2Cl_2	330	373		89
	C_6H_{12}	328	370	75	89
spiro-CN-PBD **29**	CH_2Cl_2	314, 337	404	50	107, 113
30	CH_3CN	331, 361	385	48	108
31	CH_3CN	343	404	75	108
33	$CHCl_3$	315	393		109
34	$CHCl_3$	317	382		109
35	$CHCl_3$	307	383		109
spiro-FPA **36**	C_7H_8		425		111
spiro-DPA **37**	CH_2Cl_2	360, 378, 399	429, 443[a]		112
spiro-AMO-*t*-Bu **38**	CH_2Cl_2	302, 389	477	62	107, 113
	C_6H_{12}	397	411, 434	56	89
spiro-AMPO-*t*-Bu **39**	CH_2Cl_2	306, 337, 374	497	70	107, 113
	C_6H_{12}	374	416, 441	58	89
spiro-AMO-CN **40**	CH_2Cl_2	304, 400	541		107, 113
spiro-AMPO-CN **41**	CH_2Cl_2	312, 340, 383	540		107, 113
DPASF **42**	C_6H_5Cl	353	401	24	114
DPVSF **43**	C_6H_5Cl	385	480	50	114
CHOSF **44**	C_6H_5Cl	402	495	46	114
BTSF **45**	C_6H_5Cl	433	549	∼0	114
BTCNSF **46**	C_6H_5Cl	464	601	14	114
CNSF **47**	C_6H_5Cl	481	620	31	114
PhSPDCV **49**	C_6H_{14}		500		116
	$C_6H_8O_2$		572	70	116
	CH_3Cl		624		116

Table 7 (Continued)

compounds	solvent	λ_{Abs} (nm)	λ_{Em} (nm)	Φ_F (%)	ref
pTSPDCV **50**	C_6H_{14}		516		116
	$C_6H_8O_2$		598	75	116
	CH_3Cl		658		116
SDPF **51**	CH_2Cl_2	364	422	78	117
TDAF-1 **52**	CH_3CN/C_6H_6 (1:1)	263, 298, 309, 351	393, 414, 440[a]		118
	$CHCl_3$	353	393, 412, 441	99	134
D1A1 **54**	C_6H_{12}	360	394	~28	121
	C_6H_6		448	~5.8	121
	C_4H_8O		484	~2.8	121
	CH_2Cl_2		510	~1.9	121
	CH_3CN		556	~0.7	121
D1A2 **55**	C_6H_{12}	365	440	~11	121
	C_6H_6		490	~10	121
	C_4H_8O		545	~10	121
	CH_2Cl_2		555	~6	121
	CH_3CN		600	~2	121
spiro-DPO **56**	C_6H_{12}	381	440	~16	121
	C_6H_6		490	~11.9	121
	C_4H_8O		520	~8.1	121
	CH_2Cl_2		560	~4.5	121
	CH_3CN		595	~1.1	121
spiro-DPO **56**	CH_2Cl_2	310, 329, 344, 378	570[b]	<1	107
	$CH_3(CH_2)_4CH_3$	308, 327,[c] 342, 380	401,[a] 434[c]		107
	CH_3CN	312, 332, 347,[a] 381	409,[a] 484		107
D2A2 **57**	C_6H_{12}	382	500	~4.5	121
	C_4H_8O	382	588	~1.1	121
	CH_2Cl_2	383	609	~0.5	121
	C_6H_6	384	557	~2.3	121
	CH_3CN	378	642	~0.1	121
spiro-DPSP **58**	$CH_3(CH_2)_4CH_3$	317,[a] 338,[c] 379	394, 419	7	107
	CH_2Cl_2	318,[a] 342, 380[a]	521[b]	2	107
	CH_3CN	317,[a] 343		0	107
spiro-DPSP[2] **59**	C_6H_{12}	354	544		123
	$CH_3(CH_2)_4CH_3$	354	415		123
spiro-SPO **60**	$CH_3(CH_2)_4CH_3$	317, 330,[c] 343	380,[c] 399, 420[a]		107
	CH_2Cl_2	320,[a] 331, 345[a]	386,[c] 405, 427[b]	78	107
	C_6H_{12}	345	381, 399	87	89
64	THF	362, 309	388, 411		125
spiro-MeO-DPO **72**	$CH_3(CH_2)_4CH_3$	307, 327,[c] 343, 386	389, 413, 474[c]		107
	CH_2Cl_2	310, 330, 345, 383	572[b]	<1	107
	CH_3CN	333, 350, 380	423, 521[b]	<1	107
spiro-MeO-TAD **73**	CH_2Cl_2	383, 365,[a] 305	424		91
spiro-TTB **74**	CH_2Cl_2	384, 309	413		91
spiro-TPD **76**	CH_2Cl_2	379, 309	406		91
A2 **78**	C_4H_8O	368	373	~91	120
4-Ph-spiro[2] **87**	CH_2Cl_2	352, 308, 297[a]	403, 423		91
6-spiro[2] **88**	CH_2Cl_2	357, 324, 308, 298	407, 426		91
89	$CHCl_3$	358	393, 414	16	139
spiro-*m*-TTB **95**	CH_2Cl_2	381, 310	407		91
B2 **96**	$CHCl_3$	310, 333	367, 387	70	105, 106
D2 **98**	C_4H_8O	382	392	~58	120
108	CH_2Cl_2	373, 315, 345, 303	469	49	207
TST **124**	$CHCl_3$	333	370, 387		105
168	$CHCl_3$	353	393, 412, 438	99	134
169	$CHCl_3$	353	394, 414, 440	99	134
170	$CHCl_3$	356	395, 415, 441	99	134
173	$CHCl_3$	358	393, 414	28	139
spiro-β-NPB **183**	CH_2Cl_2	385, 366,[a] 322, 281[a]	442		91
spiro-MeO-TPD **184**	CH_2Cl_2	377, 310	404		91
spiro-MeMeO-TAD **185**	CH_2Cl_2	378, 301	408		91
186	CH_2Cl_2	366, 315, 345, 303	414	73	207
187	CH_2Cl_2	353, 315, 303	452	11	207
188	CH_2Cl_2	350, 328, 315, 302	463	10	207
189	CH_2Cl_2	371, 346, 315, 303	423	82	207
190	CH_2Cl_2	394, 358, 315, 302	422	65	207
191	CH_2Cl_2	396, 354, 315, 303	488	48	207
192	CH_2Cl_2	378, 304	402	64	207
193	CH_2Cl_2	343, 335, 314	368	68	207
194	CH_2Cl_2	379, 350, 315	480	10	207
195	CH_2Cl_2	371, 335, 316	464	27	207
196	CH_2Cl_2	415, 392, 362, 336	530	13	207
197	CH_2Cl_2	375, 312	469	9	207
198	CH_2Cl_2	387, 315	502	51	207
199	CH_2Cl_2	406, 314	476	25	207

[a] Shoulder. [b] Broad. [c] Maximum.

Table 8. Optical Properties of Neat Thin Films of Spiro Compound

compounds	fabrication method[a] (solvent)	λ_{Abs} (nm)	λ_{Em} (nm)	Φ_F (%)	ref
spiro-6Φ **2**	VD	346	399,[b] 420	38	138
				38,[c] 58[d]	77
	SC (CH_2Cl_2)	347	402, 419		95
spiro-TAD **4**	VD	383	406		89
	VD	310, 365,[b] 379	406, 426		91
4-spiro[2] **5**	VD	300, 311, 356	406, 429		91
	VD	310, 353	406, 429	70 ± 10	138
	SC (CH_2Cl_2)	360	402, 420		95
spiro-4Φ **9**	SC (CH_2Cl_2)	337	390, 405, 416		95
4-spiro[3] **12**	SC (CH_2Cl_2)	299, 311, 366	426, 443		91
	SC ($CHCl_3$)	312, 362	426, 446		138
spiro-6Φ $(MeO)_4$ **13**	VD	349	430		89
spiro-α-NPB **15**	VD	371	452		91
spiro-PhOx-TAD **16**	SC (CH_2Cl_2)	311, 394			91
spiro-PhTh-TAD **17**	SC (CH_2Cl_2)	315			91
spiro-Carb **18**	VD	346	382		89
	SC (CH_2Cl_2)	295, 349	381		91
spiro-DPVBi **19**	VD	359	466		89
spiro-octo-2 **24**	VD	350	433	48	77, 89
SSS **27**	VD	312, 335	374, 392	56	105
spiro-PBD **28**	VD	334	406		89
spiro-CN-PBD **29**	SC (CH_2Cl_2)	344	425		107
33	VD	318	410	54	109
34	VD	313	415	31	109
35	VD	304	398	44	109
spiro-FPA **36**	SC (C_7H_8)	439			111
spiro-AMO-*t*-Bu **38**	SC (CH_2Cl_2)	389	477		107
	VD	389	472		89
spiro-AMPO-*t*-Bu **39**	VD	376	479		89
	SC (CH_2Cl_2)	310, 340, 379[e]	483		107
spiro-AMO-CN **40**	SC (CH_2Cl_2)	406	524		107
spiro-AMPO-CN **41**	SC (CH_2Cl_2)	322, 344,[b] 404[e]	526		107
PhSPDCV **49**	VD		500	33	116
pTSPDCV **50**	VD		516	25	116
SDFP **51**	VD		465		117
TDAF-1 **52**	VD			90	134
TDAF-1 **52**	VD	309, 351[e]	405, 430		144
spiro-DPO **56**	SC (CH_2Cl_2)	312, 332,[e] 347,[b] 381	409,[b] 484[e]		107
spiro-DPSP **58**	SC (CH_2Cl_2)	347	466		107
spiro-SPO **60**	VD	337	420		89
64	SC (C_7H_8)	298, 311, 362	394, 412		125
spiro-MeO-DPO **72**	SC (CH_2Cl_2)	333,[e] 350, 380	423, 521[e,f]		107
spiro-MeO-TAD **73**	SC (CH_2Cl_2)	308, 382	426		91
spiro-TTB **74**	SC (CH_2Cl_2)	385, 311			91
spiro-TPD **76**	VD	314, 384	406, 426		91
4-Ph-spiro[2] **87**	SC (CH_2Cl_2)	310,[b] 354	414, 435		91
6-spiro[2] **88**	SC (CH_2Cl_2)	301, 310, 330, 363	438		91
spiro-ADA **92**	SC ($C_6H_{10}O$)	438			148
spiro-*m*-TTB **95**	SC (CH_2Cl_2)	313, 385	406, 425		91
B2 **96**	VD	333	375, 393	63	105
TST **124**	VD	333	375, 393	60	105
168	VD			82	134
169	VD			87	134
170	VD			66	134
spiro-*β*-NPB **183**	SC (CH_2Cl_2)	383, 326	423, 445		91
spiro-MeO−TPD **184**	SC (CH_2Cl_2)	313, 384	406, 425		91
spiro-MeMeO-TAD **185**	SC (CH_2Cl_2)	305, 364,[b] 380	428[f]		91

[a] VD = vapor deposition; SC = spin-coating. [b] Shoulder. [c] Amorphous. [d] Polycrystalline. [e] Maximum. [f] Broad.

Table 9. Oxidation Potentials and HOMO Levels of Some Spiro Compounds[a]

compounds	RE;[b] solvent	E°_{1ox} (V)	E°_{2ox} (V)	HOMO[c] (eV)	ref
TAD **3**	Fc/Fc^+; CH_2Cl_2	0.29	0.52	5.09	132, 133
spiro-TAD **4**	Fc/Fc^+; CH_2Cl_2	0.20	0.34	∼5.00	132, 133
spiro-α-NPB **15**	Fc/Fc^+; CH_2Cl_2	0.20	0.35	∼5.00	132, 133
spiro-PhOx-TAD **16**	Fc/Fc^+; CH_2Cl_2	0.29		∼5.09	91
spiro-PhTh-TAD **17**	Fc/Fc^+; CH_2Cl_2	0.27		∼5.07	91
SSS **27**	Fc/Fc^+; CH_2Cl_2	0.92		5.72	105
33	Ag/AgCl; CH_3CN/THF (9:1 (v/v))	1.11[d]		5.81[e]	109
34	Ag/AgCl; CH_3CN/THF (9:1 (v/v))	1.17[d]		5.87[e]	109
35	Ag/AgCl; CH_3CN/THF (9:1 (v/v))	1.09[d]		5.79[e]	109
spiro-DPA **37**	Fc/Fc^+; CH_2Cl_2	0.8			112
TDAF-1 **52**	Fc/Fc^+; CH_3CN/C_6H_6 (1:1)	1.49	1.66		118
TDAF-1 **52**	Ag/AgCl; CH_2Cl_2	1.32	1.56	6.12	134

Table 9 (Continued)

compounds	RE;[b] solvent	E°_{1ox} (V)	E°_{2ox} (V)	HOMO[c] (eV)	ref
D1A1 **54**	Fc/Fc^+; CH_2Cl_2	0.47		5.27	121
D1A1 **54**	Fc/Fc^+; PhH/MeCN (4:1)	0.50			131
D1A2 **55**	Fc/Fc^+; CH_2Cl_2	0.42		5.22	121
D1A2 **55**	Fc/Fc^+; PhH/MeCN (4:1)	0.49			131
spiro-DPO **56**	Fc/Fc^+; CH_2Cl_2	0.21	0.54	~5.01	133
spiro-DPO **56**	Fc/Fc^+; CH_2Cl_2	0.09	0.42	4.89	121
D2A2 **57**	Fc/Fc^+; CH_2Cl_2	0.23	0.55	5.03	121
D2A2 **57**	Fc/Fc^+; PhH/MeCN (4:1)	0.30	0.46		131
spiro-DPSP **58**	Fc/Fc^+; CH_2Cl_2	0.20	0.52	~5.01	133
spiro-$DPSP^2$ **59**	Fc/Fc^+; CH_2Cl_2	0.19	0.52	~4.99	133
TPD **70**	Fc/Fc^+; CH_2Cl_2	0.27	0.51	~5.07	132, 133
α-NPB **71**	Fc/Fc^+; CH_2Cl_2	0.30	0.57	~5.10	132, 133
spiro-MeO-TAD **73**	Fc/Fc^+; CH_2Cl_2	0.11	0.23	~4.91	91
spiro-TTB **74**	Fc/Fc^+; CH_2Cl_2	0.07	0.24	~4.88	132, 133
TTB **75**	Fc/Fc^+; CH_2Cl_2	0.18	0.44	~4.98	132, 133
spiro-TPD **76**	Fc/Fc^+; CH_2Cl_2	0.17	0.32	~4.97	132, 133
A1 **77**	Fc/Fc^+; PhH/MeCN (4:1)	1.30[f]			131
A2 **78**	Fc/Fc^+; PhH/MeCN (4:1)	1.30[f]			131
spiro-*m*-TTB **95**	Fc/Fc^+; CH_2Cl_2	0.17	0.32	~4.97	91
B2 **96**	Fc/Fc^+; CH_2Cl_2	0.96		5.76	105
B2 **96**	Ag/AgCl; CH_2Cl_2	1.44			106
D2 **98**	Fc/Fc^+; CH_2Cl_2	0.19	0.50	4.99	121
108	Ag/Ag^+; CH_2Cl_2	0.71		5.33	207
TST **124**	Fc/Fc^+; CH_2Cl_2	0.93		5.73	105
168	Ag/AgCl; CH_2Cl_2	1.31	1.56	6.11	134
169	Ag/AgCl; CH_2Cl_2	1.31	1.56	6.11	134
170	Ag/AgCl; CH_2Cl_2	1.30	1.55	6.10	134
spiro-β-NPB **183**	Fc/Fc^+; CH_2Cl_2	0.20	0.33	~5.00	91
spiro-MeO−TPD **184**	Fc/Fc^+; CH_2Cl_2	0.23	0.37	~5.03	91
spiro-MeMeO-TAD **185**	Fc/Fc^+; CH_2Cl_2	0.10	0.24	4.90	91
186	Ag/Ag^+; CH_2Cl_2	0.54		5.15	207
187	Ag/Ag^+; CH_2Cl_2	0.52	1.15[f]	5.10	207
188	Ag/Ag^+; CH_2Cl_2	0.54	1.17[f]	5.12	207
189	Ag/Ag^+; CH_2Cl_2	0.43	0.68	5.05	207
190	Ag/Ag^+; CH_2Cl_2	0.34	0.65	4.96	207
191	Ag/Ag^+; CH_2Cl_2	0.60	0.99	5.21	207
192	Ag/Ag^+; CH_2Cl_2	0.41	0.74	4.95	207
193	Ag/Ag^+; CH_2Cl_2	0.76	1.12	5.28	207
194	Ag/Ag^+; CH_2Cl_2	0.48	0.80	5.31	207
195	Ag/Ag^+; CH_2Cl_2	0.72	0.90	5.26	207
196	Ag/Ag^+; CH_2Cl_2	0.47	0.78	5.04	207
197	Ag/Ag^+; CH_2Cl_2	0.39	0.67	4.93	207
198	Ag/Ag^+; CH_2Cl_2	0.60	0.83	5.12	207
199	Ag/Ag^+; CH_2Cl_2	0.45		4.99	207
D1 **250**	Fc/Fc^+; CH_2Cl_2	0.44		5.24	121
D1 **250**	Fc/Fc^+; PhH/MeCN (4:1)	0.50			131

[a] Potentials depend on solvent effects and the conditions of the reference electrodes (e.g., Ag/AgCl); referencing to a stable, solvent-independent potential is essential. Fc/Fc^+ (+0.35 V vs Ag/AgCl) or cobaltocene $CoCp_2/CoCp_2^+$ (−0.94 V vs Ag/AgCl) has been widely adopted. [b] Reference electrode. [c] The HOMO energy level was deduced from HOMO (eV) = −(4.8 eV + $E_{1/2}$), $E_{1/2}$ being the reversible half-wave potential with respect to ferrocene. [d] Onset potential. [e] HOMO (eV) = $-e(E^{ox}_{onset} + 4.8)$. [f] Irreversible.

Table 10. Reduction Potentials and LUMO Levels of Some Spiro Compounds[a]

compounds	RE;[b] solvent	E°_{1red} (V)	E°_{2red} (V)	LUMO[c] (eV)	ref
SSS **27**	Fc/Fc^+; THF	−2.72			105
spiro-PBD **28**	Fc/Fc^+; THF	−2.46			88
33	Ag/AgCl; CH_3CN:THF (9:1 (v/v))	−2.42[d]		2.46[e]	109
34	Ag/AgCl; CH_3CN:THF (9:1 (v/v))	−2.24[d]		2.28[e]	109
spiro-DPA **37**	Fc/Fc^+; THF	−2.44			112
TDAF-1 **52**	Fc/Fc^+; CH_3CN:C_6H_6 (1:1)	−1.91	−2.02		118
TDAF-1 **52**	Ag/AgCl; THF	−2.01	−2.21		134
D1A1 **54**	Fc/Fc^+; THF	−2.57		2.23	121
D1A1 **54**	Fc/Fc^+; PhH/MeCN (4:1)	−2.48	−2.92		131
D1A2 **55**	Fc/Fc^+; THF	−2.29	−2.63	2.51	121
D1A2 **55**	Fc/Fc^+; PhH/MeCN (4:1)	−2.22	−2.49		131
spiro-DPO **56**	Fc/Fc^+; THF	−2.60		2.20	121
spiro-DPO **56**	Fc/Fc^+; PhH/MeCN (4:1)	−2.45	−2.88		131
spiro-DPO **56**	Fc/Fc^+; THF	−2.53	−2.98		133
D2A2 **57**	Fc/Fc^+; THF	−2.31	−2.64	2.49	121
D2A2 **57**	Fc/Fc^+; PhH/MeCN (4:1)	−2.25	−2.52		131
spiro-DPSP **58**	Fc/Fc^+; THF	−2.69	−2.81		133
spiro-MeO-DPO **72**	Fc/Fc^+; THF	−2.54	−3.07		133
A1 **77**	Fc/Fc^+; THF	−2.56		2.24	121
A1 **77**	Fc/Fc^+; PhH/MeCN (4:1)	−2.51	−2.90		131
A2 **78**	Fc/Fc^+; THF	−2.29	−2.61	2.51	121
A2 **78**	Fc/Fc^+; PhH/MeCN (4:1)	−2.22	−2.49		131
B2 **96**	Fc/Fc^+; THF	−2.75			105

Table 10 (Continued)

compounds	RE;[b] solvent	E°_{1red} (V)	E°_{2red} (V)	LUMO[c] (eV)	ref
B2 **96**	Ag/AgCl; THF	−2.15			106
D2 **98**				1.86	121
108				2.44	207
TST **124**	Fc/Fc^+; THF	−2.71			105
168	Ag/AgCl; THF	−2.11	−2.23		134
169	Ag/AgCl; THF	−2.10	−2.22		134
170	Ag/AgCl; THF	−2.03	−2.17		134
186				2.06	207
187				2.00	207
188				2.05	207
189				2.08	207
190				2.04	207
191				2.42	207
192				1.84	207
193				1.93	207
194				2.32	207
195				2.23	207
196				2.39	207
197				1.98	207
198				2.22	207
199				2.38	207
D1 **250**	Fc/Fc^+; PhH/MeCN (4:1)	−3.15			131
D1 **250**				2.14	121

[a] Potentials depend on solvent effects and the conditions of the reference electrodes (e.g., Ag/AgCl); referencing to a stable, solvent-independent potential is essential. Fc/Fc^+ (+0.35 V vs Ag/AgCl) or cobaltocene $CoCp_2/CoCp_2^+$ (−0.94 V vs Ag/AgCl) has been widely adopted. [b] RE = reference electrode. [c] The LUMO energy was deduced from LUMO (eV) = HOMO (eV) − E_g (eV), where E_g is the optical band gap, calculated from the absorption onset. [d] Onset potential. [e] LUMO (eV) = $-e(E^{red}_{onset} + 4.8)$.

Table 11. Thermal Properties of Some Spiro Compounds

compounds	T_g (°C)	T_m (°C)	T_{rec} (°C)	T_d[a] (°C)	ref	compounds	T_g (°C)	T_m (°C)	T_{rec} (°C)	T_d[a] (°C)	ref
spiro-6Φ **2**	212	408	271		77, 138	TTB **75**	66				132
TAD **3**	70				132	spiro-TPD **76**	115	234		470	91
spiro-TAD **4**	133	276	185	480	91	A1 **77**	128			391	121
4-spiro[2] **5**	273	447	347	620	91, 138	A2 **78**	165			412	121
spiro-4Φ **9**	184	296			77, 87	4-Ph-spiro[2] **87**	285	446		580	91
spiro-8Φ **10**	243	440		585	77, 88	6-spiro[2] **88**	259			460	91
4-spiro[3] **12**	330				91, 138	**89**	296				139
spiro-6Φ(MeO)$_4$ **13**	191	326			89	spiro-ADA **92**	147				148
spiro-α-NPB **15**	147	294		540	91	spiro-*m*-TTB **95**	119	230		490	91
spiro-PhOx-TAD **16**				500	91	B2 **96**	174			367[b]	105
spiro-PhTh-TAD **17**				430	91	D2 **98**	112			329	121
spiro-Carb **18**	240	532		570	91	**108**	146			378[c]	207
spiro-DPVBi **19**	130	228			206	TST **124**	197			475[b]	105
spiro-octo-2 **24**	236	263			77, 89	**168**	201			425	134
SSS **27**	228			464[b]	105	**169**	210			435	134
spiro-PBD **28**	163	337			88	**170**	231			430	134
spiro-CN-PBD **29**	191	355	317		107	**173**	225				139
33	228	382			109	**174**	275	452	328		139
34	203	334			109	**175**	60	194	84		96
35	203	314			109	**176**	56				96
spiro-FPA **36**	223	397		450	111	**177**	~60				96
spiro-AMO-*t*-Bu **38**	165				107	**178**	179	348	243		96
spiro-AMPO-*t*-Bu **39**	177				107	**179**	202				96
spiro-AMO-CN **40**	168	293	235		107	spiro-β-NPB **183**	137			560	91
spiro-AMPO-CN **41**	212	299			107	spiro-MeO-TPD **184**	86	218		480	91
PhSPDCV **49**	110	253		337	116	spiro-MeMeO-TAD **185**	105	238		450	91
pTSPDCV **50**	112	232		340	116	**186**	145			405[c]	207
SDPF **51**	193	399		488[c]	117	**187**	154			414[c]	207
TDAF-1 **52**				450	134	**188**	178			440[c]	207
D1A1 **54**	139			355	121	**189**	205			480[c]	207
D1A2 **55**	187			436	121	**190**	210			430[c]	207
spiro-DPO **56**	149			406	121	**191**	215			470[c]	207
spiro-DPO **56**	139	234			107	**192**				430[c]	207
D2A2 **57**	173			442	121	**193**				450[c]	207
spiro-DPSP **58**	152	371	196		107	**194**	135			421[c]	207
spiro-DPSP[2] **59**	210				107	**195**	139	287	194	407[c]	207
spiro-SPO **60**	177				107	**196**	185			400[c]	207
TPD **70**	62				132	**197**				442[c]	207
α-NPB **71**	95				132	**198**	180			430[c]	207
spiro-MeO-DPO **72**	111				107	**199**				410[c]	207
spiro-MeO-TAD **73**	121	246		440	91	D1 **250**	89			280	121
spiro-TTB **74**	146	293	192	510	91						

[a] Decomposition temperature, corresponding to 5% weight loss. [b] Decomposition temperature, corresponding to 10% weight loss. [c] No further information.

9. References

(1) Tang, C. W.; Van Slyke, S. A. *Appl. Phys. Lett.* **1987**, *51*, 913.
(2) Burroughes, J. H.; Bradley, D. D. C.; Brown, A. R.; Marks, R. N.; Mackay, K.; Friend, R. H.; Burns, P. L.; Holmes, A. B. *Nature* **1990**, *347*, 539.
(3) Kraft, A.; Grimsdale, A. C.; Holmes, A. B. *Angew. Chem., Int. Ed.* **1998**, *37*, 402.
(4) Baldo, M. A.; Thompson, M. E.; Forrest, S. R. *Nature* **2000**, *403*, 750.
(5) Rees, I. D.; Robinson, K. L.; Holmes, A. B.; Towns, C. R.; O'Dell, R. *MRS Bull.* **2002**, 451.
(6) Forrest, S. R. *Nature* **2004**, *428*, 911.
(7) Veinot, J. G. C.; Marks, T. J. *Acc. Chem. Res.* **2005**, *38*, 632.
(8) Sariciftci, N. S.; Smilowitz, L.; Heeger, A. J.; Wudl, F. *Science* **1992**, *258*, 1474.
(9) Xue, J.; Uchida, S.; Rand, B. P.; Forrest, S. R. *Appl. Phys. Lett.* **2004**, *85*, 5757.
(10) Xue, J.; Uchida, S.; Rand, B. P.; Forrest, S. R. *Appl. Phys. Lett.* **2004**, *84*, 3013.
(11) Xue, J.; Rand, B. P.; Uchida, S.; Forrest, S. R. *Adv. Mater. (Weinheim, Ger.)* **2005**, *17*, 66.
(12) van Duren, J. K. J.; Yang, X.; Loos, J.; Bulle-Lieuwma, C. W. T.; Sieval, A. B.; Hummelen, J. C.; Janssen, R. A. J. *Adv. Funct. Mater.* **2004**, *14*, 425.
(13) Mihailetchi, V. D.; Koster, L. J. A.; Blom, P. W. M.; Melzer, C.; de Boer, B.; van Duren, J. K. J.; Janssen, R. A. J. *Adv. Funct. Mater.* **2005**, *15*, 795.
(14) Erb, T.; Zhokhavets, U.; Gobsch, G.; Raleva, S.; Stühn, B.; Schilinsky, P.; Waldauf, C.; Brabec, C. J. *Adv. Funct. Mater.* **2005**, *15*, 1193.
(15) Hoppe, H.; Sariciftci, N. S. *J. Mater. Chem.* **2006**, *16*, 45.
(16) Ma, L. P.; Liu, J.; Yang, Y. *Appl. Phys. Lett.* **2002**, *80*, 2997.
(17) Ma, L. P.; Pyo, S.; Ouyang, J.; Xu, Q. F.; Yang, Y. *Appl. Phys. Lett.* **2003**, *82*, 1419.
(18) Möller, S.; Perlov, C.; Jackson, W.; Taussig, C.; Forrest, S. R. *Nature* **2003**, *426*, 166.
(19) Möller, S.; Forrest, S. R.; Perlov, C.; Jackson, W.; Taussig, C. *J. Appl. Phys.* **2003**, *94*, 7811.
(20) Bozano, L. D.; Kean, B. W.; Deline, V. R.; Salem, J. R.; Scott, J. C. *Appl. Phys. Lett.* **2004**, *84*, 607.
(21) Ouyang, J.; Chu, C. W.; Szmanda, C.; Ma, L.; Yang, Y. *Nat. Mater.* **2004**, *3*, 918.
(22) Yang, Y.; Ma, L.; Wu, J. *MRS Bull.* **2004**, 833.
(23) Chih, C. C.; Ouyang, J.; Tseng, J. H.; Yang, Y. *Adv. Mater. (Weinheim, Ger.)* **2005**, *17*, 1440.
(24) Peumans, P.; Bulovic, V.; Forrest, S. R. *Appl. Phys. Lett.* **2000**, *76*, 3855.
(25) Narayan, K. S.; Kumar, N. *Appl. Phys. Lett.* **2001**, *79*, 1891.
(26) Rand, B. P.; Xue, J.; Lange, M.; Forrest, S. R. *IEEE Photonics Technol. Lett.* **2003**, *15*, 1279.
(27) Peumans, P.; Yakimov, A.; Forrest, S. R.; *J. Appl. Phys.* **2003**, *93*, 3693.
(28) Kabra, D.; Singh, Th. B.; Narayan, K. S. *Appl. Phys. Lett.* **2004**, *85*, 5073.
(29) Crone, B.; Dodabalapur, A.; Galperin, A.; Torsi, L.; Katz, H. E.; Lovinger, A. J.; Bao, Z. *Appl. Phys. Lett.* **2001**, *78*, 2229.
(30) Torsi, L.; Lovinger, A. J.; Crone, B.; Someya, T.; Dodabalapur, A.; Katz, H. E.; Galperin, A. *J. Phys. Chem. B* **2002**, *106*, 12563.
(31) Someya, T.; Katz, H. E.; Galperin, A.; Lovinger, A. J.; Dodabalapur, A. *Appl. Phys. Lett.* **2002**, *81*, 3079.
(32) Torsi, L.; Dodabalapur, A.; Sabbatini, L.; Zambonin, P. G. *Sens. Actuators, B* **2000**, *67*, 312.
(33) Torsi, L.; Dodabalapur, A.; Cioffi, N.; Sabbatini, L.; Zambonin, P. G. *Sens. Actuators, B* **2001**, *77*, 7.
(34) Torsi, L.; Tanese, M. C.; Cioffi, N.; Gallazzi, M. C.; Sabbatici, L.; Zambonin, P. G.; Raos, G.; Meille, S. V.; Giangregorio, M. M. *J. Phys. Chem. B* **2003**, *107*, 7589.
(35) Torsi, L.; Tafuri, A.; Cioffi, N.; Gallazzi, M. C.; Sassella, A.; Sabbatici, L.; Zambonin, P. G. *Sens. Actuators, B* **2003**, *93*, 257.
(36) Bartic, C.; Campitelli, A.; Borghi, G. *Appl. Phys. Lett.* **2003**, *82*, 475.
(37) Zhu, Z. T.; Mabeck, J. T.; Zhu, C.; Cady, N. C.; Batt, C. A.; Malliaras, G. G. *Chem. Commun.* **2004**, *13*, 1556.
(38) Torsi, L.; Tanese, M. C.; Cioffi, N.; Gallazzi, M. C.; Sabbatici, L.; Zambonin, P. G. *Sens. Actuators B* **2004**, *98*, 204.
(39) Torsi, L.; Dodabalapur, A. *Anal. Chem.* **2005**, *77*, 380A.
(40) Tanese, M. C.; Fine, D.; Dodabalapur, A.; Torsi, L. *Biosens. Bioelectron.* **2005**, *21*, 782.
(41) Wang, L.; Fine, D.; Sharma, D.; Torsi, L.; Dodabalapur, A. *Anal. Bioanal. Chem.* **2006**, *384*, 310.
(42) Bartic, C.; Borghs, G. *Anal. Bioanal. Chem.* **2006**, *384*, 354.
(43) Dimitrakopoulos, C. D.; Mascoro, D. *IBM J. Res. Dev.* **2001**, *45*, 11.
(44) Dimitrakopoulos, C. D.; Malenfant, P. R. L. *Adv. Mater.* (*Weinheim, Ger.*) **2002**, *14*, 99.
(45) Sirringhaus, H. *Adv. Mater. (Weinheim, Ger.)* **2005**, *17*, 2411.
(46) Kosolov, D.; English, D. S.; Bulovic, V.; Barbara, P. F.; Forrest, S. R.; Thompson, M. E. *J. Appl. Phys.* **2001**, *90*, 3242.
(47) Ke, L.; Chen, P.; Chua, S. J. *Appl. Phys. Lett.* **2002**, *80*, 697.
(48) Naito, K.; Miura, A. *J. Phys. Chem.* **1993**, *97*, 6240.
(49) Naito, K. *Chem. Mater.* **1994**, *6*, 2343.
(50) Shirota, Y.; Kuwabara, Y.; Okuda, D.; Okuda, R.; Ogawa, H.; Inada, H.; Wakimoto, T.; Nakada, H.; Yonemoto, Y.; Kawami, S.; Imai, K. *J. Lumin.* **1997**, *72*, 985.
(51) Wang, S.; Oldham, W. J.; Hudack, R. A.; Bazan, G. C. *J. Am. Chem. Soc.* **2000**, *122*, 5695.
(52) Shirota, Y.; Tobata, T.; Noma, N. *Chem. Lett.* **1989**, 1145.
(53) Higuchi, A.; Inada, H.; Kobata, T.; Shirota, Y. *Adv. Mater. (Weinheim, Ger.)* **1991**, *3*, 549.
(54) Ishikawa, W.; Inada, H.; Nakano, H.; Shirota, Y. *Chem. Lett.* **1991**, 1731.
(55) Inada, H.; Shirota, Y. *J. Mater. Chem.* **1993**, *3*, 319.
(56) Kuwabara, Y.; Ogawa, H.; Inada, H.; Noma, N.; Shirota, Y. *Adv. Mater. (Weinheim, Ger.)* **1994**, *6*, 677.
(57) Shirota, Y. *J. Mater. Chem.* **2000**, *10*, 1.
(58) Shirota, Y. *J. Mater. Chem.* **2005**, *15*, 75.
(59) Pudzich, R.; Fuhrmann-Lieker, T.; Salbeck. J. *Adv. Polym. Sci.* **2006**, *199*, 83.
(60) Frank, N. L.; Clerac, R.; Sutter, J. P.; Daro, N.; Kahn, O.; Coulon, C.; Green, M. T.; Golhen, S.; Ouahab, L. *J. Am. Chem. Soc.* **2000**, *122*, 2053.
(61) Huang, Y.; Liang, W.; Poon, J. K. S.; Xu, Y.; Lee, R. K.; Yariv, A. *Appl. Phys. Lett.* **2006**, *88*, 181102.
(62) Yuan, W.; Sun, L.; Tang, H.; Wen, Y.; Jiang, G.; Huang, W.; Jiang, L.; Song, Y.; Zhu, D. *Adv. Mater. (Weinheim, Ger.)* **2005**, *17*, 156.
(63) Patel, D. G.; Benedict, J. B.; Kopelman, R. A.; Frank, N. L. *Chem. Commun.* **2005**, *17*, 2208.
(64) Fu, S.; Liu, Y.; Lu, Z.; Dong, L.; Hu, W.; Xie, M. *Opt. Commun.* **2004**, *242*, 115.
(65) Li, X.; Li, J.; Wang, Y.; Matsuura, T.; Meng, J. *J. Photochem. Photobiol., A* **2004**, *161*, 201.
(66) Kopelman, R. A.; Snyder, S. M.; Frank, N. L. *J. Am. Chem. Soc.* **2003**, *125*, 13684.
(67) Alonso, M.; Reboto, V.; Guiscardo, L.; San Martin, A.; Rodriguez-Cabello, J. C. *Macromolecules* **2000**, *33*, 9480.
(68) Guo, X.; Zhang, D.; Yu, G.; Wan, M.; Li, J.; Liu, Y.; Zhu, D. *Adv. Mater. (Weinheim, Ger.)* **2004**, *16*, 636.
(69) Zhu, M. Q.; Zhu, L.; Han, J. J.; Wu, W.; Hurst, J. K.; Li, A. D. Q. *J. Am. Chem. Soc.* **2006**, *128*, 4303.
(70) Matsumoto, M.; Nakazawa, T.; Mallia, V. A.; Tamaoki, N.; Azumi, R.; Sakai, H.; Abe, M. *J. Am. Chem. Soc.* **2004**, *126*, 1006.
(71) Wu, Y.; Li, J.; Fu, Y.; Bo, Z. *Org. Lett.* **2004**, *6*, 3485.
(72) Rothe, C.; Brunner, K.; Bach, I.; Heun, S.; Monkman, A. P. *J. Chem. Phys.* **2005**, *122*, 084706.
(73) Laquai, F.; Wegner, G.; Im, C.; Bassler, H.; Heun, S. *J. Appl. Phys.* **2006**, *99*, 033710.
(74) Mueller, C. D.; Falcou, A.; Reckefuss, N.; Rojahn, M.; Wiederhirn, V.; Rudati, P.; Frohne, H.; Nuyken, O.; Becker, H.; Meerholz, K. *Nature* **2003**, *421*, 829.
(75) Rothe, C.; Al Attar, H. A.; Monkman, A. P. *Phys. Rev. B* **2005**, *72*, 155330.
(76) Buchhauser, D.; Scheffel, M.; Rogler, W.; Tschamber, C.; Heuser, K.; Hunze, A.; Gieres, G.; Henseler, D.; Jakowetz, W.; Diekmann, K.; Winnacker, A.; Becker, H.; Buesing, A.; Falcou, A.; Rau, L.; Voegele, S.; Goettling, S. *Proc. SPIE−Int. Soc. Opt. Eng.* **2004**, *5519*, 70.
(77) Salbeck, J. In *Inorganic and Organic Electroluminescence /EL96 Berlin*; Mauch, R.H., Gumlich, H.E., Eds.; Wissenschaft und Technik Verlag: Berlin, Germany, 1996; p 243.
(78) Schweig, A.; Weidner, U.; Hellwinkel, D.; Krapp, W. *Angew. Chem.* **1973**, *85*, 360.
(79) van Dantzig, N. A.; Levy, D. H.; Vigo, C.; Piotrowiak, P. *J. Chem. Phys.* **1995**, *103*, 4894.
(80) Shain, A. L.; Ackerman, J. P.; Teague, M. W. *Chem. Phys. Lett.* **1969**, *3*, 550.
(81) Prelog, V.; Bedekovic, D. *Helv. Chim. Acta* **1979**, *62*, 2285.
(82) Schartel, B.; Krüger, S.; Wachtendorf, V.; Hennecke, M. *J. Chem. Phys.* **2000**, *112*, 9822.
(83) Yip, W. T.; Levy, D. H.; Kobetic, R.; Piotrowiak, P. *J. Phys. Chem. A* **1999**, *103*, 10.
(84) Davydov, A. S. *Zh. Eksp. Teor. Fiz.* **1948**, *18*, 515.
(85) Berlman, I. B. *Mol. Cryst.* **1978**, *4*, 157.
(86) Brackmann, U. *Lambdachrome Laser Dyes*; Lambda Physik AG: Göttingen, Germany, 2000.
(87) Salbeck, J.; Yu, N.; Bauer, J.; Weissortel, F.; Bestgen, H. *Synth. Met.* **1997**, *91*, 209.

(88) Salbeck, J.; Weissoertel, F.; Bauer, J. *Macromol. Symp.* **1997**, *125*, 121.
(89) Spehr, T.; Pudzich, R.; Fuhrmann, T.; Salbeck, J. *Org. Electron.* **2003**, *4*, 61.
(90) Johansson, N.; dos Santos, D. A.; Guo, S.; Cornil, J.; Fahlman, M.; Salbeck, J.; Schenk, H.; Arwin, H.; Bredas, J. L.; Salaneck, W. R. *J. Chem. Phys.* **1997**, *107*, 2542.
(91) Weissörtel, F. Ph.D. Thesis, University of Regensburg, Regensburg, Germany, 1999.
(92) Londenberg, J.; Salbeck, J. Unpublished work.
(93) Milota, F.; Warmuth, C.; Tortschanoff, A.; Sperling, J.; Fuhrmann, T.; Salbeck, J.; Kauffmann, H. F. *Synth. Met.* **2001**, *121*, 1497.
(94) Lukeš, V.; Breza, M. *J. Mol. Struct.* **2004**, *699*, 93.
(95) Lukeš, V.; Pálszegi, T.; Milota, F.; Sperling, J.; Kauffmann, H. F. *J. Phys. Chem. A* **2006**, *110*, 1775.
(96) Katsis, D.; Geng, Y. H.; Ou, J. J.; Culligan, S. W.; Trajkovska, A.; Chen, S. H.; Rothberg, L. J. *Chem. Mater.* **2002**, *14*, 1332.
(97) Schneider, D.; Rabe, T.; Riedl, T.; Dobbertin, T.; Kröger, M.; Becker, E.; Johannes, H. H.; Kowalsky, W.; Weimann, T.; Wang, J.; Hinze, P.; Gerhard, A.; Stössel, P.; Vestweber, H. *Adv. Mater. (Weinheim, Ger.)* **2005**, *17*, 31.
(98) Schartel, B.; Damerau, T.; Hennecke, M. *Phys. Chem. Chem. Phys.* **2000**, *2*, 4690.
(99) Avilov, I.; Marsal, P.; Brédas, J. L.; Beljonne, D. *Adv. Mater. (Weinheim, Ger.)* **2004**, *16*, 1624.
(100) Hosokawa, C.; Higashi, H.; Nakamura, H.; Kusumoto, T. *Appl. Phys. Lett.* **1995**, *67*, 3853.
(101) Harada, N; Ono, H; Nishiwaki, T; Uda, H. *J. Chem. Soc., Chem. Commun.* **1991**, 1753.
(102) Alcazar, V.; Diederich, F. *Angew. Chem.* **1992**, *104*, 1503.
(103) Cuntze, J., Diederich, F. *Helv. Chim. Acta* **1997**, *80*, 897.
(104) Spehr, T.; Siebert, A.; Fuhrmann-Lieker, T.; Salbeck, S.; Rabe, T.; Riedl, T.; Johannes, H. H.; Kowalsky, W.; Wang, J.; Weimann, T.; Hinze, P. *Appl. Phys. Lett.* **2005**, *87*, 161103.
(105) Wong, K. T.; Liao, Y. L.; Lin, Y. T.; Su, H. C.; Wu, C. C. *Org. Lett.* **2005**, *7*, 5131.
(106) Chao, T. C.; Lin, Y. T.; Yang, C. Y.; Hung, T. S.; Chou, H. C.; Wu, C. C.; Wong, K. T. *Adv. Mater. (Weinheim, Ger.)* **2005**, *17*, 992.
(107) Pudzich, R. Ph.D. Thesis, University of Kassel, Kassel, Germany, 2002.
(108) Wu, F.; Riesgo, E. C.; Thummel, R. P., Juris, A.; Hissler, M.; El-Ghayoury, A.; Ziessel, R. *Tetrahedron Lett.* **1999**, *40*, 7311.
(109) Lee, S. H.; Jang, B. B.; Kafafi, Z. H. *J. Am. Chem. Soc.* **2005**, *127*, 9071.
(110) Yang, G.; Su, Z.; Qin, C. *J. Phys. Chem. A* **2006**, *110*, 4817.
(111) Shen, W. J.; Dodda, R.; Wu, C. C.; Wu, F. I.; Liu, T. H.; Chen, H. H.; Chen, C. H.; Shu, C. F. *Chem. Mater.* **2004**, *16*, 930.
(112) Gerloff, T.; Salbeck, J. Unpublished work.
(113) Pudzich, R.; Salbeck, J. *Synth. Met.* **2003**, *138*, 21.
(114) Chiang, C. L.; Shu, C. F.; Chen, C. T. *Org. Lett.* **2005**, *7*, 3717.
(115) Kim, S. Y.; Lee, M.; Boo, B. H. *J. Chem. Phys.* **1998**, *109*, 2593.
(116) Chiang, C. L.; Wu, M. F.; Dai, D. C.; Wen, Y. S.; Wang, J. K.; Chen, C. T. *Adv. Funct. Mater.* **2005**, *15*, 231.
(117) Tao, S.; Peng, Z.; Zhang, X.; Wang, P.; Lee, C. S.; Lee, S. T. *Adv. Funct. Mater.* **2005**, *15*, 1716.
(118) Choi, J. P.; Wong, K. T.; Chen, Y. M.; Yu, J. K.; Chou, P. T.; Bard, A. J. *J. Phys. Chem. B* **2003**, *107*, 14407.
(119) Wu, C. C.; Lin, Y. T., Chiang, H. H.; Cho, T. Y.; Chen, C. W.; Wong, K. T.; Liao, Y. L.; Lee, G. H.; Peng, S. M. *Appl. Phys. Lett.* **2002**, *81*, 577.
(120) Chien, Y. Y.; Wong, K. T.; Chou, P. T.; Cheng, Y. M. *Chem. Commun.* **2002**, *23*, 2874.
(121) Wong, K. T.; Ku, S. Y.; Cheng, Y. M.; Lin, X. Y.; Hung, Y. Y.; Pu, S. C.; Chou, P. T.; Lee, G. H.; Peng, S. M. *J. Org. Chem.* **2006**, *71*, 456.
(122) Saragi, T. P. I.; Pudzich, R.; Fuhrmann, T.; Salbeck, J. *Appl. Phys. Lett.* **2004**, *84*, 2334.
(123) Saragi, T. P. I.; Pudzich, R.; Fuhrmann-Lieker, T.; Salbeck, J. *Opt. Mater.* **2007**, *29*, 879.
(124) Lee, H.; Oh, J.; Chu, H. Y.; Lee, J. I.; Kim, S. H.; Yang, Y. S.; Kim, G. H.; Do, L. M.; Zyung, T.; Lee, J.; Park, Y. *Tetrahedron* **2003**, *59*, 2773.
(125) Cao, X. Y.; Zhang, W.; Hong, Z.; Pei, J. *Org. Lett.* **2004**, *6*, 4845.
(126) Chen, H. S.; Wu, F. I.; Shu, C. F.; Chien, C. H.; Tao, Y. T. *J. Mater. Chem.* **2004**, *14*, 1585.
(127) Horhant, D.; Liang, J. J.; Virboul, M.; Poriel, C.; Alcaraz, G.; Rault-Berthelot, J. *Org. Lett.* **2006**, *8*, 257.
(128) Gritzner, G.; Kuta, J. *Pure Appl. Chem.* **1984**, *56*, 461.
(129) Pommerehne, J.; Vestweber, H.; Guss, W.; Mahrt, R. F.; Bässler, H.; Porsch, M.; Daub, J. *Adv. Mater. (Weinheim, Ger.)* **1995**, *7*, 551.
(130) D'Andrade, B. W.; Datta, S.; Forrest, S. R.; Djurovich, P.; Polikarpov, E.; Thompson, M. E. *Org. Electron.* **2005**, *6*, 11.
(131) Fungo, F.; Wong, K. T.; Ku, S. Y.; Hung, Y. Y.; Bard, A. J. *J. Phys. Chem. B* **2005**, *109*, 3984.
(132) Saragi, T. P. I.; Fuhrmann-Lieker, T.; Salbeck, J. *Adv. Funct. Mat.* **2006**, *16*, 966.
(133) Ebert, T.; Salbeck, J. Unpublished work.
(134) Wong, K. T.; Chien, Y. Y.; Chen, R. T.; Wang, C. F.; Lin, Y. T.; Chiang, H. H.; Hsieh, P. Y.; Wu, C. C.; Chou, C. H.; Su, Y. O.; Lee, G. H.; Peng, S. M. *J. Am. Chem. Soc.* **2002**, *124*, 11576.
(135) Crispin, A.; Crispin, X.; Fahlmann, M.; dos Santos, D. A.; Cornil, J.; Johannson, N.; Bauer, J.; Weissörtel, F.; Salbeck, J.; Brédas, J. L.; Salaneck, W. R. *J. Chem. Phys.* **2002**, *116*, 8159.
(136) Mitschke, U.; Bäuerle, P. *J. Chem. Soc., Perkin Trans. 1* **2001**, 740.
(137) Pei, J.; Ni, J.; Zhou, X. H.; Cao, X. Y.; Lai, Y. H. *J. Org. Chem.* **2002**, *67*, 8104.
(138) Salbeck, J.; Schörner, M.; Fuhrmann, T. *Thin Solid Films* **2002**, *417*, 20.
(139) Geng, Y.; Katsis, D.; Culligan, S. W.; Ou, J. J.; Chen, S. H.; Rothberg, L. J. *Chem. Mater.* **2002**, *14*, 463.
(140) Jellison, G. E.; Modine, F. A. *Appl. Phys. Lett.* **1996**, *69*, 371.
(141) Jellison, G. E.; Modine, F. A. *Appl. Phys. Lett.* **1996**, *69*, 2137.
(142) Tammer, M.; Higgins, R. W. T.; Monkman, A. P. *J. Appl. Phys.* **2002**, *91*, 4010.
(143) Campoy-Quiles, M.; Etchegoin, P. G.; Bradley, D. D. C. *Phys. Rev. B* **2005**, *72*, 045209.
(144) Lin, H. W.; Lin, C. L.; Chang, H. H.; Lin, Y. T.; Wu, C. C.; Chen, Y. M.; Chen, R. T.; Chien, Y. Y.; Wong, K. T. *J. Appl. Phys.* **2004**, *95*, 881.
(145) Weinfurtner, K. H.; Weissörtel, F.; Harmgarth, G.; Salbeck, J. *Proc. SPIE−Int. Soc. Opt. Eng.* **1998**, *3476*, 40.
(146) Saragi, T. P. I. Ph.D. Thesis, University of Kassel, Kassel, Germany, 2004.
(147) Saragi, T. P. I.; Pudzich, R.; Fuhrmann, T.; Salbeck, J. *Mater. Res. Soc. Symp. Proc.* **2002**, *725*, 85.
(148) Chun, C.; Kim, M. J.; Vak, D.; Kim, D. Y. *J. Mater. Chem.* **2003**, *13*, 2904.
(149) Rochon, P.; Batalla, E.; Natansohn, A. *Appl. Phys. Lett.* **1995**, *66*, 136.
(150) Kim, D. Y.; Tripathy, S. K.; Li, L.; Kumar, J. *Appl. Phys. Lett.* **1995**, *66*, 1166.
(151) Fuhrmann, T.; Tsutsui, T. *Chem. Mater.* **1999**, *11*, 2226.
(152) Nakano, H.; Takahashi, T.; Shirota, Y. *Adv. Mater. (Weinheim, Ger.)* **2002**, *14*, 1157.
(153) Kim, M. J.; Seo, E. M.; Vak, D.; Kim, D. Y. *Chem. Mater.* **2003**, *15*, 4021.
(154) Müller-Wiegand, M.; Georgiev, G.; Oesterschulze, E.; Fuhrmann, T.; Salbeck, J. *Appl. Phys. Lett.* **2002**, *81*, 4940.
(155) Fuhrmann, T.; Salbeck, J.; Müller-Wiegand, M.; Oesterschulze, E. *Int. J. Nanosci.* **2004**, *3*, 609.
(156) Fuhrmann, T.; Salbeck, J.; Reinke, N.; Franke, H.; Müller-Wiegand, M.; Oesterschulze, E. In *Fusion of Nanotechnology and Organic Semiconductor*; Karthaus, O., Adachi, C., Sasabe, H., Eds.; PWC Publishing: Chitose, Japan, **2004**.
(157) Spehr, T.; Fetten, M.; Fuhrmann-Lieker, T.; Salbeck, J. Unpublished work.
(158) Schneider, D.; Rabe, T.; Riedl, T.; Dobbertin, T.; Kroeger, M.; Becker, E.; Johannes, H. H.; Kowalsky, W.; Weimann, T.; Wang, J.; Hinze, P. *Appl. Phys. Lett.* **2004**, *85*, 1659.
(159) Schneider, D.; Rabe, T.; Riedl, T.; Dobbertin, T.; Werner, O.; Kroger, M.; Becker, E.; Johannes, H. H.; Kowalsky, W.; Weimann, T.; Wang, J.; Hinze, P.; Gerhard, A.; Stossel, P.; Vestweber, H. *Appl. Phys. Lett.* **2004**, *84*, 4693.
(160) Schneider, D.; Rabe, T.; Riedl, T.; Dobbertin, T.; Kröger, M.; Becker, E.; Johannes, H. H.; Kowalsky, W.; Weimann, T.; Wang, J.; Hinze, P. *J. Appl. Phys.* **2005**, *98*, 043104.
(161) Johansson, N.; Salbeck, J.; Bauer, J.; Weissörtel, F.; Bröms, P.; Andersson, A.; Salaneck, W. R. *Adv. Mater. (Weinheim, Ger.)* **1998**, *10*, 1136.
(162) Dodabalapur, A.; Berggren, M.; Slusher, R. E.; Bao, Z.; Timko, A.; Schiortino, P.; Laskowski, E.; Katz, H. E.; Nalamasu, O. *IEEE J. Sel. Top. Quantum Electron.* **1998**, *4*, 67.
(163) Berggren, M.; Dodabalapur, A.; Slusher, R. E.; Bao, Z.; Timko, A.; Nalamasu, O. *Electron. Lett.* **1998**, *34*, 90.
(164) Meier, M.; Mekis, A.; Dodabalapur, A.; Timko, A.; Slusher, R. E.; Joannopoulos, J. D.; Nalamasu, O. *Appl. Phys. Lett.* **1999**, *74*, 7.
(165) Mekis, A.; Meier, M.; Dodabalapur, A.; Slusher, R. E.; Joannopoulos, J. D. *Appl. Phys. A* **1999**, *69*, 111.
(166) Yoshino, K.; Tatsuhara, S.; Kawagishi, Y.; Ozaki, M.; Zakhidov, A. A.; Vardeny, Z. V. *Appl. Phys. Lett.* **1999**, *74*, 2590.
(167) Koschorreck, M.; Gehlhaar, R.; Lyssenko, V. G.; Swoboda, M.; Hoffmann, M.; Leo, K. *Appl. Phys. Lett.* **2005**, *87*, 181108.
(168) Persano, L.; Del Carro, P.; Mele, E.; Cingolani, R.; Pisignano, D.; Zavelani-Rossi, M.; Longhi, S.; Lanzani, G. *Appl. Phys. Lett.* **2006**, *88*, 121110.

(169) Frolov, S. V.; Vardeny, Z. V.; Yoshino, K.; Zakhidov, A.; Baughman, R. H. *Phys. Rev. B* **1999**, *59*, R5284.
(170) Kuwata-Gonokami, M.; Jordan, R. H.; Dodabalapur, A.; Katz, H. E.; Schilling, M. L.; Slusher, R. E.; Ozawa, S. *Opt. Lett.* **1995**, *20*, 2093.
(171) Frolov, S. V.; Shkunov, M.; Vardeny, Z. V.; Yoshino, K. *Phys. Rev. B* **1997**, *56*, R4363.
(172) Kawabe, Y.; Spiegelberg, Ch.; Schulzgen, A.; Nabor, M. F.; Kippelen, B.; Mash, E. A.; Allemand, P. M.; Kuwata-Gonokami, M.; Takeda, K.; Peyghambarian, N. *Appl. Phys. Lett.* **1998**, *72*, 141.
(173) Frolov, S. V.; Fujii, A.; Chinn, D.; Hirohata, M.; Hidayat, R.; Taraguchi, M.; Masuda, T.; Yoshino, K.; Vardeny, Z. V. *Adv. Mater. (Weinheim, Ger.)* **1998**, *10*, 869.
(174) Borsenberger, P.; Weiss, D. S. *Organic Photoreceptors for Imaging Systems*; Marcel Dekker: New York, 1993; pp 273−287.
(175) Horowitz, G. In *Semiconducting Polymer: Chemistry, Physics and Engineering*; Hadziioannou, G., van Hutten, P. F., Eds.; Wiley-VCH: Weinheim, Germany, 1999; pp 463−514.
(176) Bässler, H. *Phys. Status Solidi B* **1993**, *175*, 15.
(177) Gill, W. D. *J. Appl. Phys.* **1972**, *43*, 5033.
(178) Bach, U.; de Cloedt, K.; Spreitzer, H.; Grätzel, M. *Adv. Mater. (Weinheim, Ger.)* **2000**, *12*, 1060.
(179) Poplavskyy, D.; Nelson, J. *J. Appl. Phys.* **2003**, *93*, 341.
(180) Kirkpatrick, J.; Nelson, J. *J. Chem. Phys.* **2005**, *123*, 084703.
(181) Wu, C. C.; Liu, T. L.; Hung, W. Y.; Lin, Y. T.; Wong, K. T.; Chen, R. T.; Chen, Y. M.; Chien, Y. Y. *J. Am. Chem. Soc.* **2003**, *125*, 3710.
(182) Wu, C. C.; Liu, W. G.; Hung, W. Y.; Liu, T. L.; Lin, Y. T.; Lin, H. W.; Wong, K. T.; Chien, Y. Y.; Chen, R. T.; Hung, T. H.; Chao, T. C.; Chen, Y. M. *Appl. Phys. Lett.* **2005**, *87*, 052103.
(183) Wu, C. C.; Liu, T. L.; Lin, Y. T.; Hung, W. Y.; Ke, T. H.; Wong, K. T.; Chao, T. C. *Appl. Phys. Lett.* **2004**, *85*, 1172.
(184) Saragi, T. P. I.; Fuhrmann-Lieker, T.; Salbeck, J. *Synth. Met.* **2005**, *148*, 267.
(185) Stolka, M.; Yanus, J. F.; Pai, D. M. *J. Phys. Chem.* **1984**, *88*, 4707.
(186) Brown, A. R.; Jarrett, C. P.; de Leeuw, D. M.; Matters, M. *Synth. Met.* **1997**, *88*, 37.
(187) Vissenberg, M. C. J. M.; Matters, M. *Phys. Rev. B* **1998**, *57*, 12964.
(188) Kaneko, Y.; Koike, N.; Tsutsui, K.; Tsukada, T. *Appl. Phys. Lett.* **1990**, *56*, 650.
(189) Hamilton, M. C.; Martin, S.; Kanicki, J. *IEEE Trans. Electron Devices* **2004**, *51*, 877.
(190) Xu, Y.; Berger, P. R.; Wilson, J. N.; Bunz, U. H. F. *Appl. Phys. Lett.* **2004**, *85*, 4219.
(191) Noh, Y. Y.; Kim, D. Y.; Yoshida, Y.; Yase, K.; Jung, B. J.; Lim, E.; Shim, H. K. *Appl. Phys. Lett.* **2005**, *86*, 043501.
(192) Noh, Y. Y.; Kim, D. Y.; Yase, K. *J. Appl. Phys.* **2005**, *98*, 074505.
(193) Saragi, T. P. I.; Pudzich, R.; Fuhrmann-Lieker, T.; Salbeck, J. Unpublished work.
(194) Lin, H. W.; Ku, S. Y.; Su, H. C.; Huang, C. W.; Lin, Y. T.; Wong, K. T.; Wu, C. C. *Adv. Mater. (Weinheim, Ger.)* **2005**, *17*, 2489.
(195) O'Regan, B.; Grätzel, M. *Nature* **1991**, *353*, 737.
(196) Bach, U.; Lupo, D.; Comte, P.; Moser, J. E.; Weissörtel, F.; Salbeck, J.; Spreitzer, H.; Gratäzel, M. *Nature* **1998**, *395*, 583.
(197) Bach, U.; Tachibana, Y.; Moser, J. E.; Haque, S. A.; Durrant, J. R.; Grätzel, M.; Klug, D. R. *J. Am. Chem. Soc.* **1999**, *121*, 7445.
(198) Krüger, J. Ph.D. Thesis, Ecole Polytechnique Fédérale de Laussane, Laussane, Switzerland, 2003.
(199) Krüger, J.; Plass, R.; Cevey, L.; Piccirelli, M.; Gratzel, M.; Bach, U. *Appl. Phys. Lett.* **2001**, *79*, 2085.
(200) Krüger, J.; Plass, R.; Gratzel, M.; Matthieu, H. J. *Appl. Phys. Lett.* **2002**, *81*, 367.
(201) Schmidt-Mende, L.; Bach, U.; Humphry-Baker, R.; Horiuchi, T.; Miura, H.; Ito, S.; Uchida, S.; Grätzel, M. *Adv. Mater. (Weinheim, Ger.)* **2005**, *17*, 813.
(202) Schmidt-Mende, L.; Kroeze, J. E.; Durrant, J. R.; Nazeeruddin, M. K.; Grätzel, M. *Nano Lett.* **2005**, *5*, 1315.
(203) Schmidt-Mende, L.; Zakeeruddin, S. M.; Grätzel, M. *Appl. Phys. Lett.* **2005**, *86*, 013504.
(204) Adachi, C.; Tsutsui, T.; Saito, S. *Appl. Phys. Lett.* **1989**, *55*, 1489.
(205) CIE Central Bureau, Eds. *CIE, Commission Internationale de l'Éclairage Proceedings 1931*; Cambridge University Press: Cambridge, 1932.
(206) Spreitzer, H.; Schenk, H.; Salbeck, J.; Weissörtel, F.; Riel, H.; Riess, W. *Proc. SPIE−Int. Soc. Opt. Eng.* **1999**, *3797*, 316.
(207) Shen, J. Y.; Lee, C. Y.; Huang, T. H.; Lin, J. T.; Tao, Y. T.; Chien, C. H.; Tsai, C. *J. Mater. Chem.* **2005**, *15*, 2455.
(208) Wu, C. C.; Lin, Y. T.; Wong, K. T.; Chen, R. T.; Chien, Y. Y. *Adv. Mater. (Weinheim, Ger.)* **2004**, *16*, 61.
(209) Oyston, S.; Wang, C.; Hughes, G.; Batsanov, A. S.; Perepichka, I. F.; Bryce, M. R.; Ahn, J. H.; Pearson, C.; Petty, M. C. *J. Mater. Chem.* **2005**, *15*, 194.
(210) Pfeiffer, M.; Leo, K.; Zhou, X.; Hunag, J. S.; Hofmann, M.; Werner, A.; Blochwitz-Nimoth, J. *Org. Electron.* **2003**, *4*, 89.
(211) Gebeyehu, D.; Walzer, K.; He, G.; Pfeiffer, M.; Leo, K.; Brandt, J.; Gerhard, A.; Stoessel, P.; Vestweber, H. *Synth. Met.* **2005**, *148*, 205.
(212) He, G.; Schneider, O.; Qin, D.; Zhou, X.; Pfeiffer, M.; Leo, K. *J. Appl. Phys.* **2004**, *95*, 5773.
(213) He, G.; Pfeiffer, M.; Leo, K.; Hofmann, M.; Birnstock, J.; Pudzich, R.; Salbeck, J. *Appl. Phys. Lett.* **2004**, *85*, 3911.
(214) Huang, J.; Pfeiffer, M.; Blochwitz, J.; Werner, A.; Salbeck, J.; Liu, S.; Leo, K. *Jpn. J. Appl. Phys.* **2001**, *40*, 6630.
(215) Steuber, F.; Staudigl, J.; Stössel, M.; Simmerer, J.; Winnacker, A.; Spreitzer, H.; Weissörtel, F.; Salbeck, J. *Adv. Mater. (Weinheim, Ger.)* **2000**, *12*, 130.
(216) Chuen, C. H.; Tao, Y. T.; Wu, F. I.; Shu, C. F. *Appl. Phys. Lett.* **2004**, *85*, 4609.
(217) Salis, G.; Alvarado, S. F.; Tschudy, M.; Brunschwiler, T.; Allenspach, R. *Phys. Rev. B* **2004**, *70*, 085203.
(218) Clarkson, R. G.; Gomberg, M. *J. Am. Chem. Soc.* **1930**, *52*, 2881.
(219) Tour, J. M.; Wu, R.; Schumm, J. S. *J. Am. Chem. Soc.* **1990**, *112*, 5662.
(220) Wu, R.; Schumm, J. S.; Pearson, D. L.; Tour, J. M. *J. Org. Chem.* **1996**, *61*, 6906.
(221) Poriel, C.; Ferrand, Y.; Juillard, S.; Le Maux, P.; Simonneaux, G. *Tetrahedron* **2004**, *60*, 145.
(222) Thiemann, F.; Piehler, T.; Haase, D.; Saak, W.; Luetzen, A. *Eur. J. Org. Chem.* **2005**, 1991.
(223) Wu, X. M.; Chen, X. C.; Cao, X. P.; Pan, X. F. *Ganguang Kexue Yu Guang Huaxue* **2001**, *19*, 161.
(224) Marsitzky, D.; Murray, J.; Scott, J. C.; Carter, K. R. *Chem. Mater.* **2001**, *13*, 4285.
(225) Pei, J.; Ni, J.; Zhou, X. H.; Cao, X. Y.; Lai, Y. H. *J. Org. Chem.* **2002**, *67*, 4924.
(226) Merkushev, E. B. *Synthesis* **1988**, 923.
(227) Borowitz, I. J.; Anschel, M.; Readio, P. D. *J. Org. Chem.* **1971**, *36*, 553.
(228) Ayasse, C.; Salbeck, J. Unpublished work.
(229) Park, J. H.; Ko, H. C.; Kim, J. H.; Lee, H. *Synth. Met.* **2004**, *144*, 193.
(230) Winter, Werner, B.; Diederich, F.; Gramlich, V. *Helv. Chim. Acta* **1996**, *79*, 1338.
(231) Yu, W. L.; Pei, J.; Huang, W.; Heeger, A. J. *Adv. Mater. (Weinheim, Ger.)* **2000**, *12*, 828.
(232) Kim, Y. H.; Shin, D. C.; Kim, S. H.; Ko, C. H.; Yu, H. S.; Chae, Y. S.; Kwon, S. K. *Adv. Mater. (Weinheim, Ger.)* **2001**, *13*, 1690.
(233) Shin, D. C.; Kim, Y. H.; You, H.; Kwon, S. K. *Macromolecules* **2003**, *36*, 3222.
(234) Kim, Y. H.; Kim, H. S.; Kwon, S. K. *Macromolecules* **2005**, *38*, 7950.
(235) Sutcliffe, F. K.; Shahidi, H. M.; Patterson, D. *J. Soc. Dyers Colour.* **1978**, *94*, 306.
(236) Weisburger, J. H.; Weisburger, E. K.; Ray, F. E. *J. Am. Chem. Soc.* **1950**, *72*, 4253.
(237) Chou, C. H.; Reddy, D. S.; Shu, C. F. *J. Polym. Sci., Part A: Polym. Chem.* **2002**, *40*, 3615.
(238) Wong, K. T.; Liao, Y. L.; Peng, Y. C.; Wang, C. C.; Lin, S. Y.; Yang, C. H.; Tseng, S. M.; Lee, G. H.; Peng, S. M. *Cryst. Growth Des.* **2005**, *5*, 667.
(239) Siebert, A.; Salbeck, J. Unpublished work.
(240) Doyle, M. P.; Siegfried, B.; Dellaria, J. F. J. *J. Org. Chem.* **1977**, *42*, 2426.
(241) Wu, F. I.; Dodda, R.; Reddy, D. S.; Shu, C. F. *J. Mater. Chem.* **2002**, *12*, 2893.
(242) Moore, J. S.; Weinstein, E. J.; Wu, Z. *Tetrahedron Lett.* **1991**, *32*, 2465.
(243) Haas, G.; Prelog, V. *Helv. Chim. Acta* **1969**, *52*, 1202.
(244) Alcazar Montero, V.; Tomlinson, L.; Houk, K. N.; Diederich, F. *Tetrahedron Lett.* **1991**, *32*, 5309.
(245) Cheng, X.; Zhang, Q.; Xie, J. H.; Wang, L. X.; Zhou, Q. L. *Angew. Chem., Int. Ed.* **2005**, *44*, 1118.
(246) Littke, A. F.; Dai, C.; Fu, G. C. *J. Am. Chem. Soc.* **2000**, *122*, 4020.
(247) Toda, F.; Tanaka, K. *J. Org. Chem.* **1988**, *53*, 3607.
(248) Cahn, R. S.; Ingold, C.; Prelog, V. *Angew. Chem., Int. Ed. Engl.* **1966**, *5*, 385.
(249) Cahn, R. S.; Ingold, C.; Prelog, V. *Angew. Chem.* **1966**, *78*, 413.
(250) Eliel, E. L.; Wilen, S. H. *Stereochemistry of Organic Compounds*; John Wiley & Sons, Inc.: New York, 1994.
(251) Eliel, E. L.; Wilen, S. H. *Organische Stereochemie*; Wiley VCH: Weinheim, Germany, 1998.
(252) Ritter, K. *Synthesis* **1993**, 735.
(253) Abad, A.; Agullo, C.; Cunat, A. C.; Perni, R. H. *Tetrahedron: Asymmetry* **2000**, *11*, 1607.
(254) Cheng, X.; Hou, G. H.; Xie, J. H.; Zhou, Q. L. *Org. Lett.* **2004**, *6*, 2381.

(255) Fournier, J. H.; Maris, T.; Wuest, J. D. *J. Org. Chem.* **2004**, *69*, 1762.
(256) Salbeck, J. *Ber. Bunsen-Ges.* **1996**, *100*, 1667.
(257) Miyaura, N.; Suzuki, A. *Chem. Rev.* **1995**, *95*, 2457.
(258) Kimura, M.; Kuwano, S.; Sawaki, Y.; Fujikawa, H.; Noda, K.; Taga, Y.; Takagi, K. *J. Mater. Chem.* **2005**, *15*, 2393.
(259) Wu, F. I.; Fu, C. F.; Wang, T. T.; Diau, E. W. G.; Chien, C. H.; Chuen, C. H.; Tao, Y. T. *Synth. Met.* **2005**, *151*, 285.
(260) Hartwig, J. F. *Angew. Chem.* **1998**, *110*, 2154.
(261) Tour, J. M. *Adv. Mater. (Weinheim, Ger.)* **1994**, *6*, 190.
(262) Juris, A.; Prodi, L.; Harriman, A.; Ziessel, R.; Hissler, M.; El-Ghayoury, A.; Wu, F.; Riesgo, E. C.; Thummel, R. P. *Inorg. Chem.* **2000**, *39*, 3590.
(263) Poriel, C.; Ferrand, Y.; Maux, P. L.; Raul-Berthelot, J.; Simonneaux, G. *Chem. Commun.* **2003**, 1104.
(264) Poriel, C.; Ferrand, Y.; Maux, P. L.; Raul-Berthelot, J.; Simonneaux, G. *Tetrahedron Lett.* **2003**, *44*, 1759.
(265) Chiang, C. L.; Shu, C.-F. *Chem. Mater.* **2002**, *14*, 682.
(266) Gilman, H.; Gorsich, R. D., *J. Am. Chem. Soc.* **1958**, *80*, 1883.
(267) Chang, L. S.; Corey, J. Y. *Organometallics* **1989**, *8*, 1885.
(268) Boo, B. H.; Park, J.; Yeo, H. G.; Lee, S. Y.; Park, C. J.; Kim, J. H., *J. Phys. Chem. A* **1998**, *102*, 1139.
(269) Ballweg, D.; Liu, Y.; Guzei, I. A., West, R. *Silicon Chem.* **2002**, *1*, 57.
(270) Lee, S. H.; Jang, B. B.; Kafafi, Z. *Polym. Mater.: Sci. Eng.* **2004**, *91*, 808.

CR0501341